EUROPEAN ORGANISATION FOR NUCLEAR RESEARCH (CERN)

Submitted to: J. High Energy Phys.

CERN-EP-2016-019
12th April 2016

Measurement of fiducial differential cross sections of gluon-fusion production of Higgs bosons decaying to $WW^* \to e\nu\mu\nu$ with the ATLAS detector at $\sqrt{s} = 8$ TeV

The ATLAS Collaboration

Abstract

This paper describes a measurement of fiducial and differential cross sections of gluon-fusion Higgs boson production in the $H \to WW^* \to e\nu\mu\nu$ channel, using 20.3 fb^{-1} of proton–proton collision data. The data were produced at a centre-of-mass energy of $\sqrt{s} = 8$ TeV at the CERN Large Hadron Collider and recorded by the ATLAS detector in 2012. Cross sections are measured from the observed $H \to WW^* \to e\nu\mu\nu$ signal yield in categories distinguished by the number of associated jets. The total cross section is measured in a fiducial region defined by the kinematic properties of the charged leptons and neutrinos. Differential cross sections are reported as a function of the number of jets, the Higgs boson transverse momentum, the dilepton rapidity, and the transverse momentum of the leading jet. The jet-veto efficiency, or fraction of events with no jets above a given transverse momentum threshold, is also reported. All measurements are compared to QCD predictions from Monte Carlo generators and fixed-order calculations, and are in agreement with the Standard Model predictions.

Contents

1 Introduction

Since the observation of a new particle by the ATLAS [1] and CMS [2] collaborations in the search for the Standard Model (SM) Higgs boson [3–8], the mass, spin, and charge conjugation times parity of the new particle have been measured by both collaborations [9–11]. Its mass has been measured to be $m_H = 125.09 \pm 0.24$ GeV [9] by combining ATLAS and CMS measurements. The strengths of its couplings to gauge bosons and fermions have also been explored [12, 13]. In all cases the results are consistent with SM predictions. Differential cross-section measurements have recently been made by the ATLAS and CMS collaborations in the $ZZ \to 4\ell$ [14, 15] and $\gamma\gamma$ [16, 17] final states. The results of the ATLAS collaboration have been combined in Ref. [18].

In this paper, measurements of fiducial and differential cross sections for Higgs boson production in the $H \to WW^* \to e\nu\mu\nu$ final state are presented. These measurements use 20.3 fb^{-1} of proton–proton collision data at a centre-of-mass energy of $\sqrt{s} = 8$ TeV recorded by the ATLAS experiment at the CERN Large Hadron Collider (LHC). The presented measurements characterise the gluon-fusion production mode (ggF), which is the dominant signal contribution to the $H \to WW^* \to e\nu\mu\nu$ event sample. The results are compared to quantum chromodynamics (QCD) predictions of this production mechanism. Small contributions from the vector-boson fusion (VBF), and vector-boson associated production (VH) modes are subtracted assuming the SM expectation. Contributions from associated Higgs boson production via $t\bar{t}H$ and $b\bar{b}H$ are expected to be negligible after applying the experimental event-selection criteria. To minimise the model dependencies of the correction for the detector acceptance, and to allow direct comparison with theoretical predictions, all cross sections presented in this paper are fiducial cross sections corrected for detector effects. Here, the cross sections are given in a fiducial region defined using particle-level objects where most of the event-selection requirements of the analysis are applied.

The differential ggF Higgs boson production cross sections are chosen to probe several different physical effects:

- Higher-order perturbative QCD contributions to the ggF production are probed by measuring the number of jets, N_{jet}, and transverse momentum, p_{T}, of the highest-p_{T} ("leading") jet, $p_{\text{T}}^{j_1}$.
- Multiple soft-gluon emission, as modelled by resummation calculations, and non-perturbative effects are probed by measuring the transverse momentum of the reconstructed Higgs boson, p_{T}^{H}.
- Parton distribution functions (PDFs) are probed by measuring the absolute value of the rapidity of the reconstructed dilepton system, $|y_{\ell\ell}|$.

The dilepton rapidity, $y_{\ell\ell}$, is highly correlated to the rapidity of the reconstructed Higgs boson, y_H, which is known to be sensitive to PDFs. Since it is not possible to reconstruct y_H experimentally in the $H \to WW^* \to e\nu\mu\nu$ final state, the differential cross section is measured as a function of $|y_{\ell\ell}|$. An additional important test of QCD predictions is the production cross section of the Higgs boson without additional jets (H + 0-jet), which is also a significant source of uncertainty in measurements of the total $H \to WW^*$ production rate. The H + 0-jet cross section can be calculated from the product of the total cross section and the jet-veto efficiency for H + 0-jet events, $\varepsilon_0(p_{\text{T}}^{\text{thresh}})$, where events with jets of a transverse momentum above threshold, $p_{\text{T}} > p_{\text{T}}^{\text{thresh}}$, are vetoed. In addition to the measurement of the N_{jet} distribution, a measurement of the jet-veto efficiency for H + 0-jet events, ε_0, is presented for three different values of $p_{\text{T}}^{\text{thresh}}$. All results are compared to a set of predictions from fixed-order calculations and Monte Carlo (MC) generators.

Differential cross-section measurements are performed for the first time in the $H \to WW^* \to e\nu\mu\nu$ final state. This analysis is an extension of the ggF coupling measurement performed using the Run-1 dataset [19], and uses the same object definitions, background-estimation techniques, and strategies to evaluate the systematic uncertainties. In contrast to the couplings measurement, in which the results were obtained using a likelihood-based approach to simultaneously fit several signal regions and background-dominated control regions, the analysis presented here utilizes a simplified approach. First the dominant backgrounds are estimated using control regions in data, and then the predicted backgrounds are subtracted from the observed data in the signal region to obtain the signal yield. Another difference is that events with two leptons of the same flavour ($ee/\mu\mu$) are not considered due to the large Drell–Yan ($pp \to Z/\gamma^* \to \ell\ell$) background. Using an iterative Bayesian method, the distributions are corrected for detector efficiencies and resolutions. Statistical and systematic uncertainties are propagated through these corrections, taking correlations among bins into account.

2 The ATLAS detector

The ATLAS detector [20] at the LHC covers nearly the entire solid angle around the collision point. It consists of an inner tracking detector surrounded by a thin superconducting solenoid, electromagnetic and hadronic calorimeters, and a muon spectrometer incorporating three large superconducting toroid magnets. The inner-detector system (ID) is immersed in a 2 T axial magnetic field and provides charged-particle tracking in the range $|\eta| < 2.5$.[1]

Closest to the interaction point, the silicon-pixel detector forms the three innermost layers of the inner detector. The silicon-microstrip tracker surrounding it typically provides four additional two-dimensional measurement points per track. The silicon detectors are complemented by the transition-radiation tracker, which enables radially extended track reconstruction up to $|\eta| = 2.0$ and provides electron identification information based on the fraction of hits above a higher energy-deposit threshold indicating the presence of transition radiation.

The calorimeter system covers the range $|\eta| < 4.9$. Within the region $|\eta| < 3.2$, electromagnetic calorimetry is provided by a high-granularity lead/liquid-argon (LAr) sampling calorimeter. The hadronic calorimeter consists of steel and scintillator tiles in the central region and two copper/LAr hadronic endcap calorimeters. The solid-angle coverage is completed with forward copper/LAr and tungsten/LAr calorimeter modules optimised for electromagnetic and hadronic measurements respectively.

The muon spectrometer (MS) covers the region $|\eta| < 2.7$ with precise position measurements from three layers of monitored drift tubes (MDTs). Cathode-strip chambers provide additional high-granularity coverage in the forward ($2 < |\eta| < 2.7$) region. The muon trigger system covers the range $|\eta| < 2.4$ with resistive-plate chambers in the barrel and thin-gap chambers in the endcap regions, both of which also provide position measurements in the direction normal to the bending plane, complementary to the precision hits from the MDTs.

[1] ATLAS uses a right-handed coordinate system with its origin at the nominal interaction point (IP) in the centre of the detector and the z-axis along the beam pipe. The x-axis points from the IP to the centre of the LHC ring, and the y-axis points upwards. Cylindrical coordinates (r, ϕ) are used in the transverse plane, ϕ being the azimuthal angle around the z-axis. The pseudorapidity is defined in terms of the polar angle θ as $\eta = -\ln\tan(\theta/2)$. Angular separation is measured in units of $\Delta R \equiv \sqrt{(\Delta\eta)^2 + (\Delta\phi)^2}$.

A three-level trigger system reduces the event rate to about 400 Hz [21]. The Level-1 trigger is implemented in hardware and uses a subset of detector information to reduce the event rate to a design value of at most 75 kHz. The two subsequent trigger levels, collectively referred to as the High-Level Trigger (HLT), are implemented in software.

3 Signal and background models

The ggF and VBF production modes for $H \to WW^*$ are modelled at next-to-leading order (NLO) in the strong coupling α_S with the Powheg MC generator [22–25], interfaced with Pythia8 [26] (version 8.165) for the parton shower, hadronisation, and underlying event. The CT10 [27] PDF set is used and the parameters of the Pythia8 generator controlling the modelling of the parton shower and the underlying event are those corresponding to the AU2 set [28]. The Higgs boson mass set in the generation is 125.0 GeV, which is close to the measured value. The Powheg ggF model takes into account finite quark masses and a running-width Breit–Wigner distribution that includes electroweak corrections at NLO [29]. To improve the modelling of the Higgs boson p_T distribution, a reweighting scheme is applied to reproduce the prediction of the next-to-next-to-leading-order (NNLO) and next-to-next-to-leading-logarithm (NNLL) dynamic-scale calculation given by the HRes 2.1 program [30]. Events with ≥ 2 jets are further reweighted to reproduce the p_T^H spectrum predicted by the NLO Powheg simulation of Higgs boson production in association with two jets ($H + 2$ jets) [31]. Interference with continuum WW production [32, 33] has a negligible impact on this analysis due to the transverse-mass selection criteria described in Section 4 and is not included in the signal model.

The inclusive cross sections at $\sqrt{s} = 8$ TeV for a Higgs boson mass of 125.0 GeV, calculated at NNLO+NNLL in QCD and NLO in the electroweak couplings, are 19.3 pb and 1.58 pb for ggF and VBF respectively [34]. The uncertainty on the ggF cross section has approximately equal contributions from QCD scale variations (7.5%) and PDFs (7.2%). For the VBF production, the uncertainty on the cross section is 2.7%, mainly from PDF variations. The WH and ZH processes are modelled with Pythia8 and normalised to cross sections of 0.70 pb and 0.42 pb respectively, calculated at NNLO in QCD and NLO in the electroweak couplings [34]. The uncertainty is 2.5% on the WH cross section and 4.0% on the ZH cross section.

For all of the background processes, with the exception of W + jets and multijet events, MC simulation is used to model event kinematics and as an input to the background normalisation. The W + jets and multijet background models are derived from data as described in Section 5. For the dominant WW and top-quark backgrounds, the MC generator is Powheg +Pythia6 [35] (version 6.426), also with CT10 for the input PDFs. The Perugia 2011 parameter set is used for Pythia6 [36]. For the WW background with $N_{\text{jet}} \geq 2$, to better model the additional partons, the Sherpa [37] program (version 1.4.3) with the CT10 PDF set is used. The Drell–Yan background, including $Z/\gamma^* \to \tau\tau$, is simulated with the Alpgen [38] program (version 2.14). It is interfaced with Herwig [39] (version 6.520) with parameters set to those of the ATLAS Underlying Event Tune 2 [40] and uses the CTEQ6L1 [41] PDF set. The same configuration is applied for $W\gamma$ events. Events in the Z/γ^* sample are reweighted to the MRSTmcal PDF set [42]. For the $W\gamma^*$ and Z/γ backgrounds, the Sherpa program is used, with the same version number and PDF set as the WW background with ≥ 2 jets. Additional diboson backgrounds, from WZ and ZZ, are modelled using Powheg +Pythia8.

For all MC samples, the ATLAS detector response is simulated [43] using either Geant4 [44] or Geant4 combined with a parameterised Geant4-based calorimeter simulation [45]. Multiple proton–proton (pile-

up) interactions are modelled by overlaying minimum-bias interactions generated using Pythia8. Further detail of all MC generators and cross sections used is given in Ref. [19].

4 Event selection

This section describes the reconstruction-level definition of the signal region. The definition of physics objects reconstructed in the detector follows that of Ref. [19] exactly and is summarised here. All objects are defined with respect to a primary interaction vertex, which is required to have at least three associated tracks with $p_{\mathrm{T}} \geq 400$ MeV. If more than one such vertex is present, the one with the largest value of $\sum(p_{\mathrm{T}}^2)$, where the sum is over all tracks associated with that vertex, is selected as the primary vertex.

4.1 Object reconstruction and identification

Electron candidates are built from clusters of energy depositions in the EM calorimeter with an associated well-reconstructed track. They are required to have $E_{\mathrm{T}} > 10$ GeV, where the transverse energy E_{T} is defined as $E\sin(\theta)$. Electrons reconstructed with $|\eta| < 2.47$ are used, excluding $1.37 < |\eta| < 1.52$, which corresponds to the transition region between the barrel and the endcap calorimeters. Additional identification criteria are applied to reject background, using the calorimeter shower shape, the quality of the match between the track and the cluster, and the amount of transition radiation emitted in the ID [46–48]. For electrons with 10 GeV $< E_{\mathrm{T}} <$ 25 GeV, a likelihood-based electron selection at the "very tight" operating point is used for its improved background rejection. For $E_{\mathrm{T}} > 25$ GeV, a more efficient "medium" selection is used because background is less of a concern. The efficiency of these requirements varies strongly as a function of E_{T}, starting from 65–70% for $E_{\mathrm{T}} < 25$ GeV, jumping to about 80% with the change in identification criteria at $E_{\mathrm{T}} = 25$ GeV, and then steadily increasing as a function of E_{T} [47].

Muon candidates are selected from tracks reconstructed in the ID matched to tracks reconstructed in the muon spectrometer. Tracks in both detectors are required to have a minimum number of hits to ensure robust reconstruction. Muons are required to have $|\eta| < 2.5$ and $p_{\mathrm{T}} > 10$ GeV. The reconstruction efficiency is between 96% and 98%, and stable as a function of p_{T} [49].

Additional criteria are applied to electrons and muons to reduce backgrounds from non-prompt leptons and electromagnetic signatures produced by hadronic activity. Lepton isolation is defined using track-based and calorimeter-based quantities. All isolation variables used are normalised relative to the transverse momentum of the lepton, and are optimised for the $H \to WW^* \to e\nu\mu\nu$ analysis, resulting in stricter criteria for better background rejection at lower p_{T} and looser criteria for better efficiency at higher p_{T}. Similarly, requirements on the transverse impact-parameter significance d_0/σ_{d_0} and the longitudinal impact parameter z_0 are made. The efficiency of the isolation and impact-parameter requirements for electrons satisfying all of the identification criteria requirements ranges from 68% for 10 GeV $< E_{\mathrm{T}} <$ 15 GeV to greater than 90% for electrons with $E_{\mathrm{T}} > 25$ GeV. For muons, the equivalent efficiencies are 60–96%.

Jets are reconstructed from topological clusters of calorimeter cells [50–52] using the anti-k_t algorithm with a radius parameter of $R = 0.4$ [53]. Jet energies are corrected for the effects of calorimeter non-compensation, signal losses due to noise threshold effects, energy lost in non-instrumented regions, contributions from in-time and out-of-time pile-up, and the position of the primary interaction vertex [50, 54]. Subsequently, the jets are calibrated to the hadronic energy scale [50, 55]. To reduce the chance of

using a jet produced by a pile-up interaction, jets with with $p_{\mathrm{T}} < 50$ GeV and $|\eta| < 2.4$ are required to have more than 50% of the scalar sum of the p_{T} of their associated tracks come from tracks associated with the primary vertex. Jets used for definition of the signal region are required to have $p_{\mathrm{T}} > 25$ GeV if $|\eta| < 2.5$ and $p_{\mathrm{T}} > 30$ GeV if $2.5 < |\eta| < 4.5$.

Jets containing b-hadrons are identified using a multivariate b-tagging algorithm [56, 57] which combines impact-parameter information of tracks and the reconstruction of charm- and bottom-hadron decays. The working point, chosen to maximise top-quark background rejection, has an efficiency of 85% for b-jets and a mis-tag rate for light-flavour jets (excluding jets from charm quarks) of 10.3% in simulated $t\bar{t}$ events.

Missing transverse momentum ($\boldsymbol{p}_{\mathrm{T}}^{\mathrm{miss}}$) is produced in signal events by the two neutrinos from the W boson decays. It is reconstructed as the negative vector sum of the transverse momenta of muons, electrons, photons, jets, and tracks with $p_{\mathrm{T}} > 0.5$ GeV associated with the primary vertex but unassociated with any of the previous objects.

4.2 Signal region selection

Events are selected from those with exactly one electron and one muon with opposite charge, a dilepton invariant mass $m_{\ell\ell}$ greater than 10 GeV, and $p_{\mathrm{T}}^{\mathrm{miss}} > 20$ GeV. At least one of the two leptons is required to have $p_{\mathrm{T}} > 22$ GeV and the lepton with higher p_{T} is referred to as the leading lepton. The other ("subleading") lepton is required to have $p_{\mathrm{T}} > 15$ GeV. All events are required to pass at least one single-lepton or dilepton trigger. The Level-1 p_{T} thresholds for the single-lepton triggers are 18 GeV and 15 GeV for electrons and muons, respectively. The HLT uses object reconstruction and calibrations close to those used offline, and the electron and muon triggers both have thresholds at 24 GeV and an isolation requirement. To recover efficiency, a supporting trigger with no isolation requirement but higher p_{T} thresholds, 60 GeV for electrons and 36 GeV for muons, is used. The dilepton trigger requires an electron and a muon above a threshold of 10 GeV and 6 GeV, respectively, at Level-1, and 12 GeV and 8 GeV in the HLT. This increases the signal efficiency by including events with a leading lepton below the threshold imposed by the single-lepton triggers but still on the plateau of the dilepton trigger efficiency. The reconstructed leptons are required to match those firing the trigger.

Three non-overlapping signal regions are defined, distinguished by the number of reconstructed jets: $N_{\mathrm{jet}} = 0$, $N_{\mathrm{jet}} = 1$, or $N_{\mathrm{jet}} \geq 2$. These separate the data into signal regions with different background compositions, which improves the sensitivity of the analysis. The dominant background processes are WW production for $N_{\mathrm{jet}} = 0$, top-quark production for $N_{\mathrm{jet}} \geq 2$, and a mixture of the two for $N_{\mathrm{jet}} = 1$. For jet multiplicities above two, the number of events decreases with increasing number of jets but the background composition remains dominated by top-quark production, so these events are all collected in the $N_{\mathrm{jet}} \geq 2$ signal region.

The signal regions are based on the selection used for the ggF analysis of Ref. [19], with modifications to improve the signal-to-background ratio, and to account for the treatment of VBF and VH as backgrounds. The former includes the increase in the subleading lepton p_{T} threshold and the exclusion of same-flavour events, to reduce background from W + jets and Drell–Yan events, respectively.

The selection criteria are summarised in Table 1. The b-jet veto uses jets with $p_{\mathrm{T}} > 20$ GeV and $|\eta^{\mathrm{jet}}| < 2.4$, and rejects top-quark background in the $N_{\mathrm{jet}} = 1$ and $N_{\mathrm{jet}} \geq 2$ categories. Background from $Z/\gamma^* \to \tau\tau$ and multijet events is reduced in the $N_{\mathrm{jet}} = 0$ category with a requirement on the transverse momentum of

Table 1: Event selection criteria used to define the signal regions in the $H \to WW^* \to e\nu\mu\nu$ differential cross section measurements. The preselection and signal-topology selection criteria are identical across all signal regions. The background rejection and VBF-veto selection depend on N_{jet}, and a dash ('-') indicates that no selection is applied. Definitions including the p_{T} thresholds for jet counting are given in the text.

Category	$N_{\text{jet}} = 0$	$N_{\text{jet}} = 1$	$N_{\text{jet}} \geq 2$
Preselection	Two isolated leptons ($\ell = e, \mu$) with opposite charge $p_{\text{T}}^{\text{lead}} > 22$ GeV, $p_{\text{T}}^{\text{sublead}} > 15$ GeV $m_{\ell\ell} > 10$ GeV $p_{\text{T}}^{\text{miss}} > 20$ GeV		
Background rejection	- $\Delta\phi(\ell\ell, p_{\text{T}}^{\text{miss}}) > 1.57$ $p_{\text{T}}^{\ell\ell} > 30$ GeV	$N_{b\text{-jet}} = 0$ $\max(m_{\text{T}}^{\ell}) > 50$ GeV $m_{\tau\tau} < m_Z - 25$ GeV	$N_{b\text{-jet}} = 0$ - $m_{\tau\tau} < m_Z - 25$ GeV
VBF veto	-	-	$m_{jj} < 600$ GeV or $\Delta y_{jj} < 3.6$
$H \to WW^* \to \ell\nu\ell\nu$ topology	$m_{\ell\ell} < 55$ GeV $\Delta\phi_{\ell\ell} < 1.8$ 85 GeV $< m_{\text{T}} <$ 125 GeV		

the dilepton system, $p_{\text{T}}^{\ell\ell} > 30$ GeV. In the $N_{\text{jet}} = 1$ category, this is accomplished in part by requirements on the single-lepton transverse mass m_{T}^{ℓ}, defined for each lepton as $m_{\text{T}}^{\ell} = \sqrt{2(p_{\text{T}}^{\text{miss}} p_{\text{T}}^{\ell} - \boldsymbol{p}_{\text{T}}^{\ell} \cdot \boldsymbol{p}_{\text{T}}^{\text{miss}})}$. At least one of the two leptons is required to have $m_{\text{T}}^{\ell} > 50$ GeV. For $Z/\gamma^* \to \tau\tau$ background events in the $N_{\text{jet}} = 1$ and $N_{\text{jet}} \geq 2$ categories, the p_{T} of the $\tau\tau$ system is larger, so the collinear approximation is used to calculate the $\tau\tau$ invariant mass $m_{\tau\tau}$ [58]. A requirement that $m_{\tau\tau}$ at $m_Z - 25$ GeV suppresses most background from $Z/\gamma^* \to \tau\tau$. Selection that rejects $Z/\gamma^* \to \tau\tau$ events also rejects $H \to \tau\tau$ events, which are kinematically similar. The VBF veto in the $N_{\text{jet}} \geq 2$ signal region removes events in which the two leading jets have an invariant mass $m_{jj} > 600$ GeV and a rapidity separation $\Delta y_{jj} > 3.6$, which rejects about 40% of VBF events but only 5% of ggF events.

Upper bounds on $m_{\ell\ell}$ and the azimuthal angle between the leptons $\Delta\phi_{\ell\ell}$ take advantage of the unique kinematics of the $H \to WW^*$ decay to discriminate between these signal events and the continuum WW background. The spin-zero nature of the Higgs boson, together with the structure of the weak interaction in the W boson decays, preferentially produces leptons pointing into the same hemisphere of the detector. The small dilepton invariant mass is a consequence of that and the fact that $m_H < 2m_W$, which forces one of the two W bosons off-shell, resulting in lower lepton momenta in the centre-of-mass frame of the Higgs boson decay.

Signal events are peaked in the distribution of the transverse mass m_{T}, defined as

$$m_{\text{T}} = \sqrt{(E_{\text{T}}^{\ell\ell} + p_{\text{T}}^{\text{miss}})^2 - |\boldsymbol{p}_{\text{T}}^{\ell\ell} + \boldsymbol{p}_{\text{T}}^{\text{miss}}|^2}, \tag{1}$$

where

$$E_{\text{T}}^{\ell\ell} = \sqrt{|\boldsymbol{p}_{\text{T}}^{\ell\ell}|^2 + m_{\ell\ell}^2}. \tag{2}$$

Figure 1 shows the m_{T} distribution after application of all other selection criteria in each of the signal regions. Selecting events with 85 GeV $< m_{\text{T}} <$ 125 GeV increases the signal region purity and minimises

Table 2: Bin edges for the reconstructed and unfolded distributions.

p_{T}^{H} [GeV]:	[0–20], [20–60], [60–300]
$\lvert y_{\ell\ell}\rvert$:	[0.0–0.6], [0.6–1.2], [1.2–2.5]
$p_{\mathrm{T}}^{j_1}$ [GeV]:	[0–30], [30–60], [60–300]

the total uncertainty of this measurement of the ggF cross section. Removing events with $m_{\mathrm{T}} \gtrsim m_H$ also reduces the effect of interference with the continuum WW process to negligible levels compared to the observed event yield [32].

The distributions to be measured are built using the same leptons, jets, and $p_{\mathrm{T}}^{\mathrm{miss}}$ that enter the event selection. The p_{T} of the Higgs boson is reconstructed as the magnitude of the vector sum of the missing transverse momentum and the $\boldsymbol{p}_{\mathrm{T}}$ of the two leptons. The rapidity of the dilepton system $|y_{\ell\ell}|$ is reconstructed from the charged lepton four momenta. The reconstructed and unfolded distributions are binned using the bin edges defined in Table 2. The bin edges are determined by balancing the expected statistical and systematic uncertainties in each bin. The resolution of the variables is smaller than the bin size and does not affect the binning choice. For each distribution, the upper edge of the highest bin is chosen so that less than 1% of the expected event yield in the fiducial region is excluded.

5 Background estimation

Important background processes for this analysis are WW, $t\bar{t}$, single top-quark, $Z/\gamma^* \to \tau\tau$, W + jets, and diboson processes other than WW, collectively referred to as "Other VV" and including $W\gamma^*$, $W\gamma$, WZ, and ZZ events. The background estimation techniques are described in detail in Ref. [19] and briefly here. The normalisation strategy is summarised in Table 3. As much as possible, backgrounds are estimated using a control region (CR) enriched in the target background and orthogonal to the signal region (SR), because the statistical and extrapolation uncertainties are smaller than the typical uncertainties associated with explicit prediction of the yields in exclusive N_{jet} categories. The background estimates done in the CRs are extrapolated to the SR using extrapolation factors taken from simulation. The control region definitions are summarised in Table 4, and include the lower subleading lepton p_{T} threshold of 10 GeV for all control regions except the one for WW. This is done because the gain in statistical precision of the resulting background estimates is larger than the increase of the systematic uncertainties on the extrapolation factors, particularly for the $Z/\gamma^* \to \tau\tau$ and VV processes.

For all kinematic distributions, except N_{jet}, the shapes are derived from data for the W + jets and multijet backgrounds, and from the MC-simulated background samples for all other processes. Because the signal regions are defined in terms of N_{jet}, the N_{jet} distribution is determined directly in each bin by the sum of the background predictions. Theoretical and experimental uncertainties are evaluated for all MC-simulation-derived shapes and included in the analysis, as described in Section 8.

The contribution to the signal region from the VBF and VH Higgs boson production modes, and all contributions from $H \to \tau\tau$ decays, are treated as a background assuming the Standard Model cross section, branching ratio, and acceptance for $m_H = 125$ GeV. The contribution of $H \to \tau\tau$ events is negligible due to the selection criteria rejecting $\tau\tau$ events. The largest contribution from all non-ggF Higgs boson processes is in the $N_{\mathrm{jet}} \geq 2$ category, in which events from VBF and VH contribute about

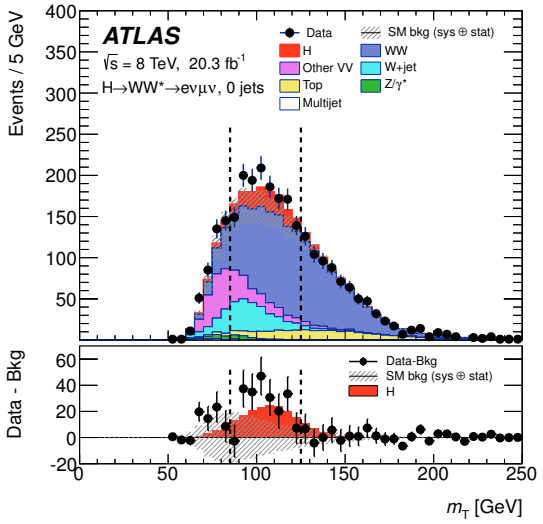

(a) $N_{\text{jet}} = 0$

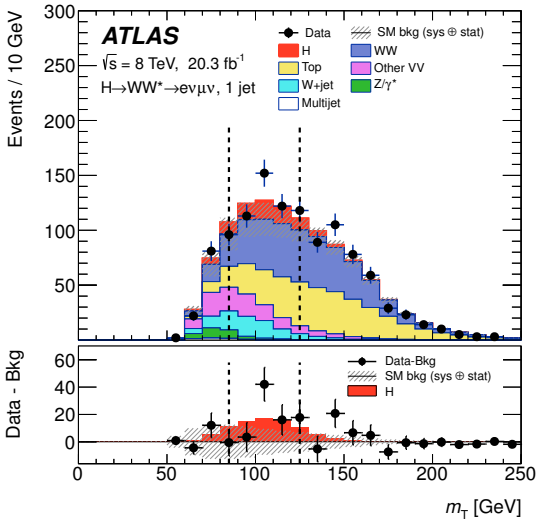

(b) $N_{\text{jet}} = 1$

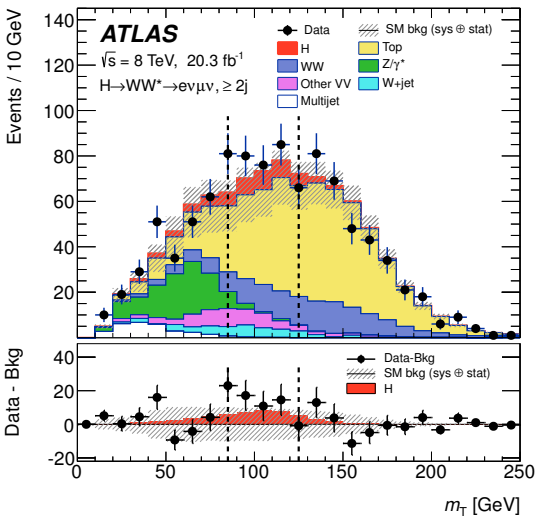

(c) $N_{\text{jet}} \geq 2$

Figure 1: Observed distributions of m_{T} with signal and background expectations after all other selection criteria have been applied for the $N_{\text{jet}} = 0$ (top left), $N_{\text{jet}} = 1$ (top right) and $N_{\text{jet}} \geq 2$ (bottom) signal regions. The background contributions are normalised as described in Section 5. The SM Higgs boson signal prediction shown is summed over all production processes. The hatched band shows the sum in quadrature of statistical and systematic uncertainties of the sum of the backgrounds. The vertical dashed lines indicate the lower and upper selection boundaries on m_{T} at 85 and 125 GeV.

half the number of events that ggF does, and constitute about 3% of the total background. The N_{jet} distribution and other shapes are taken from simulation.

For the $N_{\text{jet}} = 0$ and $N_{\text{jet}} = 1$ categories, the WW background is normalised using control regions distinguished from the SR primarily by $m_{\ell\ell}$, and the shape is taken from simulated events generated using Powheg +Pythia6 as described in Section 3. For the $N_{\text{jet}} \geq 2$ category, WW is normalised using the NLO

Table 3: Summary of background-estimation procedures for the three signal regions. Each background is categorised according to whether it is normalised using a control region (CR), a fully data-derived estimate (Data), or the theoretical cross section and acceptance from simulation (MC).

Channel	WW	Top	$Z/\gamma^* \to \tau\tau$	$Z/\gamma^* \to ee/\mu\mu$	W+jets/multijet	Other VV
$N_{\text{jet}} = 0$	CR	CR	CR	MC	Data	CR
$N_{\text{jet}} = 1$	CR	CR	CR	MC	Data	CR
$N_{\text{jet}} \geq 2$	MC	CR	CR	MC	Data	MC

Table 4: Event selection criteria used to define the control regions. Every control region starts from the same basic charged lepton and $p_{\text{T}}^{\text{miss}}$ selection as the signal regions except that the subleading lepton p_{T} threshold is lowered to 10 GeV unless otherwise stated. Jet-multiplicity requirements also match the corresponding signal region, except where noted for some top-quark control regions. The "top quark aux." lines describe auxiliary data control regions used to correct the normalisation found in the main control region. Dashes indicate that a particular control region is not defined. The definitions of $m_{\tau\tau}$, m_{T}^{ℓ}, and the jet counting p_{T} thresholds are as for the signal regions.

CR	$N_{\text{jet}} = 0$	$N_{\text{jet}} = 1$	$N_{\text{jet}} \geq 2$
WW	$55 < m_{\ell\ell} < 110$ GeV $\Delta\phi_{\ell\ell} < 2.6$ $p_{\text{T}}^{\text{sublead}} > 15$ GeV	$m_{\ell\ell} > 80$ GeV $\lvert m_{\tau\tau} - m_Z \rvert > 25$ GeV $p_{\text{T}}^{\text{sublead}} > 15$ GeV b-jet veto $\max(m_{\text{T}}^{\ell}) > 50$ GeV	-
Top quark	No N_{jet} requirement $\Delta\phi_{\ell\ell} < 2.8$	$\geq$ 1 b-jet required	$m_{\ell\ell} > 80$ GeV b-jet veto
Top quark aux.	No N_{jet} requirement $\geq$ 1 b-jet required	$N_{\text{jet}} = 2$ $\geq$ 1 b-jet required	-
Other VV	Same-sign leptons All SR cuts	Same-sign leptons All SR cuts	-
$Z/\gamma^* \to \tau\tau$	$m_{\ell\ell} < 80$ GeV $\Delta\phi_{\ell\ell} > 2.8$	$m_{\ell\ell} < 80$ GeV $m_{\tau\tau} > m_Z - 25$ GeV b-jet veto	$m_{\ell\ell} < 70$ GeV $\Delta\phi_{\ell\ell} > 2.8$ b-jet veto

cross section calculated with MCFM [59]. The efficiency for the $N_{\text{jet}} \geq 2$ requirement and other SR selections is taken from MC simulation, for which the Sherpa generator is used. It is LO in QCD but has matrix elements implemented for $WW + N$ jets, for $0 \leq N \leq 3$. For all N_{jet} categories, $WW \to \ell\nu\ell\nu$ background events produced by double parton scattering are normalised using the predicted cross section times branching ratio of 0.44 ± 0.26 pb [19]. The acceptance is modelled at LO using events generated by Pythia8. The $|y_{\ell\ell}|$ distribution in the $N_{\text{jet}} = 0$ WW CR and the p_{T}^{H} distribution in the $N_{\text{jet}} = 1$ WW CR are shown in Figure 2.

The top-quark background normalisation is estimated using control regions for all N_{jet}, and the shapes of the distributions other than N_{jet} are taken from MC simulation. The $t\bar{t}$ and single-top (i.e. Wt) backgrounds are treated together and the normalisation factor determined from the CR yield is applied to their sum. In

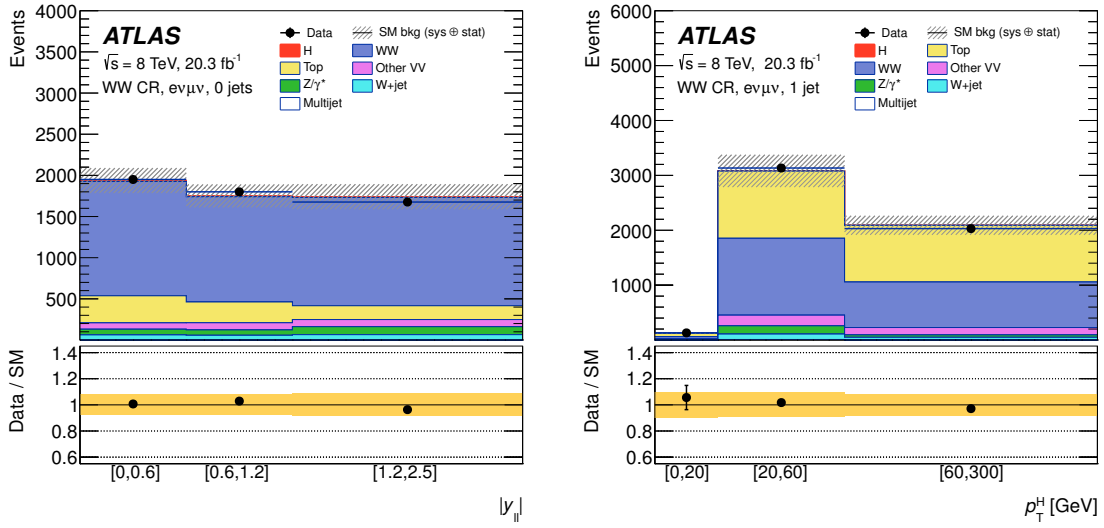

(a) $|y_{\ell\ell}|$, $N_{\text{jet}} = 0$ (b) p_{T}^{H}, $N_{\text{jet}} = 1$

Figure 2: Observed distributions of (a) $|y_{\ell\ell}|$ in the $N_{\text{jet}} = 0$ WW CR and (b) p_{T}^{H} in the $N_{\text{jet}} = 1$ WW CR, with signal and background expectations. Relevant background normalisation factors have been applied. The SM Higgs boson signal prediction shown is summed over all production processes. The hatched band in the upper panel and the shaded band in the lower panel show the sum in quadrature of statistical and systematic uncertainties of the prediction.

the $N_{\text{jet}} = 0$ category, the normalisation is derived from an inclusive sample of events meeting all of the lepton and $p_{\text{T}}^{\text{miss}}$ preselection criteria but with no requirements on the number of jets, in which the majority of events contain top quarks. The efficiency of the $N_{\text{jet}} = 0$ signal region selection is modelled using MC simulation. To reduce the uncertainty on the efficiency of the jet veto, the fraction of b-tagged events which have no additional jets is measured in a data sample with at least one b-tagged jet and compared to the fraction predicted by simulation. The efficiency of the jet veto is corrected by the square of the ratio of the measured fraction over the predicted one to account for the presence of two jets in $t\bar{t}$ production. In the $N_{\text{jet}} = 1$ category, the normalisation of the top-quark background is determined from a control region distinguished from the signal region by requiring that the jet is b-tagged. To reduce the effect of b-tagging systematic uncertainties, the extrapolation factor from the CR to the SR is corrected using an effective b-jet tagging scale factor derived from a control region with two jets, at least one of which is b-tagged. In the $N_{\text{jet}} \geq 2$ category, the number of top-quark events is sufficiently large that a CR with a b-jet veto can be defined using $m_{\ell\ell} > 80$ GeV. The $p_{\text{T}}^{j_1}$ distribution in the $N_{\text{jet}} = 1$ top-quark CR and the p_{T}^{H} distribution in the $N_{\text{jet}} \geq 2$ top-quark CR are shown in Figure 3.

The W + jets background contribution is estimated using a control sample of events in which one of the two lepton candidates satisfies the identification and isolation criteria used to define the signal sample (these lepton candidates are denoted "fully identified"), and the other ("anti-identified") lepton fails to meet the nominal selection criteria but satisfies a less restrictive one. Events in this sample are otherwise required to satisfy all of the signal-region selection criteria. The W + jets contamination in the SR is determined by scaling the number of events in the control sample by an extrapolation factor measured in a Z + jets data sample. The extrapolation factor is the ratio of the number of fully identified leptons to the number of anti-identified leptons, measured in bins of anti-identified lepton p_{T} and η. To account for differences between the composition of jets associated with W- and Z-boson production, the extrapolation

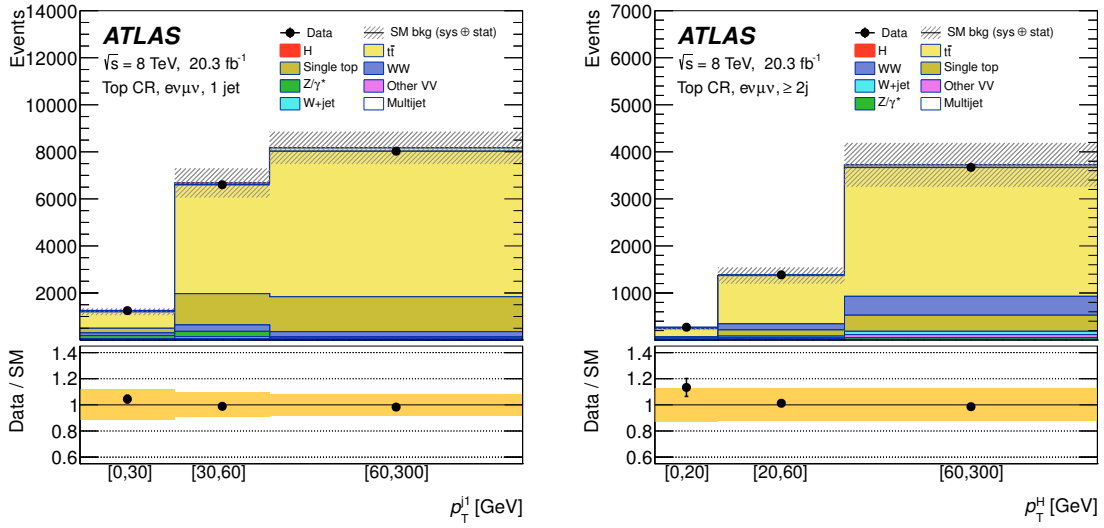

(a) $p_{\mathrm{T}}^{j_1}$, $N_{\mathrm{jet}} = 1$ (b) p_{T}^{H}, $N_{\mathrm{jet}} \geq 2$

Figure 3: Observed distributions of (a) $p_{\mathrm{T}}^{j_1}$ in the $N_{\mathrm{jet}} = 1$ top-quark CR and (b) p_{T}^{H} in the $N_{\mathrm{jet}} \geq 2$ top-quark CR, with signal and background expectations. Relevant background normalisation factors have been applied. The SM Higgs boson signal prediction shown is summed over all production processes. The hatched band in the upper panel and the shaded band in the lower panel show the sum in quadrature of statistical and systematic uncertainties of the prediction.

factors are measured in simulated $W+$jets and $Z+$jets events. The ratio of the two extrapolation factors is applied as a multiplicative correction to the extrapolation factor measured in the $Z+$jets data. The background due to multijet events is determined similarly to the $W+$jets background, using a control sample that has two anti-identified lepton candidates, but otherwise satisfies the SR selection criteria. The extrapolation factor is constructed from data events dominated by QCD-produced jet activity, and is applied to both anti-identified leptons.

The background from diboson processes other than WW, primarily from $W\gamma^*$, $W\gamma$, and WZ events, is normalised in the $N_{\mathrm{jet}} = 0$ and $N_{\mathrm{jet}} = 1$ categories using a control region identical to the signal region except that the leptons are required to have the same sign. The number and properties of same-sign and opposite-sign dilepton events produced by $W\gamma^{(*)}$ and WZ are almost identical. In the $N_{\mathrm{jet}} \geq 2$ analysis, this same-sign sample is too small to be used as a control region, and the background is estimated from the predicted inclusive cross sections and MC acceptance alone. For all N_{jet}, the MC simulation is used to predict the shapes of the distributions to be unfolded. Figure 4(a) shows the distribution of $|y_{\ell\ell}|$ in the $N_{\mathrm{jet}} = 0$ same-sign control region.

The $Z/\gamma^* \to \tau\tau$ background normalisation is derived from control regions, and the shape is derived from MC, for all three signal regions. The small contributions from $Z/\gamma^* \to ee$ and $Z/\gamma^* \to \mu\mu$, including $Z\gamma$, are estimated from MC simulation and the predicted cross sections, as described in Section 3. Figure 4(b) shows the distribution of p_{T}^{H} in the $Z/\gamma^* \to \tau\tau$ control region with $N_{\mathrm{jet}} \geq 2$.

Each control region is designed for the calculation of a normalisation factor (NF) for a particular target process, The NF is defined as $(N - B')/B$, where N is the number of data events observed in the control region, B is the expected background yield in the CR for the target process based on the predicted cross section and acceptance from MC simulation, and B' is the predicted yield from other processes in the

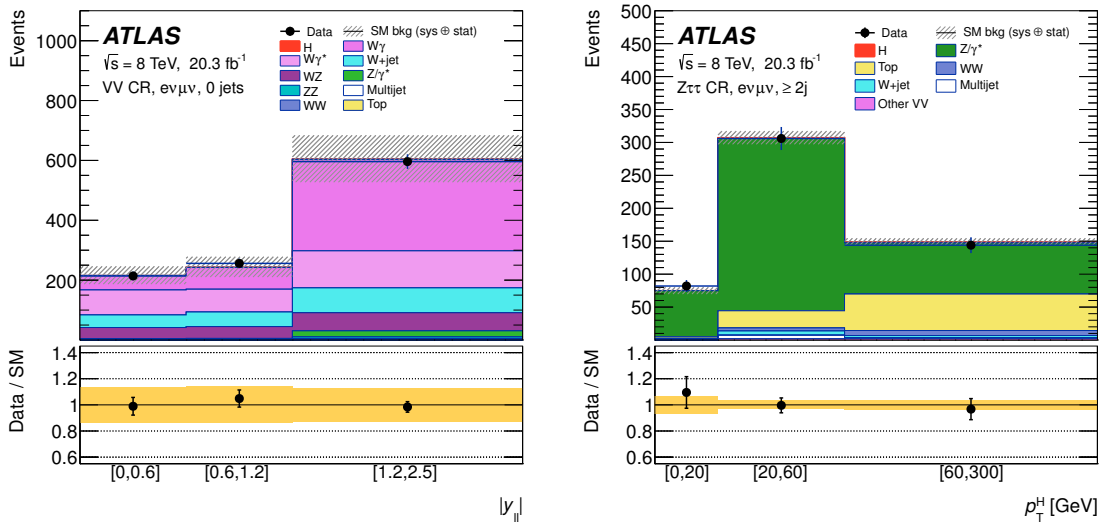

(a) $|y_{\ell\ell}|$, $N_{\text{jet}} = 0$ VV CR

(b) p_{T}^{H}, $N_{\text{jet}} \geq 2$ $Z/\gamma^* \to \tau\tau$ CR

Figure 4: Observed distributions of (a) $|y_{\ell\ell}|$ in the $N_{\text{jet}} = 0$ same-sign (VV) CR and (b) p_{T}^{H} in the $N_{\text{jet}} \geq 2$ $Z/\gamma^* \to \tau\tau$ CR, with signal and background expectations. Relevant background normalisation factors have been applied. The SM Higgs boson signal prediction shown is summed over all production processes. The hatched band in the upper panel and the shaded band in the lower panel show the sum in quadrature of statistical and systematic uncertainties of the prediction.

Table 5: Background normalisation factors (NFs) obtained from the control regions, for different background contributions and N_{jet} categories. The uncertainty quoted is the statistical uncertainty; systematic uncertainties on the predicted yield, not shown, restore compatibility of the NF with unity but do not directly enter the analysis because they are replaced by extrapolation uncertainties. A dash ('-') indicates that there is no control region corresponding to that background.

Control Regions	WW	Top	$Z/\gamma^* \to \tau\tau$	Other VV
$N_{\text{jet}} = 0$	1.22 ± 0.03	1.08 ± 0.02	0.99 ± 0.02	0.92 ± 0.07
$N_{\text{jet}} = 1$	1.05 ± 0.05	1.06 ± 0.02	1.06 ± 0.04	0.96 ± 0.12
$N_{\text{jet}} \geq 2$	-	1.05 ± 0.03	1.00 ± 0.09	-

control region. The CRs have a small contribution from the signal process, which is normalised to the SM expectation. The effect of this choice is negligible. The normalisation of each background associated with a CR is scaled by the corresponding NF. All NFs used are given in Table 5, along with their statistical uncertainties. These are included in the statistical uncertainties of the final results. The value of the $N_{\text{jet}} = 0$ WW NF has been studied in detail [19]; its deviation from unity is due to the modelling of the jet veto and higher-order corrections on the prediction of the WW cross section. A newer calculation of the inclusive WW cross section, with NNLO precision in α_{S} [60], moves the NF closer to unity, compared to the one shown here, as described in Ref. [61].

Table 6: Predicted and observed event yields in the three signal regions. Predicted numbers are given with their statistical (first) and systematic (second) uncertainties evaluated as described in Section 8. The "Non-ggF H" row includes the contributions from VBF and VH with $H \to WW^*$ and from $H \to \tau\tau$. The total background in the third-from-last row is the sum of these and of all other backgrounds.

	$N_{\text{jet}} = 0$	$N_{\text{jet}} = 1$	$N_{\text{jet}} \geq 2$
Non-ggF H	$2.2 \pm 0.2 \pm 0.2$	$7.1 \pm 0.3 \pm 0.5$	$8.2 \pm 0.3 \pm 0.4$
WW	$686 \pm 19 \pm 43$	$153 \pm 7 \pm 13$	$44 \pm 1 \pm 11$
Other VV	$88 \pm 3 \pm 12$	$44 \pm 3 \pm 11$	$21.6 \pm 1.6 \pm 3.3$
Top	$60.2 \pm 1.5 \pm 3.8$	$111.2 \pm 2.7 \pm 8.2$	$164 \pm 2 \pm 16$
Z/γ^*	$8.7 \pm 2.3 \pm 2.3$	$6.2 \pm 1.3 \pm 2.2$	$7.3 \pm 1.5 \pm 2.2$
W+jets	$90 \pm 2 \pm 21$	$33.5 \pm 2.0 \pm 7.6$	$16.9 \pm 1.2 \pm 3.9$
Multijet	$1.3 \pm 0.5 \pm 0.5$	$0.7 \pm 0.2 \pm 0.3$	$0.9 \pm 0.1 \pm 0.4$
Total background	$936 \pm 21 \pm 41$	$355 \pm 9 \pm 12$	$263 \pm 6 \pm 9$
Observed	1107	414	301
Observed − background	$171 \pm 39 \pm 41$	$59 \pm 22 \pm 12$	$38 \pm 18 \pm 9$
ggF H	$125.9 \pm 0.4 \pm 5.7$	$43.4 \pm 0.2 \pm 1.7$	$17.6 \pm 0.2 \pm 1.4$

6 Reconstructed yields and distributions

The numbers of expected and observed events satisfying all of the signal region selection criteria are shown in Table 6. The numbers of expected signal and background events are also shown, with all data-driven corrections and normalisation factors applied. In each category, the background-subtracted number of events, corresponding to the observed yield of signal events, is significantly different from zero. Taking into account the total statistical and systematic uncertainties, these yields are in agreement with those reported in Ref. [19] and with expectations from SM Higgs boson production through gluon fusion.

The four distributions under study: N_{jet}, p_{T}^{H} (reconstructed as $p_{\text{T}}(\ell\ell p_{\text{T}}^{\text{miss}})$), $|y_{\ell\ell}|$, and $p_{\text{T}}^{j_1}$ are shown in Figure 5. For presentation purposes, the reconstructed distributions are combined over the three signal regions, with the uncertainties combined accounting for correlations. In the $p_{\text{T}}^{j_1}$ distribution, $N_{\text{jet}} = 0$ events are all in the first bin, $p_{\text{T}}^{j_1} < 30$ GeV, by construction because of the definition of the jet counting. The composition of the background is shown, to illustrate how it varies as a function of the quantities being measured. The WW background decreases as a function of the number of jets, and the top-quark background increases, as can also be seen in Table 6. For the p_{T}^{H} and $p_{\text{T}}^{j_1}$ distributions, the WW background decreases with p_{T} while the top-quark background increases. The background composition does not vary substantially as a function of $|y_{\ell\ell}|$.

7 Fiducial region and correction for detector effects

Each of the reconstructed distributions is corrected for detector effects and resolution to extract the differential cross sections for the ggF Higgs boson signal. All differential cross sections are shown in a fiducial region defined based on objects at particle level, to reduce the model dependence of the results.

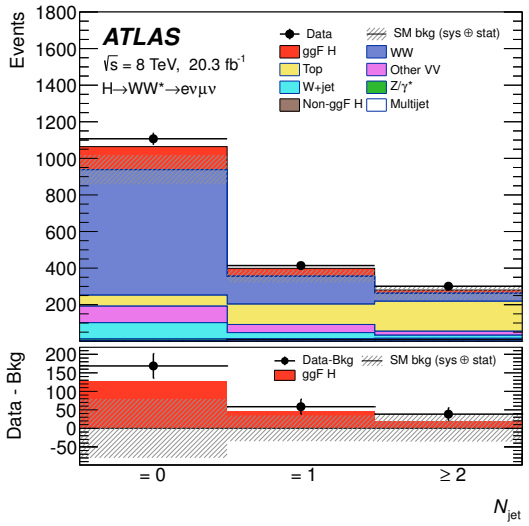

(a) N_{jet}

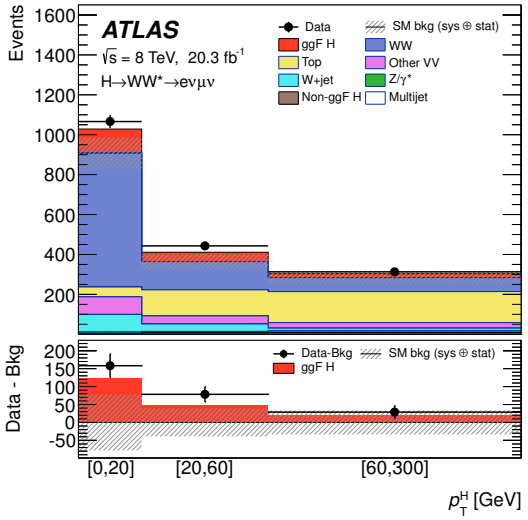

(b) p_{T}^{H}

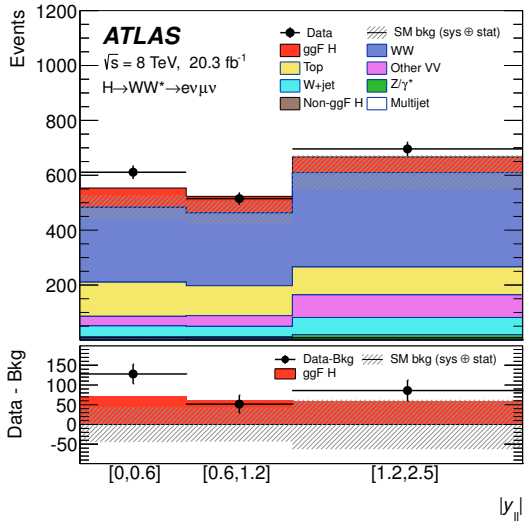

(c) $|y_{\ell\ell}|$

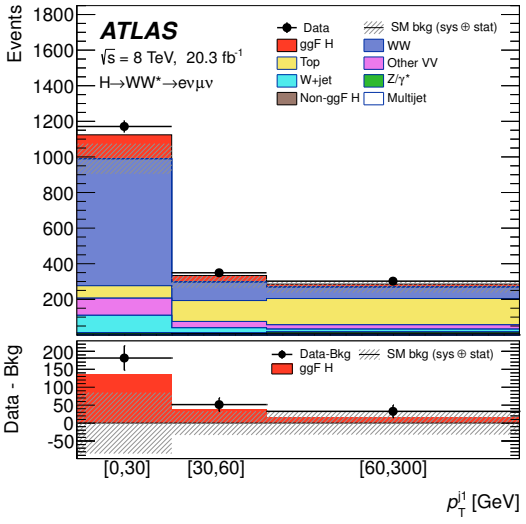

(d) $p_{\text{T}}^{j_1}$

Figure 5: Observed distributions of (a) N_{jet}, (b) p_{T}^{H}, (c) $|y_{\ell\ell}|$, and (d) $p_{\text{T}}^{j_1}$ with signal and background expectations, combined over the $N_{\text{jet}} = 0$, $= 1$, and ≥ 2 signal-region categories. The background processes are normalised as described in Section 5. The SM Higgs boson signal prediction shown is summed over all production processes. In the $p_{\text{T}}^{j_1}$ distribution, $N_{\text{jet}} = 0$ events are all in the first bin by construction because of the definition of the jet thresholds used to define the signal regions. The hatched band shows the sum in quadrature of statistical and systematic uncertainties of the sum of the backgrounds.

The particle objects and the definition of the fiducial region are described in Section 7.1. In Section 7.2, the correction procedure is discussed.

7.1 Definition of the fiducial region

The fiducial selection is designed to replicate the analysis selection described in Section 4 as closely as possible at particle level, before the simulation of detector effects. In this analysis, measurements are performed in three signal-region categories differing in the number of jets in the event. In order to present results with events from all categories, the fiducial selection only applies a selection common to all categories and using the leptons and missing transverse momentum in the final state. The criteria are summarised in Table 7.

The fiducial selection is applied to each particle-level lepton, defined as a final-state electron or muon. Here, electrons or muons from hadron decays and τ decays are rejected. The lepton momenta are corrected by adding the momenta of photons, not originating from hadron decays, within a cone of size $\Delta R = 0.1$ around each lepton; these photons arise predominantly from final-state-radiation. Selected leptons are required to satisfy the same kinematic requirements as reconstructed leptons. A selected event has exactly two different-flavour leptons with opposite charge.

The missing transverse momentum $\boldsymbol{p}_{\mathrm{T}}^{\mathrm{miss}}$ is defined as the vector sum of all final-state neutrinos excluding those produced in the decays of hadrons and τ's.

Particle-level jets are reconstructed using the anti-k_t algorithm, implemented in the FastJet package [62], with a radius parameter of $R = 0.4$. For the clustering, all stable particles with a mean lifetime greater than 30 ps are used, except for electrons, photons, muons, and neutrinos not originating from hadron decays. Selected jets are required to have $p_{\mathrm{T}} > 25$ GeV if $|\eta| < 2.5$ or $p_{\mathrm{T}} > 30$ GeV if $2.5 \leq |\eta| < 4.5$.

Selected events pass all preselection requirements introduced in Section 4 and the $H \to WW^* \to e\nu\mu\nu$ topology selection on $\Delta\phi_{\ell\ell}$ and $m_{\ell\ell}$. The m_{T} thresholds are not applied in the fiducial region since the shape of the m_{T} distribution at reconstruction level differs significantly from the shape of the distribution at particle level. All selection requirements applied are summarised in Table 7. For a SM Higgs boson the acceptance of the fiducial region with respect to the full phase space of $H \to WW^* \to e\nu\mu\nu$ is 11.3%.

7.2 Correction for detector effects

To extract the differential cross sections, the measured distributions, shown in Figure 5, are corrected for detector effects and extrapolated to the fiducial region. For the corrections, the reconstructed distributions of the different jet-binned signal-region categories are not combined, but instead are simultaneously corrected for detector effects as a function of the variable under study and the number of jets. Thus, the correlation of the variable under study with N_{jet} is correctly taken into account. Final results are presented integrated over all values of N_{jet} for the p_{T}^{H}, $|y(\ell\ell)|$ and $p_{\mathrm{T}}^{j_1}$ variables.

In the following, each bin of the reconstructed distribution is referred to by the index j, while each bin of the particle-level distribution is referred to by the index i. The correction itself is done as follows:

$$N_i^{\mathrm{part}} = \frac{1}{\varepsilon_i} \cdot \sum_j \left(M^{-1}\right)_{ij} \cdot f_j^{\text{reco-only}} \cdot (N_j^{\mathrm{reco}} - N_j^{\mathrm{bkg}}), \tag{3}$$

Table 7: Summary of the selection defining the fiducial region for the cross-section measurements. The momenta of the electrons and muons are corrected for radiative energy losses by adding the momenta of nearby photons, as described in the text.

Object selection	
Electrons	$p_{\mathrm{T}} > 15$ GeV, $\lvert\eta\rvert < 1.37$ or $1.52 < \lvert\eta\rvert < 2.47$
Muons	$p_{\mathrm{T}} > 15$ GeV, $\lvert\eta\rvert < 2.5$
Jets	$p_{\mathrm{T}} > 25$ GeV if $\lvert\eta\rvert < 2.4$, $p_{\mathrm{T}} > 30$ GeV if $2.4 \leq \lvert\eta\rvert < 4.5$
Event selection	
Preselection	$p_{\mathrm{T}}^{\mathrm{lead}}(\ell) > 22$ GeV $m_{\ell\ell} > 10$ GeV $p_{\mathrm{T}}^{\mathrm{miss}} > 20$ GeV
Topology	$\Delta\phi_{\ell\ell} < 1.8$ $m_{\ell\ell} < 55$ GeV

where N_i^{part} is the number of particle-level events in a given bin i of the particle-level distribution in the fiducial region. The quantity N_j^{reco} is the number of reconstructed events in a given bin j of the reconstructed distribution in the signal region, and N_j^{bkg} is the number of background events in bin j estimated as explained in Section 5. The correction factor $f_j^{\text{reco-only}}$, the selection efficiency ε_i, and the migration matrix M_{ij} are discussed below. To evaluate the cross section in particle-level bin i, it is also necessary to take the integrated luminosity and the bin width into account.

The migration matrix accounts for the detector resolution and is defined as the probability to observe an event in bin j when its particle-level value is located in bin i. The migration matrix is built by relating the variables at reconstruction and particle level in simulated ggF signal events that meet both the signal-region and fiducial-region selection criteria. To properly account for the migration of events between the different signal-region categories, the migration matrix accounts for the migrations within one distribution, as well as migrations between different values of N_{jet}. The inverse of the migration matrix is determined using an iterative Bayesian unfolding procedure [63] with two iterations.

The selection efficiency ε_i is defined as an overall efficiency, combining reconstruction, identification, isolation, trigger and selection, including also the differences between the fiducial and the signal region selection. It is derived from MC simulation and its values are in the range 0.14 to 0.43 for all variables. Events in the fiducial region that are not selected in the signal region are taken into account by ε_i.

Events outside the fiducial region may be selected in a signal region owing to migrations. Such migrations are accounted for via the correction factor $f_j^{\text{reco-only}}$, which is derived from MC simulation. Reconstructed $H\rightarrow WW^*$ events where the W boson decays into $\tau\nu$ and the τ lepton decays leptonically are not included in the fiducial region, but are accounted for also with the same procedure. The correction factor $f_j^{\text{reco-only}}$ is in the range 0.84 to 0.92 for all variables.

8 Statistical and systematic uncertainties

Sources of uncertainty in the differential cross sections can be grouped into five categories: statistical uncertainties, experimental systematic uncertainties, theoretical systematic uncertainties in the signal

model, uncertainties arising from the correction procedure, and theoretical systematic uncertainties in the background model. These uncertainties affect the analysis through the background normalisation, the background shape, the migration matrix, the selection efficiency, and the correction factor.

The effect of each systematic uncertainty is analysed by repeating the full analysis for the variation in the signal, background, or experimental parameter. For experimental uncertainties, the migration matrix, selection efficiency, correction factor, and background estimation are varied simultaneously. For uncertainties that only apply to the background processes, the nominal migration matrix, selection efficiency, and correction factor are used. The total uncertainty in the result from any individual source of uncertainty is taken as the difference between the shifted and the nominal result after the correction of detector effects.

The input uncertainties are summarised in this section. Their effect on the measured results, individually and collectively, are given with the results in the tables in Section 10. The total uncertainty in each measurement bin is defined as the sum in quadrature of all uncertainty components.

8.1 Statistical uncertainties

The statistical uncertainties in the differential cross sections are estimated using pseudo-experiments. The content of each bin in the measured distribution is fluctuated according to a Poisson distribution. In each pseudo-experiment the background is subtracted and the correction for detector effects is performed. Then, the root mean square of the spread of the result in each bin is taken as the estimator of the statistical uncertainty. Values for the data statistical uncertainty are evaluated using pseudo-experiments; the data statistical uncertainties in the presented measurement range from 17% to 61%.

The uncertainty due to the statistics of the background MC samples is evaluated by fluctuating the bin contents of the background template using a Gaussian distribution with a width corresponding to the uncertainty in that bin. In case of the signal MC sample, the bins of the migration matrix, the selection efficiency, and the correction factor are fluctuated simultaneously. In each pseudo-experiment the correction for detector effects is performed using the respective fluctuated template. The root mean square of the spread of results of the pseudo-experiments is taken as the estimator of the uncertainty.

For results integrated over all values of N_{jet}, and for normalised results, each pseudo-experiment is integrated or normalised and the uncertainty is re-evaluated for the integrated (normalised) bin to take into account all correlations arising from bin migration.

The statistical uncertainties in the background normalisations from the data yields in the control regions are calculated as the square root of the number of events observed.

8.2 Experimental systematic uncertainties

Experimental systematic uncertainties arise primarily from object calibrations, such as the jet energy scale, and affect the subtracted background normalisation and shape as well as the migration matrix, the selection efficiency, and the correction factor. The variations used for the experimental uncertainties are identical to those of Ref. [19] and are not described here. The effect of these variations have been reevaluated in the context of this analysis. The dominant experimental uncertainties are those associated with the jet energy scale (JES) and resolution (JER), the lepton identification efficiencies, and the uncertainty in the extrapolation factor used to estimate the W + jets background. For each uncertainty, the upward and

downward variations are performed separately. Each variation is applied simultaneously to the migration matrix, the selection efficiency, the correction factor, and the background subtraction so that correlations are correctly preserved. The background-subtracted yields are allowed to assume negative values under these variations.

8.3 Systematic uncertainties in the signal model

Theoretical uncertainties in the ggF signal model can affect the migration matrix, the selection efficiency, and the correction factor. Sources of theoretical uncertainty in the signal acceptance are the choice of QCD renormalisation and factorisation scales, PDF, parton shower/underlying event (PS/UE) model, and matrix-element generator. It was shown in Ref. [19] that the theoretical uncertainty in the signal acceptance is dominated by the PS/UE model. This uncertainty is evaluated by constructing the migration matrix and the correction factors with Powheg +Herwig and Powheg +Pythia8 and applying both sets in the detector correction. The results with each of the simulations are then compared for each of the measured distributions. The full difference between the distributions is taken as an uncertainty, which is at the level of a few percent.

In addition to the uncertainty in the signal acceptance, an uncertainty in the theoretical predictions of the exclusive ggF $H + n$-jet cross sections is assigned. The uncertainties in the exclusive cross sections are evaluated using the jet-veto efficiency method [64, 65]. Here, uncertainties due to renormalisation, factorisation, and resummation scale choices in the analytical calculations are taken into account. The correlations of the uncertainties in the different $H + n$-jet cross sections are determined using a covariance matrix as described in Ref. [66]. To evaluate the effect this uncertainty has on the migration matrix, the selection efficiency, and the correction factor, the particle-level N_{jet} distribution in the signal ggF MC sample is reweighted to account for the uncertainties in the exclusive $H + n$-jet cross sections and the correlations between them. Then, the reconstructed distribution of the reweighted ggF signal MC sample is unfolded for each variable to evaluate the change arising from the uncertainty in the exclusive ggF $H + n$-jet cross sections. The contribution of this uncertainty to the differential distributions is a few percent for p_{T}^{H} and $p_{\text{T}}^{j_1}$ and negligible for $|y_{\ell\ell}|$.

8.4 Systematic uncertainty in the correction procedure

The ggF signal simulation is used to build the migration matrix and can bias the result of the correction procedure. This bias is partly evaluated with the uncertainties in the SM prediction of the signal determined in Section 8.3. To evaluate this bias independently of the SM prediction and its uncertainty, the simulated ggF signal sample is reweighted to reproduce the amount of disagreement in shape between the reconstructed simulated distribution and the background-subtracted measured distribution. For this reweighting, only the nominal distributions are compared; uncertainties are not taken into account. The reweighted reconstructed distribution is then corrected for detector effects using the nominal migration matrix. The difference between the corrected distribution and the reweighted simulated particle-level distribution is taken as an uncertainty in the correction procedure. The resulting uncertainty is smaller than 5% in each measurement bin.

8.5 Systematic uncertainties in the background model

Systematic uncertainties in the background model are evaluated by comparing the background predictions as evaluated under different conditions. For the dominant WW and top-quark backgrounds, shape uncertainties in each measured distribution are considered in addition to normalisation uncertainties. For the backgrounds normalised by a control region, the normalisation uncertainty is derived by varying the extrapolation factor, and for backgrounds estimated directly from the MC simulation, such as the WW background in the $N_{\text{jet}} \geq 2$ signal region, the systematic uncertainty is derived by varying the full event yield in the SR rather than an extrapolation factor, and accounts for the uncertainty in the cross section and acceptance.

The nominal MC sample used to model the WW background yield for the $N_{\text{jet}} = 0$ and $= 1$ categories is Powheg +Pythia6. The theoretical uncertainties assessed are:

- QCD scales, by independently varying the values of the renormalisation scale μ_{R} and the factorisation scales μ_{F}, in aMC@NLO calculations [67]. Both scales are independently multiplied by a factor of 2.0 or 0.5 relative to the nominal value $\mu_0 = m_{WW}$, where m_{WW} is the invariant mass of the WW system, while maintaining the constraint $0.5 \leq \mu_{\text{R}}/\mu_{\text{F}} \leq 2$.
- PDF uncertainties, from the envelope of the CT10 68% CL eigenvectors added in quadrature with the maximal difference between the results obtained with CT10 and those obtained with either MSTW [68] or NNPDF [69].
- The choice of parton-shower and underlying-event models (PS/UE), by comparing the nominal Powheg prediction interfaced with Pythia6 and Herwig.
- The choice of matrix-element generator, by comparing the nominal Powheg to aMC@NLO, both interfaced with Herwig.

The normalisation uncertainties are summarised in Table 8. These are all varied in a correlated way for the $N_{\text{jet}} = 0$ and $N_{\text{jet}} = 1$ signal regions. Each source is also considered as a shape uncertainty, except for the PDF uncertainty, which is much smaller than the others. The changes observed are typically 1–10% for p_{T}^{H} and $p_{\text{T}}^{j_1}$, and less than 1% for $|y_{\ell\ell}|$. The largest changes observed are from the effect the PS/UE variation has on p_{T}^{H} and occur in sparsely populated bins, 50% for $N_{\text{jet}} = 0$ events with $p_{\text{T}}^{H} > 60$ GeV and 30% for $N_{\text{jet}} = 1$ events with $p_{\text{T}}^{H} < 20$ GeV. The shape and normalisation are varied simultaneously for the PS/UE and matrix-element-generator uncertainties. The QCD-scale uncertainties are taken from the variation exhibiting the largest difference from nominal, which is $\mu_{\text{R}}/\mu_0 = 2.0$ and $\mu_{\text{F}}/\mu_0 = 2.0$ for both the $N_{\text{jet}} = 0$ and $N_{\text{jet}} = 1$ normalisation uncertainties. The shape uncertainties are set similarly, but the variation with the largest difference to the nominal is not always the one driving the normalisation uncertainty. The resulting shape uncertainties are not correlated with the normalisation uncertainties.

The theoretical uncertainties in the WW background yield for the $N_{\text{jet}} \geq 2$ category are evaluated similarly. The QCD-scale uncertainty is evaluated by varying the renormalisation and factorisation scale μ, which has the nominal value of $\mu_0 = m_{WW}$, in the range $0.5 \leq \mu/\mu_0 \leq 2$ in MadGraph [70], and applying the relative uncertainty to the nominal Sherpa prediction. The choices of matrix-element generator and parton shower are varied together by comparing MadGraph +Pythia6 to Sherpa. Uncertainties in the predicted shape are also accounted for, and are between 1% and 15%. The larger uncertainties in the $N_{\text{jet}} \geq 2$ category are due to the use of a different MC generator (multi-leg LO in QCD) and the absence of a CR. For the same reasons, they are not correlated with the uncertainties in the $N_{\text{jet}} = 0$ and $N_{\text{jet}} = 1$ categories.

Table 8: Theoretical uncertainties (in %) in the WW background normalisation estimate in each signal region. The relative sign between entries in a row indicates correlation or anti-correlation among the $N_{\text{jet}} = 0$ and $N_{\text{jet}} = 1$ signal regions, as a single variation is applied simultaneously to both of them. The $N_{\text{jet}} \geq 2$ uncertainties are treated as uncorrelated.

	$N_{\text{jet}} = 0$	$N_{\text{jet}} = 1$	$N_{\text{jet}} \geq 2$
QCD scales	−1.1	−1.7	+22
PDF	+0.6	+0.6	+9.7
PS/UE	−1.3	−4.5	–
Generator	+5.2	+1.5	+2.7

Table 9: Theoretical uncertainties (in %) in the top-quark background estimate in each signal region. The relative sign between entries in a row indicates correlation or anti-correlation among the signal regions.

	$N_{\text{jet}} = 0$	$N_{\text{jet}} = 1$	$N_{\text{jet}} \geq 2$
QCD scales	−1.2	−0.6	−0.8
PDF	+0.4	+2.2	+1.0
PS/UE	−0.6	+2.7	+4.5
Generator	−4.1	−3.5	−1.1

Shape and normalisation uncertainties in the top-quark background yield are evaluated following the procedure applied for the WW background. The normalisation uncertainties for each signal region are summarised in Table 9. In contrast to the WW background, there is a non-negligible PDF shape uncertainty, which is evaluated by comparing CT10, MSTW, and NNPDF. For most uncertainty sources, the changes observed due to shape variations of the top-quark background are typically 5% or smaller. Exceptions are the PS/UE uncertainty for $N_{\text{jet}} = 0$ events with $p_{\text{T}}^{H} > 60$ GeV, which is about 12%, and the PDF uncertainty in the $|y_{\ell\ell}|$ shape, which is up to 8%.

Very few MC-simulated events from the $Z/\gamma^* \to \tau\tau$ background pass the full SR and $Z/\gamma^* \to \tau\tau$ CR event selection, so the corresponding theoretical uncertainties are calculated with modified and reduced SR and CR selections, in order for the relevant comparisons to be made with sufficient statistical precision. No shape uncertainty is assessed for the same reason, and the effect of any such uncertainty would be negligible due to the small contribution from this background. The p_{T}^{Z} distribution for $N_{\text{jet}} = 0$ events is reweighted using the ratio of data to MC simulation for $Z/\gamma^* \to \mu\mu$ events produced with the same MC generator and PS/UE model, and the uncertainty in the reweighting procedure is also included in the analysis. The extrapolation uncertainty to the WW control region is also evaluated, because the contribution of $Z/\gamma^* \to \tau\tau$ to that CR is not negligible. As with the other backgrounds, each variation is applied simultaneously across all signal and control regions.

The systematic uncertainties in the contributions from WZ, $W\gamma$, $W\gamma^*$, and other small sources of background are unmodified from Ref. [19]. Within the signal regions, for $W\gamma$ the corresponding uncertainties are 9%, 53%, and 100% for $N_{\text{jet}} = 0$, $N_{\text{jet}} = 1$, and $N_{\text{jet}} \geq 2$, respectively. For $W\gamma^*$ they are 7%, 30%, and 26%. For the $N_{\text{jet}} \leq 1$ signal regions, identical uncertainties apply in the SR and in the same-sign VV CR for these processes. This results in a strong cancellation of the uncertainties in the predicted yields in the signal regions.

Table 10: Summary of the ggF predictions used in comparison with the measured fiducial cross sections. The right column states the accuracy of each prediction in QCD.

Total cross-section predictions	
LHC-XS [71]	NNLO+NNLL
Differential cross-section predictions	
JetVHeto [72–74]	NNLO+NNLL
ST [75]	NNLO
BLPTW [66]	NNLO+NNLL
STWZ [76]	NNLO+NNLL′
N^3LO+NNLL+LL_R [77]	N^3LO+NNLL+LL_R
Monte Carlo event generators	
Powheg NNLOPS [78, 79]	NNLO$_{\geq 0j}$, NLO$_{\geq 1j}$
Sherpa 2.1.1 [37, 80–83]	H + 0, 1, 2 jets @NLO
MG5_aMC@NLO [67, 84, 85]	H + 0, 1, 2 jets @NLO

For the VBF $H \rightarrow WW^*$ contribution to the signal region, the cross-section uncertainties in the QCD scale (between +2.6% and −2.8%) and PDF (±0.2%) are included [34]. These have a negligible effect on the analysis, so additional uncertainties in the VBF acceptance in the ggF phase space are not considered.

9 Theory predictions

The results of the fiducial cross-section measurements are compared to analytical predictions calculated at parton level and to predictions by MC event generators at particle level. An overview of the ggF predictions used is given in Table 10. All predictions are for $m_H = 125.0$ GeV and $\sqrt{s} = 8$ TeV, and use the CT10 PDF set unless stated otherwise. The values of the predictions are shown together with the results of the measurement in the following section.

The default prediction for the cross section of ggF Higgs boson production follows the recommendation of the LHC Higgs cross section working group (LHC-XS) as introduced in Section 3. The $H \rightarrow WW^* \rightarrow e\nu\mu\nu$ decay is included in the calculations and MC, with a branching fraction of 0.25%.

For the efficiency ε_0 of the jet veto, a parton-level prediction is calculated at NNLO+NNLL accuracy by JetVHeto [72–74]. The uncertainty is taken as the maximum effect of the scale variations on the calculation, or the maximum deviation of the other calculations of ε_0 that differ by higher-order terms. An alternative prediction for ε_0 is given by the STWZ calculation [76]. The calculation has NNLO accuracy and is matched to a resummation at NNLL that accounts for the correct boundary conditions for the next-to-next-to-next-to-leading-logarithm resummation (NNLL′). This calculation also predicts the spectrum of $p_{\mathrm{T}}^{j_1}$. Another parton-level prediction of ε_0 follows the Stewart–Tackmann (ST) prescription [75] utilising the total inclusive ggF cross section at NNLO accuracy in QCD and the inclusive H + 1-jet cross section at NLO accuracy, calculated with HNNLO [30, 86, 87]. Recently, a prediction for ε_0 has become available at N^3LO+NNLL accuracy with small-R resummation (LL_R) [77]. A parton-level prediction for the N_{jet} distribution is given by the BLPTW method [66], combining the NNLO+NNLL-accurate

inclusive and the NLO+NLL-accurate inclusive H + 1-jet cross sections, including resummation in the covariance matrix.

For comparisons to data, all parton-level predictions are corrected to particle level using the acceptance of the fiducial region and non-perturbative correction factors to account for the impact of hadronisation and underlying-event activity. These factors are determined using Powheg NNLOPS+Pythia8 [78, 79] with the associated uncertainties from the renormalisation and factorisation scales as well as the PDFs. An uncertainty is assigned to the non-perturbative correction by comparing Pythia8 with Herwig. The uncertainties applied are between 0.5% and 7%. All factors are given in HEPDATA.

Particle-level predictions for the measured differential cross sections are provided by MC event generators. The most precise prediction for inclusive ggF production is given by Powheg NNLOPS, which is accurate to NNLO for the inclusive production and to NLO for the inclusive H + 1-jet production, combining the MINLO [31] method with an NNLO calculation of the Higgs boson rapidity using HNNLO. Furthermore, it includes finite quark masses [79]. The sample is generated using the CT10nnlo PDF set [88] and is interfaced to Pythia8 for parton showering. The uncertainties include a 27-point QCD scale variation described in Ref. [78], as well as a PDF uncertainty, obtained from variations of the CT10 PDF set.

Another ggF MC prediction is generated with Sherpa (v.2.1.1) [37, 80]. Here, the inclusive Higgs boson, inclusive H + 1-jet, and inclusive H + 2-jets production cross sections are calculated at NLO accuracy. The H + 2-jets matrix elements are generated via an MCFM interface within Sherpa. These calculations are combined using the MEPS@NLO method [81, 82]. The factorisation, renormalisation, resummation, and merging scales are varied to determine an uncertainty as described in Ref. [83]. Additionally, the variations of the CT10 PDF set are included.

A similar NLO-merged H+ (0, 1, 2)-jets sample is generated with MG5_aMC@NLO (v.2.3.2.2) [67, 84] where the different calculations are combined using the FxFx scheme [85]. MG5_aMC@NLO is interfaced to Pythia8 for parton showering. Variations of the factorisation, renormalisation, and merging scales, and of the CT10 PDF set, are evaluated for each prediction. The differences in the predictions are taken as uncertainties.

10 Results

The cross section of ggF Higgs boson production in the fiducial region defined in Table 7 is measured to be:

$$\begin{aligned}\sigma_{\text{ggF}}^{\text{fid}} &= 36.0 \pm 7.2(\text{stat}) \pm 6.4(\text{sys}) \pm 1.0(\text{lumi}) \text{ fb} \\ &= 36.0 \pm 9.7 \text{ fb}\end{aligned}$$

where (stat) includes all statistical uncertainties from the signal and control regions, and (sys) refers to the sum in quadrature of the experimental and theoretical systematic uncertainties. The mass of the Higgs boson is assumed to be $m_H = 125.0$ GeV. The fiducial cross section is calculated from the number of events after the event selection and detector corrections, using an integrated luminosity of 20.3 fb^{-1} with an associated uncertainty of 2.8%. This is derived following the same methodology as in Ref. [89]. More details of the sources of systematic uncertainty are given in Table 11. The uncertainty categories used in this and all tables in this section are as follows. Statistical uncertainties are quoted separately for

Table 11: Relative uncertainties (in %) in the measured total fiducial cross section.

Source	$\Delta\sigma^{\text{fid}}_{\text{ggF}}/\sigma^{\text{fid}}_{\text{ggF}}$ [%]
SR data statistical	17
MC statistical	3.0
CR data statistical	9.9
Exp. JER	4.9
Exp. JES	2.1
Exp. b-tag	3.3
Exp. leptons	5.5
Exp. $p_{\text{T}}^{\text{miss}}$	2.2
Exp. other	4.2
Theory (WW)	14
Theory (top)	7.1
Theory (other backgrounds)	5.6
Theory (signal)	2.5
Detector corrections	0.4
Total	27

the signal region data, the control region data, and the MC simulated events. Experimental uncertainties ("Exp.") are grouped according to the reconstructed object they effect. The "Exp. other" category includes uncertainties in the modelling of pile-up events, electrons from conversions, and the modelling of the p_{T} of Z bosons with $N_{\text{jet}} = 0$. Theory uncertainties are grouped by process, with the subdominant background uncertainties collected in the "Theory other backgrounds" line. The "Detector corrections" line gives the effect of the use of the ggF signal MC sample to construct the migration matrix, as described in Section 8.4.

The prediction of the fiducial cross section is given by the LHC-XS calculation as

$$\text{LHC-XS: } \sigma^{\text{fid}}_{\text{ggF}} = 25.1^{+1.8}_{-2.0}(\text{QCDscales})^{+1.9}_{-1.7}(\text{PDF}) \text{ fb} = 25.1 \pm 2.6 \text{ fb}.$$

Reference [19] also reports ggF fiducial cross sections for events with $N_{\text{jet}} = 0$ and $N_{\text{jet}} = 1$, but with modified fiducial region selections, among which the most important one is a lower threshold of 10 GeV on the subleading lepton p_{T}. The ratio of the observed to predicted SM cross sections in that analysis is statistically compatible with the results shown here.

The dependence of the cross-section measurement on m_H is mainly due to acceptance effects and is approximated by a linear function, which is sufficient within the experimental uncertainties in the Higgs boson mass [9]. The function is determined using dedicated signal samples with different values of m_H and has a slope of -0.20 fb/ GeV.

10.1 Differential fiducial cross sections

Differential fiducial cross sections are measured in bins of the N_{jet}, p_{T}^{H}, $|y_{\ell\ell}|$ and $p_{\text{T}}^{j_1}$ distributions. For the p_{T}^{H}, $|y_{\ell\ell}|$ and $p_{\text{T}}^{j_1}$ distributions, the cross sections are measured in separate bins of N_{jet} to fully take correlations into account between the different N_{jet} categories and the variable itself. After detector corrections

Table 12: Measured and predicted fiducial cross section in fb as a function of N_{jet}. Predicted values are from POWHEG NNLOPS+PYTHIA8, normalised to the LHC-XS working group recommended cross section, as described in Section 9. Total uncertainties in the measurement are given along with their relative composition in terms of source.

N_{jet}	0	1	≥ 2
$d\sigma/dN_{\text{jet}}$ [fb]	19.0	8.2	8.8
Statistical uncertainty	4.5	3.5	5.0
Total uncertainty	6.8	4.0	5.9
Predicted $d\sigma/dN_{\text{jet}}$ [fb] (NNLOPS)	14.7	7.0	3.4
Uncertainty in prediction	1.8	0.9	0.6
SR data statistical	20%	38%	54%
MC statistical	4%	7%	9%
CR data statistical	12%	18%	14%
Exp. JER	5%	4%	7%
Exp. JES	1%	10%	6%
Exp. b-tag	1%	4%	8%
Exp. leptons	6%	6%	6%
Exp. $p_{\text{T}}^{\text{miss}}$	2%	4%	4%
Exp. other	5%	4%	3%
Theory (WW)	24%	15%	5%
Theory (top)	2%	4%	24%
Theory (other backgrounds)	5%	6%	21%
Theory (signal)	4%	6%	3%
Detector corrections	<1%	4%	5%
Total uncertainty	36%	48%	67%

the distributions are integrated over N_{jet}, and the uncertainties are combined accounting for correlations. The measured differential fiducial cross sections as a function of N_{jet}, p_{T}^{H}, $|y_{\ell\ell}|$, and $p_{\text{T}}^{j_1}$ are given in Tables 12–15, together with a summary of the associated uncertainties.

Figure 6 shows the measured differential cross sections as a function of N_{jet}, p_{T}^{H}, $|y_{\ell\ell}|$, and $p_{\text{T}}^{j_1}$. The results are compared to particle-level predictions from POWHEG NNLOPS, SHERPA, and MG5_aMC@NLO for ggF Higgs boson production. The predictions are generated as described in Section 9 and normalised to the cross-section predictions calculated according to the prescription from the LHC-XS working group. In addition, the results for the N_{jet} distribution are compared to the parton-level BLPTW calculation, and the results for the $p_{\text{T}}^{j_1}$ distribution are compared to the parton-level STWZ calculation. The ratios of the results to the predictions are given in the lower panel of each figure. The measured distributions agree with the predictions within the uncertainties, except for $|y_{\ell\ell}|$, where the data have a more central mean $|y_{\ell\ell}|$ than the predictions. The statistical and systematic uncertainties are comparable for most bins. The dominant systematic uncertainties are in the background model, in particular the top-quark and WW backgrounds, although uncertainties in the experimental inputs are non-negligible.

Table 13: Measured and predicted differential fiducial cross section in fb/ GeV as a function of p_{T}^{H}. Predicted values are from Powheg NNLOPS+Pythia8, normalised to the LHC-XS working group recommended cross section, as described in Section 9. Total uncertainties in the measurement are given along with their relative composition in terms of source.

p_{T}^{H} [GeV]	$[0, 20]$	$[20, 60]$	$[60, 300]$
$\mathrm{d}\sigma/\mathrm{d}p_{\mathrm{T}}^{H}$ [fb/ GeV]	0.61	0.39	0.034
Statistical uncertainty	0.16	0.09	0.021
Total uncertainty	0.29	0.15	0.027
Predicted $\mathrm{d}\sigma/\mathrm{d}p_{\mathrm{T}}^{H}$ [fb/ GeV] (NNLOPS)	0.48	0.25	0.022
Uncertainty in prediction	0.05	0.03	0.005
SR data statistical	22%	22%	60%
MC statistical	4%	4%	10%
CR data statistical	13%	5%	18%
Exp. JER	7%	4%	16%
Exp. JES	6%	10%	17%
Exp. b-tag	2%	4%	8%
Exp. leptons	7%	6%	7%
Exp. $p_{\mathrm{T}}^{\mathrm{miss}}$	9%	8%	7%
Exp. other	7%	4%	4%
Theory (WW)	31%	17%	13%
Theory (top)	4%	7%	25%
Theory (other backgrounds)	6%	8%	14%
Theory (signal)	14%	1%	6%
Detector corrections	<1%	3%	3%
Total	47%	37%	77%

10.2 Normalised differential fiducial cross sections

To reduce the impact of systematic uncertainties, normalised differential cross sections $1/\sigma \cdot (\mathrm{d}\sigma/\mathrm{d}X_i)$ are calculated by dividing the differential cross section by the total fiducial cross section evaluated by integrating over all bins of variable X. The normalised differential cross sections as functions of N_{jet}, p_{T}^{H}, $|y_{\ell\ell}|$, and $p_{\mathrm{T}}^{j_1}$ are given in Tables 16–19, along with details of the associated uncertainties. The distributions are shown in Figure 7 compared to particle-level predictions of ggF Higgs boson production by Powheg NNLOPS, Sherpa, and MG5_aMC@NLO that are generated as described in Section 9. In each figure, the ratio of the result to the predictions is shown below the distribution. The reduced uncertainties result in a more stringent comparison of the measured and predicted distributions. The level of agreement is still good although the trend in $|y_{\ell\ell}|$ is enhanced and a slight trend towards higher N_{jet} and $p_{\mathrm{T}}^{j_1}$ appears in the data.

Table 14: Measured and predicted differential fiducial cross section in fb per unit rapidity as a function of $|y_{\ell\ell}|$. Predicted values are from POWHEG NNLOPS+PYTHIA8, normalised to the LHC-XS working group recommended cross section, as described in Section 9. Total uncertainties in the measurement are given along with their relative composition in terms of source.

$\|y_{\ell\ell}\|$	[0.0, 0.6]	[0.6, 1.2]	[1.2, 2.5]
$d\sigma/d\|y_{\ell\ell}\|$ [fb]	31	9.5	9.5
Statistical uncertainty	7.3	5.0	3.5
Total uncertainty	10	6.5	5.2
Predicted $d\sigma/d\|y_{\ell\ell}\|$ [fb] (NNLOPS)	15.9	13.0	5.9
Uncertainty in prediction	1.7	1.4	0.6
SR data statistical	22%	52%	33%
MC statistical	3%	9%	6%
CR data statistical	9%	1%	16%
Exp. JER	4%	10%	4%
Exp. JES	5%	9%	6%
Exp. b-tag	3%	4%	5%
Exp. leptons	4%	10%	9%
Exp. $p_{\mathrm{T}}^{\mathrm{miss}}$	3%	8%	4%
Exp. other	4%	8%	6%
Theory (WW)	15%	31%	20%
Theory (top)	12%	14%	8%
Theory (other backgrounds)	3%	7%	17%
Theory (signal)	4%	6%	3%
Detector corrections	<1%	<1%	1%
Total	33%	69%	53%

10.3 Jet-veto efficiency

The jet-veto efficiency ε_0 for the H + 0-jet events is defined at particle level as the fraction of events in the fiducial region with the leading particle-level jet below a given threshold. This is measured using the leading-jet p_{T} distribution, since the lowest-p_{T} bin contains exactly the fraction of events with the leading jet below the threshold of either $p_{\mathrm{T}}^{j_1} = 30$ GeV or $p_{\mathrm{T}}^{j_1} = 40$ GeV. The jet-veto efficiency for the jet selection used in the analysis, 25 GeV for central jets ($|\eta| < 2.5$) and 30 GeV for forward jets ($2.5 < |\eta| < 4.5$), corresponds to the $N_{\mathrm{jet}} = 0$ fraction from the normalised differential cross section measured as a function of N_{jet} (see Table 16). Results for the jet selection in this analysis, and thresholds of 30 GeV and 40 GeV, are given in Table 20 and compared to predictions in Figure 8. The predictions are calculated with JetVHeto, ST, STWZ, N^{3}LO+NNLL+LL_R, and POWHEG NNLOPS, as described in Section 9. The results are in agreement with the predictions. The predictions are more precise than the measurements reported here, which are limited by their large statistical uncertainties.

Table 15: Measured and predicted differential fiducial cross section in fb/ GeV as a function of $p_{\mathrm{T}}^{j_1}$. Predicted values are from POWHEG NNLOPS+PYTHIA8, normalised to the LHC-XS working group recommended cross section, as described in Section 9. Total uncertainties in the measurement are given along with their relative composition in terms of source.

$p_{\mathrm{T}}^{j_1}$ [GeV]	$[0, 30]$	$[30, 60]$	$[60, 300]$
$\mathrm{d}\sigma/\mathrm{d}p_{\mathrm{T}}^{j_1}$ [fb/ GeV]	0.69	0.26	0.034
Statistical uncertainty	0.16	0.10	0.021
Total uncertainty	0.24	0.13	0.025
Predicted $\mathrm{d}\sigma/\mathrm{d}p_{\mathrm{T}}^{j_1}$ [fb/ GeV] (NNLOPS)	0.53	0.17	0.016
Uncertainty in prediction	0.06	0.02	0.004
SR data statistical	19%	40%	61%
MC statistical	3%	7%	10%
CR data statistical	12%	2%	18%
Exp. JER	4%	6%	10%
Exp. JES	2%	14%	15%
Exp. b-tag	1%	8%	10%
Exp. leptons	6%	6%	8%
Exp. $p_{\mathrm{T}}^{\mathrm{miss}}$	2%	6%	4%
Exp. other	5%	5%	4%
Theory (WW)	23%	12%	14%
Theory (top)	2%	13%	23%
Theory (other backgrounds)	5%	13%	13%
Theory (signal)	5%	4%	3%
Detector corrections	<1%	<1%	<1%
Total	34%	51%	75%

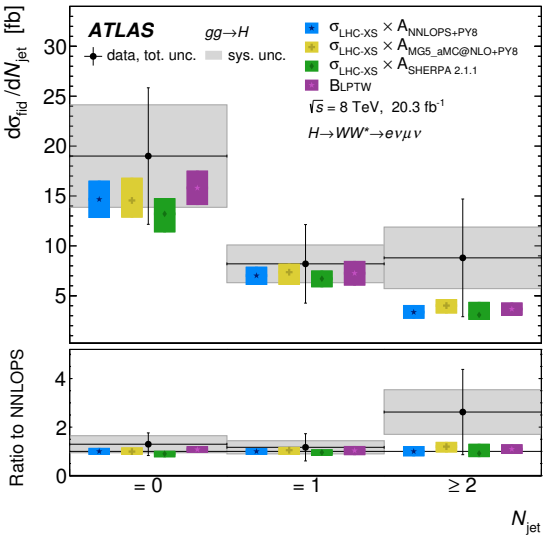

(a) N_{jet}

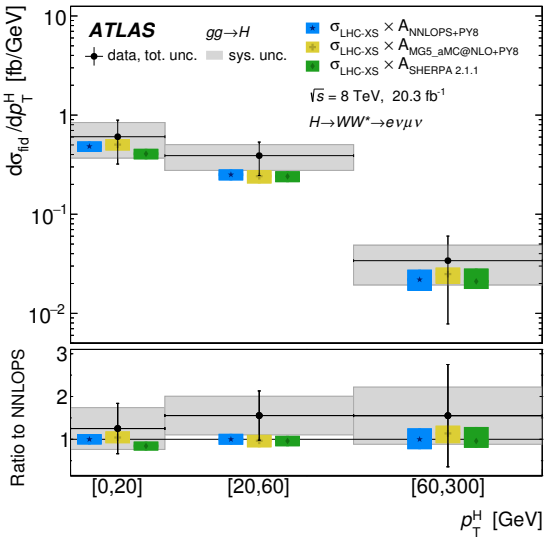

(b) p_{T}^{H}

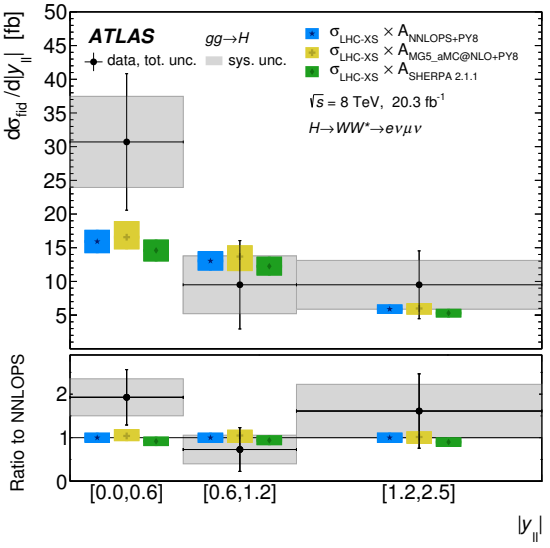

(c) $|y_{\ell\ell}|$

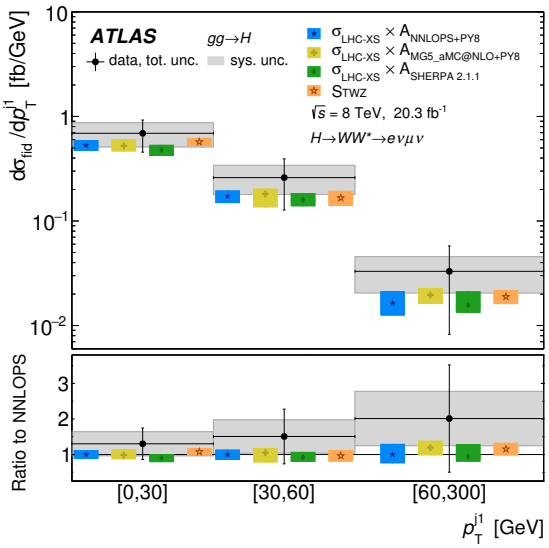

(d) $p_{\text{T}}^{j_1}$

Figure 6: Measured fiducial differential cross section as a function of (a) N_{jet}, (b) p_{T}^{H}, (c) $|y_{\ell\ell}|$, and (d) $p_{\text{T}}^{j_1}$, overlaid with the signal predictions. The [0, 30] GeV bin of the $p_{\text{T}}^{j_1}$ distribution includes events with no reconstructed jets. The systematic uncertainty at each point is shown by a grey band labelled "sys. unc." and includes the experimental and theoretical uncertainties. The uncertainty bar, labelled "data, tot. unc." is the total uncertainty and includes all systematic and statistical uncertainties. The measured results are compared to various theoretical predictions.

Table 16: Measured and predicted normalised differential fiducial cross section as a function of N_{jet}. Predicted values are from POWHEG NNLOPS+PYTHIA8, normalised to the LHC-XS working group recommended cross section, as described in Section 9. Total uncertainties in the measurement are given along with their relative composition in terms of source.

N_{jet}	0	1	≥ 2
$1/\sigma\ \mathrm{d}\sigma/\mathrm{d}N_{\text{jet}}$	0.53	0.23	0.24
Statistical uncertainty	0.11	0.09	0.12
Total uncertainty	0.14	0.10	0.14
Predicted $1/\sigma\ \mathrm{d}\sigma/\mathrm{d}N_{\text{jet}}$ (NNLOPS)	0.59	0.28	0.13
Uncertainty in prediction	0.04	0.02	0.02
SR data statistical	19%	34%	42%
MC statistical	4%	8%	17%
CR data statistical	9%	16%	14%
Exp. JER	<1%	1%	2%
Exp. JES	3%	7%	4%
Exp. b-tag	3%	3%	5%
Exp. leptons	2%	2%	4%
Exp. $p_{\text{T}}^{\text{miss}}$	1%	4%	4%
Exp. other	2%	2%	3%
Theory (WW)	12%	15%	17%
Theory (top)	7%	5%	18%
Theory (other backgrounds)	6%	5%	16%
Theory (signal)	1%	3%	5%
Detector corrections	<1%	4%	4%
Total	26%	43%	57%

Table 17: Measured and predicted normalised differential fiducial cross section as a function of p_{T}^{H}. Predicted values are from Powheg NNLOPS+Pythia8, normalised to the LHC-XS working group recommended cross section, as described in Section 9. Total uncertainties in the measurement are given along with their relative composition in terms of source.

p_{T}^{H} [GeV]	$[0, 20]$	$[20, 60]$	$[60, 300]$
$1/\sigma\ \mathrm{d}\sigma/\mathrm{d}p_{\mathrm{T}}^{H}$ [10^{-3} GeV^{-1}]	17.0	11.0	0.96
Statistical uncertainty	3.5	2.0	0.50
Total uncertainty	6.0	3.4	0.63
Predicted $1/\sigma\ \mathrm{d}\sigma/\mathrm{d}p_{\mathrm{T}}^{H}$ [10^{-3} GeV^{-1}] (NNLOPS)	19.4	10.0	0.88
Uncertainty in prediction	0.7	0.5	0.2
SR data statistical	20%	18%	48%
MC statistical	4%	3%	8%
CR data statistical	8%	7%	18%
Exp. JER	2%	4%	11%
Exp. JES	8%	9%	16%
Exp. b-tag	4%	4%	6%
Exp. leptons	3%	2%	5%
Exp. $p_{\mathrm{T}}^{\mathrm{miss}}$	10%	8%	7%
Exp. other	4%	2%	4%
Theory (WW)	19%	15%	21%
Theory (top)	9%	8%	17%
Theory (other backgrounds)	7%	8%	12%
Theory (signal)	10%	2%	10%
Detector corrections	<1%	3%	3%
Total	37%	31%	65%

Table 18: Measured and predicted normalised differential fiducial cross section as a function of $|y_{\ell\ell}|$. Predicted values are from POWHEG NNLOPS+PYTHIA8, normalised to the LHC-XS working group recommended cross section, as described in Section 9. Total uncertainties in the measurement are given along with their relative composition in terms of source.

$\|y(\ell\ell)\|$	$[0.0, 0.6]$	$[0.6, 1.2]$	$[1.2, 2.5]$
$1/\sigma\ \mathrm{d}\sigma/\mathrm{d}\|y(\ell\ell)\|$	0.83	0.27	0.26
Statistical uncertainty	0.17	0.13	0.08
Total uncertainty	0.22	0.15	0.11
Predicted$1/\sigma\ \mathrm{d}\sigma/\mathrm{d}\|y(\ell\ell)\|$ (NNLOPS)	0.636	0.521	0.235
Uncertainty in prediction	0.004	0.001	0.004
SR data statistical	18%	48%	26%
MC statistical	3%	8%	5%
CR data statistical	7%	6%	14%
Exp. JER	2%	5%	2%
Exp. JES	4%	9%	7%
Exp. b-tag	3%	5%	5%
Exp. leptons	3%	5%	5%
Exp. $p_{\mathrm{T}}^{\mathrm{miss}}$	3%	7%	4%
Exp. other	3%	6%	5%
Theory (WW)	11%	21%	18%
Theory (top)	10%	15%	9%
Theory (other backgrounds)	5%	8%	17%
Theory (signal)	<1%	2%	1%
Detector corrections	<1%	<1%	<1%
Total	27%	60%	43%

Table 19: Measured and predicted normalised differential cross section as a function of $p_{\mathrm{T}}^{j_1}$. Predicted values are from POWHEG NNLOPS+PYTHIA8, normalised to the LHC-XS working group recommended cross section, as described in Section 9. Total uncertainties in the measurement are given along with their relative composition in terms of source.

$p_{\mathrm{T}}^{j_1}$ [GeV]	$[0, 30]$	$[30, 60]$	$[60, 300]$
$1/\sigma\ \mathrm{d}\sigma/\mathrm{d}p_{\mathrm{T}}^{j_1}$ [10^{-3} GeV^{-1}]	19.0	7.0	0.91
Statistical uncertainty	3.7	2.7	0.51
Total uncertainty	4.7	3.3	0.58
Predicted $1/\sigma\ \mathrm{d}\sigma/\mathrm{d}p_{\mathrm{T}}^{j_1}$ [10^{-3} GeV^{-1}] (NNLOPS)	21.2	6.9	0.66
Uncertainty in prediction	0.7	0.5	0.16
SR data statistical	17%	36%	49%
MC statistical	3%	6%	9%
CR data statistical	7%	8%	18%
Exp. JER	2%	3%	5%
Exp. JES	3%	13%	14%
Exp. b-tag	3%	7%	9%
Exp. leptons	2%	3%	5%
Exp. $p_{\mathrm{T}}^{\mathrm{miss}}$	1%	6%	4%
Exp. other	2%	3%	5%
Theory (WW)	11%	17%	17%
Theory (top)	7%	9%	18%
Theory (other backgrounds)	5%	11%	11%
Theory (signal)	2%	2%	5%
Detector corrections	<1%	<1%	<1%
Total	24%	47%	63%

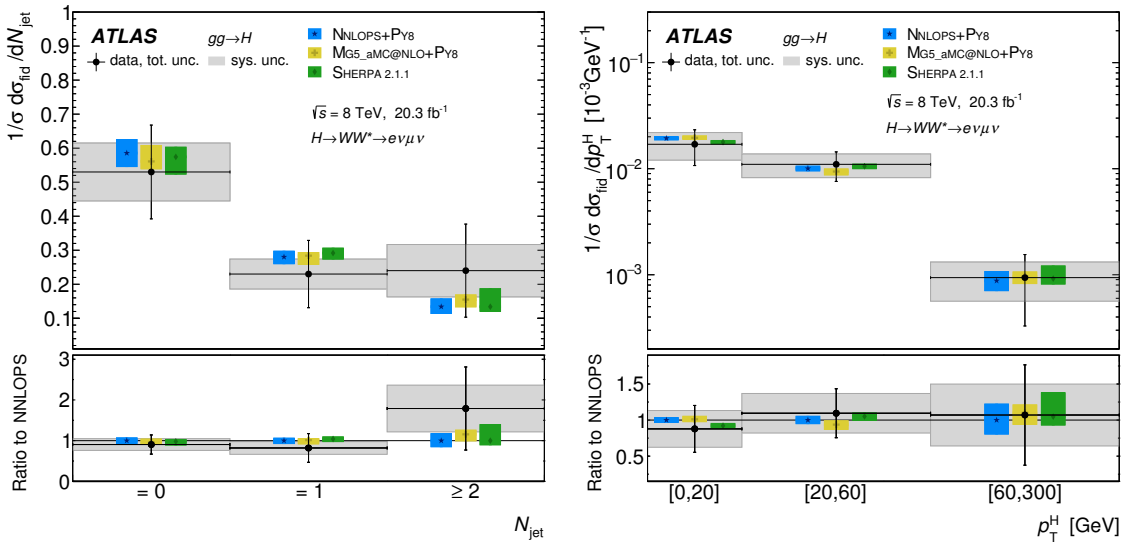

(a) N_{jet} (b) p_{T}^{H}

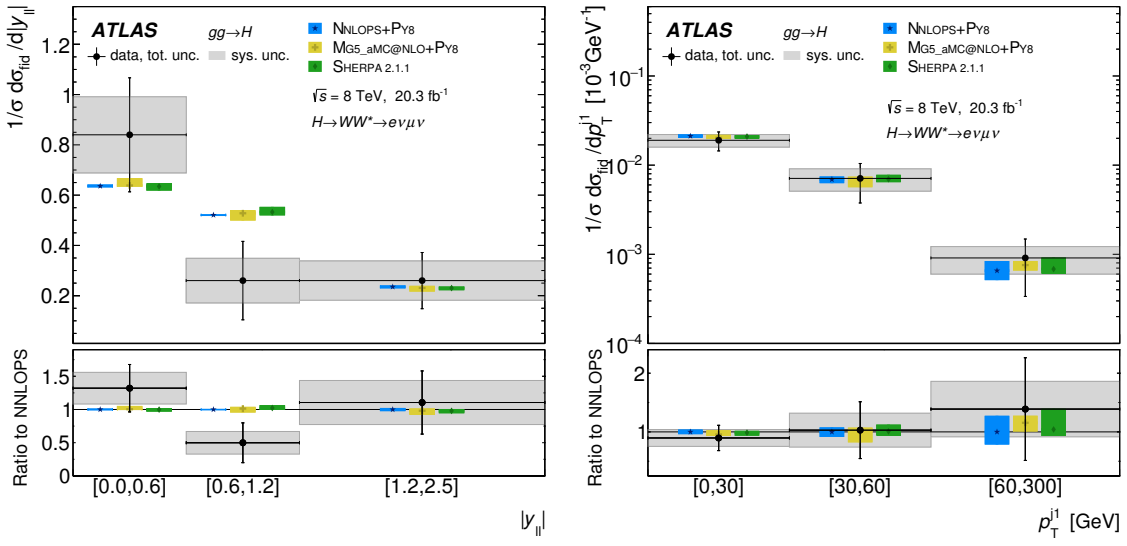

(c) $|y_{\ell\ell}|$ (d) $p_{\text{T}}^{j_1}$

Figure 7: Normalised fiducial differential cross section measurements as a function of (a) N_{jet}, (b) p_{T}^{H}, (c) $|y_{\ell\ell}|$, and (d) $p_{\text{T}}^{j_1}$, overlaid with the signal predictions. The $[0, 30]$ GeV bin of the $p_{\text{T}}^{j_1}$ distribution includes events with no reconstructed jets. The systematic uncertainty at each point is shown by a grey band labelled "sys. unc." and includes the experimental and theoretical uncertainties. The uncertainty bar, labelled "data, tot. unc." is the total uncertainty and includes all systematic and statistical uncertainties. The measured results are compared to various theoretical predictions.

Table 20: Measured and predicted jet-veto efficiency ε_0 for different jet p_{T} thresholds and the associated statistical and systematic uncertainties. The asterisk for the 25 GeV column header indicates that the results are for a mixed p_{T} threshold, which is raised from 25 GeV to 30 GeV for jets with $2.5 < |\eta| < 4.5$, corresponding to the selection used to define the signal regions for the analysis. Total uncertainties in the measurement are given along with their relative composition in terms of source.

Jet p_{T} threshold	25 GeV*	30 GeV	40 GeV
ε_0	0.53	0.57	0.64
Statistical uncertainty	0.11	0.11	0.12
Total uncertainty	0.14	0.14	0.17
Predicted ε_0 (NNLOPS)	0.59	0.63	0.73
Uncertainty in prediction	0.04	0.04	0.04
SR data statistical	19%	17%	17%
MC statistical	4%	3%	3%
CR data statistical	9%	7%	8%
Exp. JER	0%	2%	3%
Exp. JES	3%	3%	5%
Exp. b-tag	3%	3%	4%
Exp. leptons	2%	2%	2%
Exp. $p_{\mathrm{T}}^{\mathrm{miss}}$	1%	1%	1%
Exp. other	2%	2%	5%
Theory (WW)	12%	11%	12%
Theory (top)	7%	7%	9%
Theory (other backgrounds)	6%	5%	8%
Theory (signal)	1%	2%	2%
Detector corrections	<1%	<1%	<1%
Total	26%	24%	27%

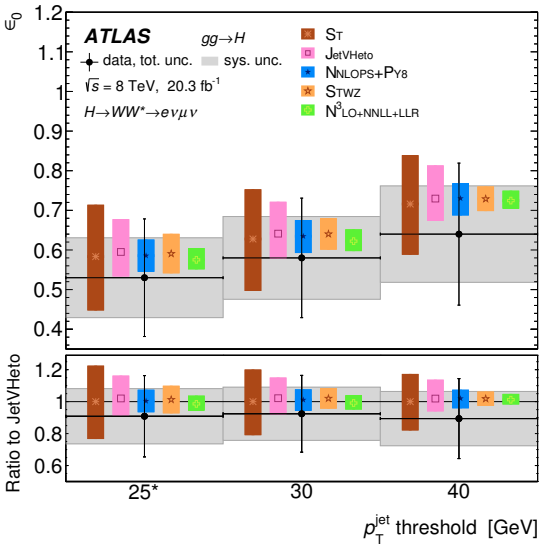

Figure 8: Measured jet-veto efficiency as a function of the jet p_{T} threshold, compared to the signal predictions. The asterisk on the 25 GeV bin label indicates that the results are for a mixed p_{T} threshold, which is raised from 25 GeV to 30 GeV for jets with $2.5 < |\eta| < 4.5$, corresponding to the selection used to define the signal regions for the analysis. The total uncertainty includes all statistical, experimental, and theoretical uncertainties.

11 Conclusion

Measurements of total and differential fiducial cross sections in the $gg \to H \to WW^* \to e\nu\mu\nu$ final state of gluon-fusion Higgs boson production are presented. They are based on 20.3 fb^{-1} of proton–proton collision data produced at a centre-of-mass energy of $\sqrt{s} = 8$ TeV at the LHC and recorded by the ATLAS experiment in 2012. The data are corrected for detector efficiencies and resolution using an iterative Bayesian method. Results are presented in a fiducial region requiring two opposite-charge leptons of different flavour and missing transverse momentum of more than 20 GeV. Additional selection requirements are applied on the dilepton system to select Higgs boson candidate events. The fiducial cross section of ggF Higgs boson production is measured to be:

$$\sigma_{\text{ggF}}^{\text{fid}} = 36.0 \pm 7.2(\text{stat}) \pm 6.4(\text{sys}) \pm 1.0(\text{lumi}) \text{ fb} \tag{4}$$

for a Higgs boson of mass 125.0 GeV produced in the fiducial region described in Table 7. The SM prediction is $\sigma_{\text{ggF}}^{\text{fid}} = 25.1 \pm 2.6$ fb.

In addition, differential and normalised differential cross sections are measured in the fiducial region as functions of the number of jets, the Higgs boson transverse momentum, the rapidity of the dilepton system, and the transverse momentum of the leading jet. These measurements probe directly the Higgs boson production and decay kinematics, as well as the jet activity produced in association with the Higgs boson. Jet-veto efficiencies for H + 0-jet events are also reported for three different thresholds for the transverse momentum of the leading jet; the jet-veto efficiency for a threshold of 30 GeV is (57 ± 14)%. All results are compared to a set of predictions from fixed-order calculations and Monte-Carlo generators and are in agreement with the predictions of the Standard Model.

Acknowledgements

We thank CERN for the very successful operation of the LHC, as well as the support staff from our institutions without whom ATLAS could not be operated efficiently.

We acknowledge the support of ANPCyT, Argentina; YerPhI, Armenia; ARC, Australia; BMWFW and FWF, Austria; ANAS, Azerbaijan; SSTC, Belarus; CNPq and FAPESP, Brazil; NSERC, NRC and CFI, Canada; CERN; CONICYT, Chile; CAS, MOST and NSFC, China; COLCIENCIAS, Colombia; MSMT CR, MPO CR and VSC CR, Czech Republic; DNRF and DNSRC, Denmark; IN2P3-CNRS, CEA-DSM/IRFU, France; GNSF, Georgia; BMBF, HGF, and MPG, Germany; GSRT, Greece; RGC, Hong Kong SAR, China; ISF, I-CORE and Benoziyo Center, Israel; INFN, Italy; MEXT and JSPS, Japan; CNRST, Morocco; FOM and NWO, Netherlands; RCN, Norway; MNiSW and NCN, Poland; FCT, Portugal; MNE/IFA, Romania; MES of Russia and NRC KI, Russian Federation; JINR; MESTD, Serbia; MSSR, Slovakia; ARRS and MIZŠ, Slovenia; DST/NRF, South Africa; MINECO, Spain; SRC and Wallenberg Foundation, Sweden; SERI, SNSF and Cantons of Bern and Geneva, Switzerland; MOST, Taiwan; TAEK, Turkey; STFC, United Kingdom; DOE and NSF, United States of America. In addition, individual groups and members have received support from BCKDF, the Canada Council, CANARIE, CRC, Compute Canada, FQRNT, and the Ontario Innovation Trust, Canada; EPLANET, ERC, FP7, Horizon 2020 and Marie Skłodowska-Curie Actions, European Union; Investissements d'Avenir Labex and Idex, ANR, Région Auvergne and Fondation Partager le Savoir, France; DFG and AvH Foundation, Germany; Herakleitos, Thales and Aristeia programmes co-financed by EU-ESF and the Greek NSRF; BSF, GIF and Minerva, Israel; BRF, Norway; the Royal Society and Leverhulme Trust, United Kingdom.

The crucial computing support from all WLCG partners is acknowledged gratefully, in particular from CERN and the ATLAS Tier-1 facilities at TRIUMF (Canada), NDGF (Denmark, Norway, Sweden), CC-IN2P3 (France), KIT/GridKA (Germany), INFN-CNAF (Italy), NL-T1 (Netherlands), PIC (Spain), ASGC (Taiwan), RAL (UK) and BNL (USA) and in the Tier-2 facilities worldwide.

References

[1] ATLAS Collaboration, *Observation of a new particle in the search for the Standard Model Higgs boson with the ATLAS detector at the LHC*, Phys. Lett. B **716** (2012) 1, arXiv:1207.7214 [hep-ex].

[2] CMS Collaboration, *Observation of a new boson at a mass of 125 GeV with the CMS experiment at the LHC*, Phys. Lett. B **716** (2012) 30, arXiv:1207.7235 [hep-ex].

[3] F. Englert and R. Brout, *Broken symmetry and the mass of gauge vector mesons*, Phys. Rev. Lett. **13** (1964) 321–323.

[4] P. W. Higgs, *Broken symmetries, massless particles and gauge fields*, Phys. Lett. **12** (1964) 132–133.

[5] P. W. Higgs, *Broken symmetries and the masses of gauge bosons*, Phys. Rev. Lett. **13** (1964) 508–509.

[6] G. Guralnik, C. Hagen and T. Kibble, *Global conservation laws and massless particles*, Phys. Rev. Lett. **13** (1964) 585–587.

[7] P. W. Higgs, *Spontaneous symmetry breakdown without massless bosons*, Phys. Rev. **145** (1966) 1156–1163.

[8] T. Kibble, *Symmetry breaking in non-Abelian gauge theories*, Phys. Rev. **155** (1967) 1554–1561.

[9] ATLAS and CMS Collaborations, *Combined Measurement of the Higgs Boson Mass in pp Collisions at $\sqrt{s} = 7$ and 8 TeV with the ATLAS and CMS Experiments*, Phys. Rev. Lett. **114** (2015) 191803, arXiv:1503.07589 [hep-ex].

[10] ATLAS Collaboration, *Study of the spin and parity of the Higgs boson in diboson decays with the ATLAS detector*, Eur. Phys. J. C **75** (2015) 476, arXiv:1506.05669 [hep-ex].

[11] CMS Collaboration, *Constraints on the spin-parity and anomalous HVV couplings of the Higgs boson in proton collisions at 7 and 8 TeV*, Phys. Rev. D **92** (2015) 012004, arXiv:1411.3441 [hep-ex].

[12] ATLAS Collaboration, *Measurements of the Higgs boson production and decay rates and coupling strengths using pp collision data at $\sqrt{s} = 7$ and 8 TeV in the ATLAS experiment*, Eur. Phys. J. C **76** (2016) 6, arXiv:1507.04548 [hep-ex].

[13] CMS Collaboration, *Precise determination of the mass of the Higgs boson and tests of compatibility of its couplings with the standard model predictions using proton collisions at 7 and 8 TeV*, Eur. Phys. J. C **75** (2015) 212, arXiv:1412.8662 [hep-ex].

[14] ATLAS Collaboration,
Fiducial and differential cross sections of Higgs boson production measured in the four-lepton decay channel in pp collisions at $\sqrt{s} = 8$ TeV with the ATLAS detector,
Phys. Lett. B **738** (2014) 234, arXiv:1408.3226 [hep-ex].

[15] CMS Collaboration, *Measurement of differential and integrated fiducial cross sections for Higgs boson production in the four-lepton decay channel in pp collisions at $\sqrt{s} = 7$ and 8 TeV*, (2015), arXiv:1512.08377 [hep-ex].

[16] ATLAS Collaboration, *Measurements of fiducial and differential cross sections for Higgs boson production in the diphoton decay channel at $\sqrt{s} = 8$ TeV with ATLAS*, JHEP **1409** (2014) 112, arXiv:1407.4222 [hep-ex].

[17] CMS Collaboration, *Measurement of differential cross sections for Higgs boson production in the diphoton decay channel in pp collisions at $\sqrt{s} = 8$ TeV*, Eur. Phys. J. C **76** (2016) 13, arXiv:1508.07819 [hep-ex].

[18] ATLAS Collaboration,
Measurements of the Total and Differential Higgs Boson Production Cross Sections Combining the $H \to \gamma\gamma$ and $H \to ZZ^* \to 4\ell$ Decay Channels at $\sqrt{s} = 8$ TeV with the ATLAS Detector,
Phys. Rev. Lett. **115** (2015) 091801, arXiv:1504.05833 [hep-ex].

[19] ATLAS Collaboration,
Observation and measurement of Higgs boson decays to WW^* with the ATLAS detector,
Phys. Rev. D **92** (2015) 012006, arXiv:1412.2641 [hep-ex].

[20] ATLAS Collaboration, *The ATLAS Experiment at the CERN Large Hadron Collider*,
JINST **3** (2008) S08003.

[21] ATLAS Collaboration, *Performance of the ATLAS Trigger System in 2010*,
Eur. Phys. J. C **72** (2012) 1849, arXiv:1110.1530 [hep-ex].

[22] P. Nason, *A new method for combining NLO QCD with shower Monte Carlo algorithms*,
JHEP **0411** (2004) 040, arXiv:hep-ph/0409146.

[23] S. Alioli et al., *NLO Higgs boson production via gluon fusion matched with shower in POWHEG*,
JHEP **0904** (2009) 002, arXiv:0812.0578 [hep-ph].

[24] P. Nason and C. Oleari,
NLO Higgs boson production via vector-boson fusion matched with shower in POWHEG,
JHEP **1002** (2010) 037, arXiv:0911.5299 [hep-ph].

[25] E. Bagnaschi et al.,
Higgs production via gluon fusion in the POWHEG approach in the SM and in the MSSM,
JHEP **1202** (2012) 88, arXiv:1111.2854 [hep-ph].

[26] T. Sjöstrand, S. Mrenna, and P. Z. Skands, *A Brief Introduction to PYTHIA 8.1*,
Comput. Phys. Commun. **178** (2008) 852–867, arXiv:0710.3820 [hep-ph].

[27] H.-L. Lai et al., *New parton distributions for collider physics*, Phys. Rev. D **82** (2010) 074024,
arXiv:1007.2241 [hep-ph].

[28] ATLAS Collaboration, *Summary of ATLAS Pythia 8 tunes*, ATL-PHYS-PUB-2012-003, 2012,
URL: http://cds.cern.ch/record/1474107.

[29] D. de Florian and M. Grazzini,
Higgs production at the LHC: updated cross sections at $\sqrt{s} = 8$ TeV,
Phys. Lett. B **718** (2013) 117–120, arXiv:1206.4133 [hep-ph].

[30] M. Grazzini and H. Sargsyan, *Heavy-quark mass effects in Higgs boson production at the LHC*, JHEP **1309** (2013) 129, arXiv:1306.4581 [hep-ph].

[31] K. Hamilton, P. Nason and G. Zanderighi, *MINLO: Multi-Scale Improved NLO*, JHEP **1210** (2012) 155, arXiv:1206.3572 [hep-ph].

[32] J. M. Campbell, R. K. Ellis and C. Williams, *Gluon-Gluon Contributions to W+ W- Production and Higgs Interference Effects*, JHEP **1110** (2011) 005, arXiv:1107.5569 [hep-ph].

[33] J. M. Campbell, R. K. Ellis and C. Williams, *Bounding the Higgs width at the LHC: Complementary results from $H \to WW$*, Phys. Rev. D **89** (2014) 053011, arXiv:1312.1628 [hep-ph].

[34] LHC Higgs Cross Section Working Group, *Handbook of LHC Higgs Cross Sections: 3. Higgs Properties*, CERN-2013-004 (2013), arXiv:1307.1347 [hep-ph].

[35] T. Sjöstrand, S. Mrenna, and P. Z. Skands, *PYTHIA 6.4 physics and manual*, JHEP **0605** (2006) 026, arXiv:hep-ph/0603175.

[36] P. Z. Skands, *Tuning Monte Carlo Generators: The Perugia Tunes*, Phys. Rev. D **82** (2010) 074018, arXiv:1005.3457 [hep-ph].

[37] T. Gleisberg et al., *Event generation with SHERPA 1.1*, JHEP **0902** (2009) 007, arXiv:0811.4622 [hep-ph].

[38] M. L. Mangano et al., *ALPGEN, a generator for hard multi-parton processes in hadronic collisions*, JHEP **0307** (2003) 001, arXiv:hep-ph/0206293.

[39] G. Corcella et al., *HERWIG 6: An event generator for hadron emission reactions with interfering gluons (including super-symmetric processes)*, JHEP **0101** (2001) 010.

[40] ATLAS Collaboration, *New ATLAS event generator tunes to 2010 data*, ATL-PHYS-PUB-2011-008, 2011, URL: http://cds.cern.ch/record/1345343.

[41] P. M. Nadolsky et al., *Implications of CTEQ global analysis for collider observables*, Phys. Rev. D **78** (2008) 013004, arXiv:0802.0007 [hep-ph].

[42] A. Sherstnev and R. S. Thorne, *Parton Distributions for LO Generators*, Eur. Phys. J. C **55** (2008) 553–575, arXiv:0711.2473 [hep-ph].

[43] ATLAS Collaboration, *The ATLAS Simulation Infrastructure*, Eur. Phys. J. C **70** (2010) 823, arXiv:1005.4568 [hep-ex].

[44] S. Agostinelli et al., *GEANT4: A simulation toolkit*, Nucl. Instrum. Meth. A **506** (2003) 250–303.

[45] ATLAS Collaboration, *The simulation principle and performance of the ATLAS fast calorimeter simulation FastCaloSim*, ATL-PHYS-PUB-2010-013, 2010, URL: http://cds.cern.ch/record/1300517.

[46] ATLAS Collaboration, *Electron reconstruction and identification efficiency measurements with the ATLAS detector using the 2011 LHC proton–proton collision data*, Eur. Phys. J. C **74** (2014) 2941, arXiv:1404.2240 [hep-ex].

[47] ATLAS Collaboration, *Electron efficiency measurements with the ATLAS detector using the 2012 LHC proton–proton collision data*, ATLAS-CONF-2014-032, 2014, URL: http://cdsweb.cern.ch/record/1706245.

[48] ATLAS Collaboration,
Electron and photon energy calibration with the ATLAS detector using LHC Run 1 data,
Eur. Phys. J. C **74** (2014) 3071, arXiv:1407.5063 [hep-ex].

[49] ATLAS Collaboration, *Measurement of the muon reconstruction performance of the ATLAS detector using 2011 and 2012 LHC proton–proton collision data*, Eur. Phys. J. C **74** (2014) 3130, arXiv:1407.3935 [hep-ex].

[50] ATLAS Collaboration, *Jet energy measurement and its systematic uncertainty in proton–proton collisions at* $\sqrt{s} = 7$ *TeV with the ATLAS detector*, Eur. Phys. J. C **75** (2015) 17, arXiv:1406.0076 [hep-ex].

[51] W. Lampl et al., *Calorimeter Clustering Algorithms: Description and Performance*, ATL-LARG-PUB-2008-002, 2008, URL: http://cds.cern.ch/record/1099735.

[52] ATLAS Collaboration, *Tagging and suppression of pileup jets with the ATLAS detector*, ATLAS-CONF-2014-018, 2014, URL: http://cdsweb.cern.ch/record/1700870.

[53] M. Cacciari, G. P. Salam and G. Soyez, *The anti-k_t jet clustering algorithm*, JHEP **0804** (2008) 063, arXiv:0802.1189 [hep-ex].

[54] ATLAS Collaboration,
Pile-up corrections for jets from proton–proton collisions at $\sqrt{s} = 7$ *TeV in ATLAS in 2011*, ATLAS-CONF-2012-064, 2012, URL: http://cdsweb.cern.ch/record/1459529.

[55] ATLAS Collaboration,
Jet energy measurement with the ATLAS detector in proton–proton collisions at $\sqrt{s} = 7$ *TeV*, Eur. Phys. J. C **73** (2013) 2304, arXiv:1112.6426 [hep-ex].

[56] ATLAS Collaboration, *Calibration of b-tagging using dileptonic top pair events in a combinatorial likelihood approach with the ATLAS experiment*, ATLAS-CONF-2014-004, 2014, URL: http://cdsweb.cern.ch/record/1664335.

[57] ATLAS Collaboration,
Calibration of the performance of b-tagging for c and light-flavour jets in the 2012 ATLAS data, ATLAS-CONF-2014-046, 2014, URL: http://cdsweb.cern.ch/record/1741020.

[58] T. Plehn, D. L. Rainwater and D. Zeppenfeld,
A Method for identifying $H \to \tau^+\tau^- \to e^\pm\mu^\mp p_T$ *at the CERN LHC*,
Phys. Rev. D **61** (2000) 093005, arXiv:hep-ph/9911385.

[59] J. M. Campbell, R. K. Ellis and G. Zanderighi,
Next-to-Leading order Higgs + 2 jet production via gluon fusion, JHEP **0610** (2006) 028, arXiv:hep-ph/0608194.

[60] T. Gehrmann et al.,
W^+W^- *Production at Hadron Colliders in Next to Next to Leading Order QCD*,
Phys. Rev. Lett. **113** (2014) 212001, arXiv:1408.5243 [hep-ph].

[61] ATLAS Collaboration,
Measurement of total and differential W^+W^- *production cross sections in proton-proton collisions at* $\sqrt{s} = 8$ *TeV with the ATLAS detector and limits on anomalous triple-gauge-boson couplings*, Submitted to JHEP (2016), arXiv:1603.01702 [hep-ex].

[62] M. Cacciari, G. P. Salam and G. Soyez, *FastJet User Manual*, Eur. Phys. J. C **72** (2012) 1896, arXiv:1111.6097 [hep-ph].

[63] G. D'Agostini, *A Multidimensional unfolding method based on Bayes' theorem*, Nucl. Instrum. Meth. A **362** (1995) 487–498.

[64] LHC Higgs cross section working group, *Handbook of LHC Higgs Cross Sections: 2. Differential Distributions*, CERN-2012-002 (2012), arXiv:1201.3084 [hep-ph].

[65] J. R. Andersen et al., *Les Houches 2013: Physics at TeV Colliders: Standard Model Working Group Report*, (2014), arXiv:1405.1067 [hep-ph].

[66] R. Boughezal et al., *Combining Resummed Higgs Predictions Across Jet Bins*, Phys. Rev. D **89** (2014) 074044, arXiv:1312.4535 [hep-ph].

[67] J. Alwall et al., *The automated computation of tree-level and next-to-leading order differential cross sections, and their matching to parton shower simulations*, JHEP **1407** (2014) 079, arXiv:1405.0301 [hep-ph].

[68] A. D. Martin et al., *Parton distributions for the LHC*, Eur. Phys. J. C **63** (2009) 189–285, arXiv:0901.0002 [hep-ph].

[69] R. D. Ball et al., *Parton distributions with LHC data*, Nucl. Phys. B **867** (2013) 244–289, arXiv:1207.1303 [hep-ph].

[70] J. Alwall et al., *MadGraph 5 : Going Beyond*, JHEP **1106** (2011) 128, arXiv:1106.0522 [hep-ph].

[71] LHC Higgs cross section working group, *Handbook of LHC Higgs cross sections: 1. Inclusive observables*, CERN-2011-002 (2011), arXiv:1101.0593 [hep-ph].

[72] A. Banfi et al., *Higgs and Z-boson production with a jet veto*, Phys. Rev. Lett. **109** (2012) 202001, arXiv:1206.4998 [hep-ph].

[73] A. Banfi, G. P. Salam and G. Zanderighi, *NLL+NNLO predictions for jet-veto efficiencies in Higgs-boson and Drell-Yan production*, JHEP **1206** (2012) 159, arXiv:1203.5773 [hep-ph].

[74] A. Banfi, P. F. Monni and G. Zanderighi, *Quark masses in Higgs production with a jet veto*, JHEP **1401** (2014) 097, arXiv:1308.4634 [hep-ph].

[75] I. W. Stewart and F. J. Tackmann, *Theory Uncertainties for Higgs and Other Searches Using Jet Bins*, Phys. Rev. D **85** (2012) 034011, arXiv:1107.2117 [hep-ph].

[76] I. W. Stewart et al., *Jet p_T resummation in Higgs production at NNLL′ + NNLO*, Phys. Rev. D **89** (2014) 054001, arXiv:1307.1808 [hep-ph].

[77] A. Banfi et al., *Jet-vetoed Higgs cross section in gluon fusion at N3LO+NNLL with small-R resummation*, (2015), arXiv:1511.02886 [hep-ph].

[78] K. Hamilton et al., *NNLOPS simulation of Higgs boson production*, JHEP **1310** (2013) 222, arXiv:1309.0017 [hep-ph].

[79] K. Hamilton, P. Nason and G. Zanderighi, *Finite quark-mass effects in the NNLOPS POWHEG+MiNLO Higgs generator*, JHEP **1505** (2015) 140, arXiv:1501.04637 [hep-ph].

[80] F. Krauss, R. Kuhn and G. Soff, *AMEGIC++ 1.0: A Matrix element generator in C++*, JHEP **0202** (2002) 044, arXiv:hep-ph/0109036.

[81] S. Hoeche et al., *QCD matrix elements + parton showers: The NLO case*, JHEP **1304** (2013) 027, arXiv:1207.5030 [hep-ph].

[82] T. Gehrmann et al., *NLO QCD matrix elements + parton showers in $e^+e^- \to$ hadrons*, JHEP **1301** (2013) 144, arXiv:1207.5031 [hep-ph].

[83] S. Hoeche, F. Krauss and M. Schonherr, *Uncertainties in MEPS@NLO calculations of h+jets*, Phys. Rev. D **90** (2014) 014012, arXiv:1401.7971 [hep-ph].

[84] P. Artoisenet et al., *A framework for Higgs characterisation*, JHEP **1311** (2013) 043, arXiv:1306.6464 [hep-ph].

[85] R. Frederix and S. Frixione, *Merging meets matching in MC@NLO*, JHEP **1212** (2012) 061, arXiv:1209.6215 [hep-ph].

[86] S. Catani and M. Grazzini, *An NNLO subtraction formalism in hadron collisions and its application to Higgs boson production at the LHC*, Phys. Rev. Lett. **98** (2007) 222002, arXiv:hep-ph/0703012.

[87] M. Grazzini, *NNLO predictions for the Higgs boson signal in the $H \to WW \to \ell\nu\ell\nu$ and $H \to ZZ \to 4\ell$ decay channels*, JHEP **0802** (2008) 043, arXiv:0801.3232 [hep-ph].

[88] J. Gao et al., *CT10 next-to-next-to-leading order global analysis of QCD*, Phys. Rev. D **89** (2014) 033009, arXiv:1302.6246 [hep-ph].

[89] ATLAS Collaboration, *Improved luminosity determination in pp collisions at $\sqrt{s} = 7$ TeV using the ATLAS detector at the LHC*, Eur. Phys. J. C **73** (2013) 2518, arXiv:1302.4393 [hep-ex].

The ATLAS Collaboration

G. Aad[86], B. Abbott[113], J. Abdallah[151], O. Abdinov[11], B. Abeloos[117], R. Aben[107], M. Abolins[91], O.S. AbouZeid[137], H. Abramowicz[153], H. Abreu[152], R. Abreu[116], Y. Abulaiti[146a,146b], B.S. Acharya[163a,163b,a], L. Adamczyk[39a], D.L. Adams[26], J. Adelman[108], S. Adomeit[100], T. Adye[131], A.A. Affolder[75], T. Agatonovic-Jovin[13], J. Agricola[55], J.A. Aguilar-Saavedra[126a,126f], S.P. Ahlen[23], F. Ahmadov[66,b], G. Aielli[133a,133b], H. Akerstedt[146a,146b], T.P.A. Åkesson[82], A.V. Akimov[96], G.L. Alberghi[21a,21b], J. Albert[168], S. Albrand[56], M.J. Alconada Verzini[72], M. Aleksa[31], I.N. Aleksandrov[66], C. Alexa[27b], G. Alexander[153], T. Alexopoulos[10], M. Alhroob[113], G. Alimonti[92a], J. Alison[32], S.P. Alkire[36], B.M.M. Allbrooke[149], B.W. Allen[116], P.P. Allport[18], A. Aloisio[104a,104b], A. Alonso[37], F. Alonso[72], C. Alpigiani[138], B. Alvarez Gonzalez[31], D. Álvarez Piqueras[166], M.G. Alviggi[104a,104b], B.T. Amadio[15], K. Amako[67], Y. Amaral Coutinho[25a], C. Amelung[24], D. Amidei[90], S.P. Amor Dos Santos[126a,126c], A. Amorim[126a,126b], S. Amoroso[31], N. Amram[153], G. Amundsen[24], C. Anastopoulos[139], L.S. Ancu[50], N. Andari[108], T. Andeen[32], C.F. Anders[59b], G. Anders[31], J.K. Anders[75], K.J. Anderson[32], A. Andreazza[92a,92b], V. Andrei[59a], S. Angelidakis[9], I. Angelozzi[107], P. Anger[45], A. Angerami[36], F. Anghinolfi[31], A.V. Anisenkov[109,c], N. Anjos[12], A. Annovi[124a,124b], M. Antonelli[48], A. Antonov[98], J. Antos[144b], F. Anulli[132a], M. Aoki[67], L. Aperio Bella[18], G. Arabidze[91], Y. Arai[67], J.P. Araque[126a], A.T.H. Arce[46], F.A. Arduh[72], J-F. Arguin[95], S. Argyropoulos[64], M. Arik[19a], A.J. Armbruster[31], L.J. Armitage[77], O. Arnaez[31], H. Arnold[49], M. Arratia[29], O. Arslan[22], A. Artamonov[97], G. Artoni[120], S. Artz[84], S. Asai[155], N. Asbah[43], A. Ashkenazi[153], B. Åsman[146a,146b], L. Asquith[149], K. Assamagan[26], R. Astalos[144a], M. Atkinson[165], N.B. Atlay[141], K. Augsten[128], G. Avolio[31], B. Axen[15], M.K. Ayoub[117], G. Azuelos[95,d], M.A. Baak[31], A.E. Baas[59a], M.J. Baca[18], H. Bachacou[136], K. Bachas[74a,74b], M. Backes[31], M. Backhaus[31], P. Bagiacchi[132a,132b], P. Bagnaia[132a,132b], Y. Bai[34a], J.T. Baines[131], O.K. Baker[175], E.M. Baldin[109,c], P. Balek[129], T. Balestri[148], F. Balli[136], W.K. Balunas[122], E. Banas[40], Sw. Banerjee[172,e], A.A.E. Bannoura[174], L. Barak[31], E.L. Barberio[89], D. Barberis[51a,51b], M. Barbero[86], T. Barillari[101], M. Barisonzi[163a,163b], T. Barklow[143], N. Barlow[29], S.L. Barnes[85], B.M. Barnett[131], R.M. Barnett[15], Z. Barnovska[5], A. Baroncelli[134a], G. Barone[24], A.J. Barr[120], L. Barranco Navarro[166], F. Barreiro[83], J. Barreiro Guimarães da Costa[34a], R. Bartoldus[143], A.E. Barton[73], P. Bartos[144a], A. Basalaev[123], A. Bassalat[117], A. Basye[165], R.L. Bates[54], S.J. Batista[158], J.R. Batley[29], M. Battaglia[137], M. Bauce[132a,132b], F. Bauer[136], H.S. Bawa[143,f], J.B. Beacham[111], M.D. Beattie[73], T. Beau[81], P.H. Beauchemin[161], P. Bechtle[22], H.P. Beck[17,g], K. Becker[120], M. Becker[84], M. Beckingham[169], C. Becot[110], A.J. Beddall[19e], A. Beddall[19b], V.A. Bednyakov[66], M. Bedognetti[107], C.P. Bee[148], L.J. Beemster[107], T.A. Beermann[31], M. Begel[26], J.K. Behr[120], C. Belanger-Champagne[88], A.S. Bell[79], W.H. Bell[50], G. Bella[153], L. Bellagamba[21a], A. Bellerive[30], M. Bellomo[87], K. Belotskiy[98], O. Beltramello[31], N.L. Belyaev[98], O. Benary[153], D. Benchekroun[135a], M. Bender[100], K. Bendtz[146a,146b], N. Benekos[10], Y. Benhammou[153], E. Benhar Noccioli[175], J. Benitez[64], J.A. Benitez Garcia[159b], D.P. Benjamin[46], J.R. Bensinger[24], S. Bentvelsen[107], L. Beresford[120], M. Beretta[48], D. Berge[107], E. Bergeaas Kuutmann[164], N. Berger[5], F. Berghaus[168], J. Beringer[15], S. Berlendis[56], N.R. Bernard[87], C. Bernius[110], F.U. Bernlochner[22], T. Berry[78], P. Berta[129], C. Bertella[84], G. Bertoli[146a,146b], F. Bertolucci[124a,124b], I.A. Bertram[73], C. Bertsche[113], D. Bertsche[113], G.J. Besjes[37], O. Bessidskaia Bylund[146a,146b], M. Bessner[43], N. Besson[136], C. Betancourt[49], S. Bethke[101], A.J. Bevan[77], W. Bhimji[15], R.M. Bianchi[125], L. Bianchini[24], M. Bianco[31], O. Biebel[100], D. Biedermann[16], R. Bielski[85], N.V. Biesuz[124a,124b], M. Biglietti[134a], J. Bilbao De Mendizabal[50], H. Bilokon[48], M. Bindi[55], S. Binet[117], A. Bingul[19b], C. Bini[132a,132b], S. Biondi[21a,21b], D.M. Bjergaard[46], C.W. Black[150], J.E. Black[143], K.M. Black[23], D. Blackburn[138], R.E. Blair[6], J.-B. Blanchard[136], J.E. Blanco[78], T. Blazek[144a], I. Bloch[43], C. Blocker[24], W. Blum[84,*], U. Blumenschein[55], S. Blunier[33a],

G.J. Bobbink[107], V.S. Bobrovnikov[109,c], S.S. Bocchetta[82], A. Bocci[46], C. Bock[100], M. Boehler[49], D. Boerner[174], J.A. Bogaerts[31], D. Bogavac[13], A.G. Bogdanchikov[109], C. Bohm[146a], V. Boisvert[78], T. Bold[39a], V. Boldea[27b], A.S. Boldyrev[163a,163c], M. Bomben[81], M. Bona[77], M. Boonekamp[136], A. Borisov[130], G. Borissov[73], J. Bortfeldt[100], D. Bortoletto[120], V. Bortolotto[61a,61b,61c], K. Bos[107], D. Boscherini[21a], M. Bosman[12], J.D. Bossio Sola[28], J. Boudreau[125], J. Bouffard[2], E.V. Bouhova-Thacker[73], D. Boumediene[35], C. Bourdarios[117], N. Bousson[114], S.K. Boutle[54], A. Boveia[31], J. Boyd[31], I.R. Boyko[66], J. Bracinik[18], A. Brandt[8], G. Brandt[55], O. Brandt[59a], U. Bratzler[156], B. Brau[87], J.E. Brau[116], H.M. Braun[174,*], W.D. Breaden Madden[54], K. Brendlinger[122], A.J. Brennan[89], L. Brenner[107], R. Brenner[164], S. Bressler[171], T.M. Bristow[47], D. Britton[54], D. Britzger[43], F.M. Brochu[29], I. Brock[22], R. Brock[91], G. Brooijmans[36], T. Brooks[78], W.K. Brooks[33b], J. Brosamer[15], E. Brost[116], J.H Broughton[18], P.A. Bruckman de Renstrom[40], D. Bruncko[144b], R. Bruneliere[49], A. Bruni[21a], G. Bruni[21a], BH Brunt[29], M. Bruschi[21a], N. Bruscino[22], P. Bryant[32], L. Bryngemark[82], T. Buanes[14], Q. Buat[142], P. Buchholz[141], A.G. Buckley[54], I.A. Budagov[66], F. Buehrer[49], M.K. Bugge[119], O. Bulekov[98], D. Bullock[8], H. Burckhart[31], S. Burdin[75], C.D. Burgard[49], B. Burghgrave[108], K. Burka[40], S. Burke[131], I. Burmeister[44], E. Busato[35], D. Büscher[49], V. Büscher[84], P. Bussey[54], J.M. Butler[23], A.I. Butt[3], C.M. Buttar[54], J.M. Butterworth[79], P. Butti[107], W. Buttinger[26], A. Buzatu[54], A.R. Buzykaev[109,c], S. Cabrera Urbán[166], D. Caforio[128], V.M. Cairo[38a,38b], O. Cakir[4a], N. Calace[50], P. Calafiura[15], A. Calandri[86], G. Calderini[81], P. Calfayan[100], L.P. Caloba[25a], D. Calvet[35], S. Calvet[35], T.P. Calvet[86], R. Camacho Toro[32], S. Camarda[31], P. Camarri[133a,133b], D. Cameron[119], R. Caminal Armadans[165], C. Camincher[56], S. Campana[31], M. Campanelli[79], A. Campoverde[148], V. Canale[104a,104b], A. Canepa[159a], M. Cano Bret[34e], J. Cantero[83], R. Cantrill[126a], T. Cao[41], M.D.M. Capeans Garrido[31], I. Caprini[27b], M. Caprini[27b], M. Capua[38a,38b], R. Caputo[84], R.M. Carbone[36], R. Cardarelli[133a], F. Cardillo[49], T. Carli[31], G. Carlino[104a], L. Carminati[92a,92b], S. Caron[106], E. Carquin[33a], G.D. Carrillo-Montoya[31], J.R. Carter[29], J. Carvalho[126a,126c], D. Casadei[79], M.P. Casado[12,h], M. Casolino[12], D.W. Casper[162], E. Castaneda-Miranda[145a], A. Castelli[107], V. Castillo Gimenez[166], N.F. Castro[126a,i], A. Catinaccio[31], J.R. Catmore[119], A. Cattai[31], J. Caudron[84], V. Cavaliere[165], D. Cavalli[92a], M. Cavalli-Sforza[12], V. Cavasinni[124a,124b], F. Ceradini[134a,134b], L. Cerda Alberich[166], B.C. Cerio[46], A.S. Cerqueira[25b], A. Cerri[149], L. Cerrito[77], F. Cerutti[15], M. Cerv[31], A. Cervelli[17], S.A. Cetin[19d], A. Chafaq[135a], D. Chakraborty[108], I. Chalupkova[129], S.K. Chan[58], Y.L. Chan[61a], P. Chang[165], J.D. Chapman[29], D.G. Charlton[18], A. Chatterjee[50], C.C. Chau[158], C.A. Chavez Barajas[149], S. Che[111], S. Cheatham[73], A. Chegwidden[91], S. Chekanov[6], S.V. Chekulaev[159a], G.A. Chelkov[66,j], M.A. Chelstowska[90], C. Chen[65], H. Chen[26], K. Chen[148], S. Chen[34c], S. Chen[155], X. Chen[34f], Y. Chen[68], H.C. Cheng[90], H.J Cheng[34a], Y. Cheng[32], A. Cheplakov[66], E. Cheremushkina[130], R. Cherkaoui El Moursli[135e], V. Chernyatin[26,*], E. Cheu[7], L. Chevalier[136], V. Chiarella[48], G. Chiarelli[124a,124b], G. Chiodini[74a], A.S. Chisholm[18], A. Chitan[27b], M.V. Chizhov[66], K. Choi[62], A.R. Chomont[35], S. Chouridou[9], B.K.B. Chow[100], V. Christodoulou[79], D. Chromek-Burckhart[31], J. Chudoba[127], A.J. Chuinard[88], J.J. Chwastowski[40], L. Chytka[115], G. Ciapetti[132a,132b], A.K. Ciftci[4a], D. Cinca[54], V. Cindro[76], I.A. Cioara[22], A. Ciocio[15], F. Cirotto[104a,104b], Z.H. Citron[171], M. Ciubancan[27b], A. Clark[50], B.L. Clark[58], P.J. Clark[47], R.N. Clarke[15], C. Clement[146a,146b], Y. Coadou[86], M. Cobal[163a,163c], A. Coccaro[50], J. Cochran[65], L. Coffey[24], L. Colasurdo[106], B. Cole[36], S. Cole[108], A.P. Colijn[107], J. Collot[56], T. Colombo[31], G. Compostella[101], P. Conde Muiño[126a,126b], E. Coniavitis[49], S.H. Connell[145b], I.A. Connelly[78], V. Consorti[49], S. Constantinescu[27b], C. Conta[121a,121b], G. Conti[31], F. Conventi[104a,k], M. Cooke[15], B.D. Cooper[79], A.M. Cooper-Sarkar[120], T. Cornelissen[174], M. Corradi[132a,132b], F. Corriveau[88,l], A. Corso-Radu[162], A. Cortes-Gonzalez[12], G. Cortiana[101], G. Costa[92a], M.J. Costa[166], D. Costanzo[139], G. Cottin[29], G. Cowan[78], B.E. Cox[85], K. Cranmer[110], S.J. Crawley[54], G. Cree[30], S. Crépé-Renaudin[56], F. Crescioli[81], W.A. Cribbs[146a,146b], M. Crispin Ortuzar[120], M. Cristinziani[22], V. Croft[106], G. Crosetti[38a,38b],

T. Cuhadar Donszelmann[139], J. Cummings[175], M. Curatolo[48], J. Cúth[84], C. Cuthbert[150], H. Czirr[141], P. Czodrowski[3], S. D'Auria[54], M. D'Onofrio[75], M.J. Da Cunha Sargedas De Sousa[126a,126b], C. Da Via[85], W. Dabrowski[39a], T. Dai[90], O. Dale[14], F. Dallaire[95], C. Dallapiccola[87], M. Dam[37], J.R. Dandoy[32], N.P. Dang[49], A.C. Daniells[18], N.S. Dann[85], M. Danninger[167], M. Dano Hoffmann[136], V. Dao[49], G. Darbo[51a], S. Darmora[8], J. Dassoulas[3], A. Dattagupta[62], W. Davey[22], C. David[168], T. Davidek[129], M. Davies[153], P. Davison[79], Y. Davygora[59a], E. Dawe[89], I. Dawson[139], R.K. Daya-Ishmukhametova[87], K. De[8], R. de Asmundis[104a], A. De Benedetti[113], S. De Castro[21a,21b], S. De Cecco[81], N. De Groot[106], P. de Jong[107], H. De la Torre[83], F. De Lorenzi[65], D. De Pedis[132a], A. De Salvo[132a], U. De Sanctis[149], A. De Santo[149], J.B. De Vivie De Regie[117], W.J. Dearnaley[73], R. Debbe[26], C. Debenedetti[137], D.V. Dedovich[66], I. Deigaard[107], J. Del Peso[83], T. Del Prete[124a,124b], D. Delgove[117], F. Deliot[136], C.M. Delitzsch[50], M. Deliyergiyev[76], A. Dell'Acqua[31], L. Dell'Asta[23], M. Dell'Orso[124a,124b], M. Della Pietra[104a,k], D. della Volpe[50], M. Delmastro[5], P.A. Delsart[56], C. Deluca[107], D.A. DeMarco[158], S. Demers[175], M. Demichev[66], A. Demilly[81], S.P. Denisov[130], D. Denysiuk[136], D. Derendarz[40], J.E. Derkaoui[135d], F. Derue[81], P. Dervan[75], K. Desch[22], C. Deterre[43], K. Dette[44], P.O. Deviveiros[31], A. Dewhurst[131], S. Dhaliwal[24], A. Di Ciaccio[133a,133b], L. Di Ciaccio[5], W.K. Di Clemente[122], A. Di Domenico[132a,132b], C. Di Donato[132a,132b], A. Di Girolamo[31], B. Di Girolamo[31], A. Di Mattia[152], B. Di Micco[134a,134b], R. Di Nardo[48], A. Di Simone[49], R. Di Sipio[158], D. Di Valentino[30], C. Diaconu[86], M. Diamond[158], F.A. Dias[47], M.A. Diaz[33a], E.B. Diehl[90], J. Dietrich[16], S. Diglio[86], A. Dimitrievska[13], J. Dingfelder[22], P. Dita[27b], S. Dita[27b], F. Dittus[31], F. Djama[86], T. Djobava[52b], J.I. Djuvsland[59a], M.A.B. do Vale[25c], D. Dobos[31], M. Dobre[27b], C. Doglioni[82], T. Dohmae[155], J. Dolejsi[129], Z. Dolezal[129], B.A. Dolgoshein[98,*], M. Donadelli[25d], S. Donati[124a,124b], P. Dondero[121a,121b], J. Donini[35], J. Dopke[131], A. Doria[104a], M.T. Dova[72], A.T. Doyle[54], E. Drechsler[55], M. Dris[10], Y. Du[34d], J. Duarte-Campderros[153], E. Duchovni[171], G. Duckeck[100], O.A. Ducu[27b], D. Duda[107], A. Dudarev[31], L. Duflot[117], L. Duguid[78], M. Dührssen[31], M. Dunford[59a], H. Duran Yildiz[4a], M. Düren[53], A. Durglishvili[52b], D. Duschinger[45], B. Dutta[43], M. Dyndal[39a], C. Eckardt[43], K.M. Ecker[101], R.C. Edgar[90], W. Edson[2], N.C. Edwards[47], T. Eifert[31], G. Eigen[14], K. Einsweiler[15], T. Ekelof[164], M. El Kacimi[135c], V. Ellajosyula[86], M. Ellert[164], S. Elles[5], F. Ellinghaus[174], A.A. Elliot[168], N. Ellis[31], J. Elmsheuser[100], M. Elsing[31], D. Emeliyanov[131], Y. Enari[155], O.C. Endner[84], M. Endo[118], J.S. Ennis[169], J. Erdmann[44], A. Ereditato[17], G. Ernis[174], J. Ernst[2], M. Ernst[26], S. Errede[165], E. Ertel[84], M. Escalier[117], H. Esch[44], C. Escobar[125], B. Esposito[48], A.I. Etienvre[136], E. Etzion[153], H. Evans[62], A. Ezhilov[123], F. Fabbri[21a,21b], L. Fabbri[21a,21b], G. Facini[32], R.M. Fakhrutdinov[130], S. Falciano[132a], R.J. Falla[79], J. Faltova[129], Y. Fang[34a], M. Fanti[92a,92b], A. Farbin[8], A. Farilla[134a], C. Farina[125], T. Farooque[12], S. Farrell[15], S.M. Farrington[169], P. Farthouat[31], F. Fassi[135e], P. Fassnacht[31], D. Fassouliotis[9], M. Faucci Giannelli[78], A. Favareto[51a,51b], W.J. Fawcett[120], L. Fayard[117], O.L. Fedin[123,m], W. Fedorko[167], S. Feigl[119], L. Feligioni[86], C. Feng[34d], E.J. Feng[31], H. Feng[90], A.B. Fenyuk[130], L. Feremenga[8], P. Fernandez Martinez[166], S. Fernandez Perez[12], J. Ferrando[54], A. Ferrari[164], P. Ferrari[107], R. Ferrari[121a], D.E. Ferreira de Lima[54], A. Ferrer[166], D. Ferrere[50], C. Ferretti[90], A. Ferretto Parodi[51a,51b], F. Fiedler[84], A. Filipčič[76], M. Filipuzzi[43], F. Filthaut[106], M. Fincke-Keeler[168], K.D. Finelli[150], M.C.N. Fiolhais[126a,126c], L. Fiorini[166], A. Firan[41], A. Fischer[2], C. Fischer[12], J. Fischer[174], W.C. Fisher[91], N. Flaschel[43], I. Fleck[141], P. Fleischmann[90], G.T. Fletcher[139], G. Fletcher[77], R.R.M. Fletcher[122], T. Flick[174], A. Floderus[82], L.R. Flores Castillo[61a], M.J. Flowerdew[101], G.T. Forcolin[85], A. Formica[136], A. Forti[85], A.G. Foster[18], D. Fournier[117], H. Fox[73], S. Fracchia[12], P. Francavilla[81], M. Franchini[21a,21b], D. Francis[31], L. Franconi[119], M. Franklin[58], M. Frate[162], M. Fraternali[121a,121b], D. Freeborn[79], S.M. Fressard-Batraneanu[31], F. Friedrich[45], D. Froidevaux[31], J.A. Frost[120], C. Fukunaga[156], E. Fullana Torregrosa[84], T. Fusayasu[102], J. Fuster[166], C. Gabaldon[56], O. Gabizon[174], A. Gabrielli[21a,21b], A. Gabrielli[15], G.P. Gach[39a], S. Gadatsch[31], S. Gadomski[50], G. Gagliardi[51a,51b], L.G. Gagnon[95], P. Gagnon[62], C. Galea[106], B. Galhardo[126a,126c], E.J. Gallas[120], B.J. Gallop[131], P. Gallus[128], G. Galster[37], K.K. Gan[111], J. Gao[34b,86], Y. Gao[47],

Y.S. Gao[143,f], F.M. Garay Walls[47], C. García[166], J.E. García Navarro[166], M. Garcia-Sciveres[15], R.W. Gardner[32], N. Garelli[143], V. Garonne[119], A. Gascon Bravo[43], C. Gatti[48], A. Gaudiello[51a,51b], G. Gaudio[121a], B. Gaur[141], L. Gauthier[95], I.L. Gavrilenko[96], C. Gay[167], G. Gaycken[22], E.N. Gazis[10], Z. Gecse[167], C.N.P. Gee[131], Ch. Geich-Gimbel[22], M.P. Geisler[59a], C. Gemme[51a], M.H. Genest[56], C. Geng[34b,n], S. Gentile[132a,132b], S. George[78], D. Gerbaudo[162], A. Gershon[153], S. Ghasemi[141], H. Ghazlane[135b], B. Giacobbe[21a], S. Giagu[132a,132b], P. Giannetti[124a,124b], B. Gibbard[26], S.M. Gibson[78], M. Gignac[167], M. Gilchriese[15], T.P.S. Gillam[29], D. Gillberg[30], G. Gilles[174], D.M. Gingrich[3,d], N. Giokaris[9], M.P. Giordani[163a,163c], F.M. Giorgi[21a], F.M. Giorgi[16], P.F. Giraud[136], P. Giromini[58], D. Giugni[92a], C. Giuliani[101], M. Giulini[59b], B.K. Gjelsten[119], S. Gkaitatzis[154], I. Gkialas[154], E.L. Gkougkousis[117], L.K. Gladilin[99], C. Glasman[83], J. Glatzer[31], P.C.F. Glaysher[47], A. Glazov[43], M. Goblirsch-Kolb[101], J. Godlewski[40], S. Goldfarb[90], T. Golling[50], D. Golubkov[130], A. Gomes[126a,126b,126d], R. Gonçalo[126a], J. Goncalves Pinto Firmino Da Costa[136], L. Gonella[18], A. Gongadze[66], S. González de la Hoz[166], G. Gonzalez Parra[12], S. Gonzalez-Sevilla[50], L. Goossens[31], P.A. Gorbounov[97], H.A. Gordon[26], I. Gorelov[105], B. Gorini[31], E. Gorini[74a,74b], A. Gorišek[76], E. Gornicki[40], A.T. Goshaw[46], C. Gössling[44], M.I. Gostkin[66], C.R. Goudet[117], D. Goujdami[135c], A.G. Goussiou[138], N. Govender[145b], E. Gozani[152], L. Graber[55], I. Grabowska-Bold[39a], P.O.J. Gradin[164], P. Grafström[21a,21b], J. Gramling[50], E. Gramstad[119], S. Grancagnolo[16], V. Gratchev[123], H.M. Gray[31], E. Graziani[134a], Z.D. Greenwood[80,o], C. Grefe[22], K. Gregersen[79], I.M. Gregor[43], P. Grenier[143], K. Grevtsov[5], J. Griffiths[8], A.A. Grillo[137], K. Grimm[73], S. Grinstein[12,p], Ph. Gris[35], J.-F. Grivaz[117], S. Groh[84], J.P. Grohs[45], E. Gross[171], J. Grosse-Knetter[55], G.C. Grossi[80], Z.J. Grout[149], L. Guan[90], W. Guan[172], J. Guenther[128], F. Guescini[50], D. Guest[162], O. Gueta[153], E. Guido[51a,51b], T. Guillemin[5], S. Guindon[2], U. Gul[54], C. Gumpert[31], J. Guo[34e], Y. Guo[34b,n], S. Gupta[120], G. Gustavino[132a,132b], P. Gutierrez[113], N.G. Gutierrez Ortiz[79], C. Gutschow[45], C. Guyot[136], C. Gwenlan[120], C.B. Gwilliam[75], A. Haas[110], C. Haber[15], H.K. Hadavand[8], N. Haddad[135e], A. Hadef[86], P. Haefner[22], S. Hageböck[22], Z. Hajduk[40], H. Hakobyan[176,*], M. Haleem[43], J. Haley[114], D. Hall[120], G. Halladjian[91], G.D. Hallewell[86], K. Hamacher[174], P. Hamal[115], K. Hamano[168], A. Hamilton[145a], G.N. Hamity[139], P.G. Hamnett[43], L. Han[34b], K. Hanagaki[67,q], K. Hanawa[155], M. Hance[137], B. Haney[122], P. Hanke[59a], R. Hanna[136], J.B. Hansen[37], J.D. Hansen[37], M.C. Hansen[22], P.H. Hansen[37], K. Hara[160], A.S. Hard[172], T. Harenberg[174], F. Hariri[117], S. Harkusha[93], R.D. Harrington[47], P.F. Harrison[169], F. Hartjes[107], M. Hasegawa[68], Y. Hasegawa[140], A. Hasib[113], S. Hassani[136], S. Haug[17], R. Hauser[91], L. Hauswald[45], M. Havranek[127], C.M. Hawkes[18], R.J. Hawkings[31], A.D. Hawkins[82], D. Hayden[91], C.P. Hays[120], J.M. Hays[77], H.S. Hayward[75], S.J. Haywood[131], S.J. Head[18], T. Heck[84], V. Hedberg[82], L. Heelan[8], S. Heim[122], T. Heim[15], B. Heinemann[15], J.J. Heinrich[100], L. Heinrich[110], C. Heinz[53], J. Hejbal[127], L. Helary[23], S. Hellman[146a,146b], C. Helsens[31], J. Henderson[120], R.C.W. Henderson[73], Y. Heng[172], S. Henkelmann[167], A.M. Henriques Correia[31], S. Henrot-Versille[117], G.H. Herbert[16], Y. Hernández Jiménez[166], G. Herten[49], R. Hertenberger[100], L. Hervas[31], G.G. Hesketh[79], N.P. Hessey[107], J.W. Hetherly[41], R. Hickling[77], E. Higón-Rodriguez[166], E. Hill[168], J.C. Hill[29], K.H. Hiller[43], S.J. Hillier[18], I. Hinchliffe[15], E. Hines[122], R.R. Hinman[15], M. Hirose[157], D. Hirschbuehl[174], J. Hobbs[148], N. Hod[107], M.C. Hodgkinson[139], P. Hodgson[139], A. Hoecker[31], M.R. Hoeferkamp[105], F. Hoenig[100], M. Hohlfeld[84], D. Hohn[22], T.R. Holmes[15], M. Homann[44], T.M. Hong[125], B.H. Hooberman[165], W.H. Hopkins[116], Y. Horii[103], A.J. Horton[142], J-Y. Hostachy[56], S. Hou[151], A. Hoummada[135a], J. Howard[120], J. Howarth[43], M. Hrabovsky[115], I. Hristova[16], J. Hrivnac[117], T. Hryn'ova[5], A. Hrynevich[94], C. Hsu[145c], P.J. Hsu[151,r], S.-C. Hsu[138], D. Hu[36], Q. Hu[34b], Y. Huang[43], Z. Hubacek[128], F. Hubaut[86], F. Huegging[22], T.B. Huffman[120], E.W. Hughes[36], G. Hughes[73], M. Huhtinen[31], T.A. Hülsing[84], N. Huseynov[66,b], J. Huston[91], J. Huth[58], G. Iacobucci[50], G. Iakovidis[26], I. Ibragimov[141], L. Iconomidou-Fayard[117], E. Ideal[175], Z. Idrissi[135e], P. Iengo[31], O. Igonkina[107], T. Iizawa[170], Y. Ikegami[67], M. Ikeno[67], Y. Ilchenko[32,s], D. Iliadis[154], N. Ilic[143], T. Ince[101],

G. Introzzi[121a,121b], P. Ioannou[9,*], M. Iodice[134a], K. Iordanidou[36], V. Ippolito[58], A. Irles Quiles[166], C. Isaksson[164], M. Ishino[69], M. Ishitsuka[157], R. Ishmukhametov[111], C. Issever[120], S. Istin[19a], F. Ito[160], J.M. Iturbe Ponce[85], R. Iuppa[133a,133b], J. Ivarsson[82], W. Iwanski[40], H. Iwasaki[67], J.M. Izen[42], V. Izzo[104a], S. Jabbar[3], B. Jackson[122], M. Jackson[75], P. Jackson[1], V. Jain[2], K.B. Jakobi[84], K. Jakobs[49], S. Jakobsen[31], T. Jakoubek[127], D.O. Jamin[114], D.K. Jana[80], E. Jansen[79], R. Jansky[63], J. Janssen[22], M. Janus[55], G. Jarlskog[82], N. Javadov[66,b], T. Javůrek[49], F. Jeanneau[136], L. Jeanty[15], J. Jejelava[52a,t], G.-Y. Jeng[150], D. Jennens[89], P. Jenni[49,u], J. Jentzsch[44], C. Jeske[169], S. Jézéquel[5], H. Ji[172], J. Jia[148], H. Jiang[65], Y. Jiang[34b], S. Jiggins[79], J. Jimenez Pena[166], S. Jin[34a], A. Jinaru[27b], O. Jinnouchi[157], P. Johansson[139], K.A. Johns[7], W.J. Johnson[138], K. Jon-And[146a,146b], G. Jones[169], R.W.L. Jones[73], S. Jones[7], T.J. Jones[75], J. Jongmanns[59a], P.M. Jorge[126a,126b], J. Jovicevic[159a], X. Ju[172], A. Juste Rozas[12,p], M.K. Köhler[171], A. Kaczmarska[40], M. Kado[117], H. Kagan[111], M. Kagan[143], S.J. Kahn[86], E. Kajomovitz[46], C.W. Kalderon[120], A. Kaluza[84], S. Kama[41], A. Kamenshchikov[130], N. Kanaya[155], S. Kaneti[29], V.A. Kantserov[98], J. Kanzaki[67], B. Kaplan[110], L.S. Kaplan[172], A. Kapliy[32], D. Kar[145c], K. Karakostas[10], A. Karamaoun[3], N. Karastathis[10], M.J. Kareem[55], E. Karentzos[10], M. Karnevskiy[84], S.N. Karpov[66], Z.M. Karpova[66], K. Karthik[110], V. Kartvelishvili[73], A.N. Karyukhin[130], K. Kasahara[160], L. Kashif[172], R.D. Kass[111], A. Kastanas[14], Y. Kataoka[155], C. Kato[155], A. Katre[50], J. Katzy[43], K. Kawade[103], K. Kawagoe[71], T. Kawamoto[155], G. Kawamura[55], S. Kazama[155], V.F. Kazanin[109,c], R. Keeler[168], R. Kehoe[41], J.S. Keller[43], J.J. Kempster[78], H. Keoshkerian[85], O. Kepka[127], B.P. Kerševan[76], S. Kersten[174], R.A. Keyes[88], F. Khalil-zada[11], H. Khandanyan[146a,146b], A. Khanov[114], A.G. Kharlamov[109,c], T.J. Khoo[29], V. Khovanskiy[97], E. Khramov[66], J. Khubua[52b,v], S. Kido[68], H.Y. Kim[8], S.H. Kim[160], Y.K. Kim[32], N. Kimura[154], O.M. Kind[16], B.T. King[75], M. King[166], S.B. King[167], J. Kirk[131], A.E. Kiryunin[101], T. Kishimoto[68], D. Kisielewska[39a], F. Kiss[49], K. Kiuchi[160], O. Kivernyk[136], E. Kladiva[144b], M.H. Klein[36], M. Klein[75], U. Klein[75], K. Kleinknecht[84], P. Klimek[146a,146b], A. Klimentov[26], R. Klingenberg[44], J.A. Klinger[139], T. Klioutchnikova[31], E.-E. Kluge[59a], P. Kluit[107], S. Kluth[101], J. Knapik[40], E. Kneringer[63], E.B.F.G. Knoops[86], A. Knue[54], A. Kobayashi[155], D. Kobayashi[157], T. Kobayashi[155], M. Kobel[45], M. Kocian[143], P. Kodys[129], T. Koffas[30], E. Koffeman[107], L.A. Kogan[120], T. Kohriki[67], T. Koi[143], H. Kolanoski[16], M. Kolb[59b], I. Koletsou[5], A.A. Komar[96,*], Y. Komori[155], T. Kondo[67], N. Kondrashova[43], K. Köneke[49], A.C. König[106], T. Kono[67,w], R. Konoplich[110,x], N. Konstantinidis[79], R. Kopeliansky[62], S. Koperny[39a], L. Köpke[84], A.K. Kopp[49], K. Korcyl[40], K. Kordas[154], A. Korn[79], A.A. Korol[109,c], I. Korolkov[12], E.V. Korolkova[139], O. Kortner[101], S. Kortner[101], T. Kosek[129], V.V. Kostyukhin[22], V.M. Kotov[66], A. Kotwal[46], A. Kourkoumeli-Charalampidi[154], C. Kourkoumelis[9], V. Kouskoura[26], A. Koutsman[159a], A.B. Kowalewska[40], R. Kowalewski[168], T.Z. Kowalski[39a], W. Kozanecki[136], A.S. Kozhin[130], V.A. Kramarenko[99], G. Kramberger[76], D. Krasnopevtsev[98], A. Krasznahorkay[31], J.K. Kraus[22], A. Kravchenko[26], M. Kretz[59c], J. Kretzschmar[75], K. Kreutzfeldt[53], P. Krieger[158], K. Krizka[32], K. Kroeninger[44], H. Kroha[101], J. Kroll[122], J. Kroseberg[22], J. Krstic[13], U. Kruchonak[66], H. Krüger[22], N. Krumnack[65], A. Kruse[172], M.C. Kruse[46], M. Kruskal[23], T. Kubota[89], H. Kucuk[79], S. Kuday[4b], J.T. Kuechler[174], S. Kuehn[49], A. Kugel[59c], F. Kuger[173], A. Kuhl[137], T. Kuhl[43], V. Kukhtin[66], R. Kukla[136], Y. Kulchitsky[93], S. Kuleshov[33b], M. Kuna[132a,132b], T. Kunigo[69], A. Kupco[127], H. Kurashige[68], Y.A. Kurochkin[93], V. Kus[127], E.S. Kuwertz[168], M. Kuze[157], J. Kvita[115], T. Kwan[168], D. Kyriazopoulos[139], A. La Rosa[101], J.L. La Rosa Navarro[25d], L. La Rotonda[38a,38b], C. Lacasta[166], F. Lacava[132a,132b], J. Lacey[30], H. Lacker[16], D. Lacour[81], V.R. Lacuesta[166], E. Ladygin[66], R. Lafaye[5], B. Laforge[81], T. Lagouri[175], S. Lai[55], S. Lammers[62], W. Lampl[7], E. Lançon[136], U. Landgraf[49], M.P.J. Landon[77], V.S. Lang[59a], J.C. Lange[12], A.J. Lankford[162], F. Lanni[26], K. Lantzsch[22], A. Lanza[121a], S. Laplace[81], C. Lapoire[31], J.F. Laporte[136], T. Lari[92a], F. Lasagni Manghi[21a,21b], M. Lassnig[31], P. Laurelli[48], W. Lavrijsen[15], A.T. Law[137], P. Laycock[75], T. Lazovich[58], M. Lazzaroni[92a,92b], O. Le Dortz[81], E. Le Guirriec[86], E. Le Menedeu[12], E.P. Le Quilleuc[136], M. LeBlanc[168], T. LeCompte[6],

F. Ledroit-Guillon[56], C.A. Lee[26], S.C. Lee[151], L. Lee[1], G. Lefebvre[81], M. Lefebvre[168], F. Legger[100], C. Leggett[15], A. Lehan[75], G. Lehmann Miotto[31], X. Lei[7], W.A. Leight[30], A. Leisos[154,y], A.G. Leister[175], M.A.L. Leite[25d], R. Leitner[129], D. Lellouch[171], B. Lemmer[55], K.J.C. Leney[79], T. Lenz[22], B. Lenzi[31], R. Leone[7], S. Leone[124a,124b], C. Leonidopoulos[47], S. Leontsinis[10], G. Lerner[149], C. Leroy[95], A.A.J. Lesage[136], C.G. Lester[29], M. Levchenko[123], J. Levêque[5], D. Levin[90], L.J. Levinson[171], M. Levy[18], A.M. Leyko[22], M. Leyton[42], B. Li[34b,z], H. Li[148], H.L. Li[32], L. Li[46], L. Li[34e], Q. Li[34a], S. Li[46], X. Li[85], Y. Li[141], Z. Liang[137], H. Liao[35], B. Liberti[133a], A. Liblong[158], P. Lichard[31], K. Lie[165], J. Liebal[22], W. Liebig[14], C. Limbach[22], A. Limosani[150], S.C. Lin[151,aa], T.H. Lin[84], B.E. Lindquist[148], E. Lipeles[122], A. Lipniacka[14], M. Lisovyi[59b], T.M. Liss[165], D. Lissauer[26], A. Lister[167], A.M. Litke[137], B. Liu[151,ab], D. Liu[151], H. Liu[90], H. Liu[26], J. Liu[86], J.B. Liu[34b], K. Liu[86], L. Liu[165], M. Liu[46], M. Liu[34b], Y.L. Liu[34b], Y. Liu[34b], M. Livan[121a,121b], A. Lleres[56], J. Llorente Merino[83], S.L. Lloyd[77], F. Lo Sterzo[151], E. Lobodzinska[43], P. Loch[7], W.S. Lockman[137], F.K. Loebinger[85], A.E. Loevschall-Jensen[37], K.M. Loew[24], A. Loginov[175], T. Lohse[16], K. Lohwasser[43], M. Lokajicek[127], B.A. Long[23], J.D. Long[165], R.E. Long[73], L. Longo[74a,74b], K.A. Looper[111], L. Lopes[126a], D. Lopez Mateos[58], B. Lopez Paredes[139], I. Lopez Paz[12], A. Lopez Solis[81], J. Lorenz[100], N. Lorenzo Martinez[62], M. Losada[20], P.J. Lösel[100], X. Lou[34a], A. Lounis[117], J. Love[6], P.A. Love[73], H. Lu[61a], N. Lu[90], H.J. Lubatti[138], C. Luci[132a,132b], A. Lucotte[56], C. Luedtke[49], F. Luehring[62], W. Lukas[63], L. Luminari[132a], O. Lundberg[146a,146b], B. Lund-Jensen[147], D. Lynn[26], R. Lysak[127], E. Lytken[82], V. Lyubushkin[66], H. Ma[26], L.L. Ma[34d], G. Maccarrone[48], A. Macchiolo[101], C.M. Macdonald[139], B. Maček[76], J. Machado Miguens[122,126b], D. Madaffari[86], R. Madar[35], H.J. Maddocks[164], W.F. Mader[45], A. Madsen[43], J. Maeda[68], S. Maeland[14], T. Maeno[26], A. Maevskiy[99], E. Magradze[55], J. Mahlstedt[107], C. Maiani[117], C. Maidantchik[25a], A.A. Maier[101], T. Maier[100], A. Maio[126a,126b,126d], S. Majewski[116], Y. Makida[67], N. Makovec[117], B. Malaescu[81], Pa. Malecki[40], V.P. Maleev[123], F. Malek[56], U. Mallik[64], D. Malon[6], C. Malone[143], S. Maltezos[10], V.M. Malyshev[109], S. Malyukov[31], J. Mamuzic[43], G. Mancini[48], B. Mandelli[31], L. Mandelli[92a], I. Mandić[76], J. Maneira[126a,126b], L. Manhaes de Andrade Filho[25b], J. Manjarres Ramos[159b], A. Mann[100], B. Mansoulie[136], R. Mantifel[88], M. Mantoani[55], S. Manzoni[92a,92b], L. Mapelli[31], G. Marceca[28], L. March[50], G. Marchiori[81], M. Marcisovsky[127], M. Marjanovic[13], D.E. Marley[90], F. Marroquim[25a], S.P. Marsden[85], Z. Marshall[15], L.F. Marti[17], S. Marti-Garcia[166], B. Martin[91], T.A. Martin[169], V.J. Martin[47], B. Martin dit Latour[14], M. Martinez[12,p], S. Martin-Haugh[131], V.S. Martoiu[27b], A.C. Martyniuk[79], M. Marx[138], F. Marzano[132a], A. Marzin[31], L. Masetti[84], T. Mashimo[155], R. Mashinistov[96], J. Masik[85], A.L. Maslennikov[109,c], I. Massa[21a,21b], L. Massa[21a,21b], P. Mastrandrea[5], A. Mastroberardino[38a,38b], T. Masubuchi[155], P. Mättig[174], J. Mattmann[84], J. Maurer[27b], S.J. Maxfield[75], D.A. Maximov[109,c], R. Mazini[151], S.M. Mazza[92a,92b], N.C. Mc Fadden[105], G. Mc Goldrick[158], S.P. Mc Kee[90], A. McCarn[90], R.L. McCarthy[148], T.G. McCarthy[30], L.I. McClymont[79], K.W. McFarlane[57,*], J.A. Mcfayden[79], G. Mchedlidze[55], S.J. McMahon[131], R.A. McPherson[168,l], M. Medinnis[43], S. Meehan[138], S. Mehlhase[100], A. Mehta[75], K. Meier[59a], C. Meineck[100], B. Meirose[42], B.R. Mellado Garcia[145c], F. Meloni[17], A. Mengarelli[21a,21b], S. Menke[101], E. Meoni[161], K.M. Mercurio[58], S. Mergelmeyer[16], P. Mermod[50], L. Merola[104a,104b], C. Meroni[92a], F.S. Merritt[32], A. Messina[132a,132b], J. Metcalfe[6], A.S. Mete[162], C. Meyer[84], C. Meyer[122], J-P. Meyer[136], J. Meyer[107], H. Meyer Zu Theenhausen[59a], R.P. Middleton[131], S. Miglioranzi[163a,163c], L. Mijović[22], G. Mikenberg[171], M. Mikestikova[127], M. Mikuž[76], M. Milesi[89], A. Milic[31], D.W. Miller[32], C. Mills[47], A. Milov[171], D.A. Milstead[146a,146b], A.A. Minaenko[130], Y. Minami[155], I.A. Minashvili[66], A.I. Mincer[110], B. Mindur[39a], M. Mineev[66], Y. Ming[172], L.M. Mir[12], K.P. Mistry[122], T. Mitani[170], J. Mitrevski[100], V.A. Mitsou[166], A. Miucci[50], P.S. Miyagawa[139], J.U. Mjörnmark[82], T. Moa[146a,146b], K. Mochizuki[86], S. Mohapatra[36], W. Mohr[49], S. Molander[146a,146b], R. Moles-Valls[22], R. Monden[69], M.C. Mondragon[91], K. Mönig[43], J. Monk[37], E. Monnier[86], A. Montalbano[148], J. Montejo Berlingen[31], F. Monticelli[72], S. Monzani[92a,92b], R.W. Moore[3], N. Morange[117], D. Moreno[20], M. Moreno Llácer[55], P. Morettini[51a],

D. Mori[142], T. Mori[155], M. Morii[58], M. Morinaga[155], V. Morisbak[119], S. Moritz[84], A.K. Morley[150], G. Mornacchi[31], J.D. Morris[77], S.S. Mortensen[37], L. Morvaj[148], M. Mosidze[52b], J. Moss[143], K. Motohashi[157], R. Mount[143], E. Mountricha[26], S.V. Mouraviev[96,*], E.J.W. Moyse[87], S. Muanza[86], R.D. Mudd[18], F. Mueller[101], J. Mueller[125], R.S.P. Mueller[100], T. Mueller[29], D. Muenstermann[73], P. Mullen[54], G.A. Mullier[17], F.J. Munoz Sanchez[85], J.A. Murillo Quijada[18], W.J. Murray[169,131], H. Musheghyan[55], A.G. Myagkov[130,ac], M. Myska[128], B.P. Nachman[143], O. Nackenhorst[50], J. Nadal[55], K. Nagai[120], R. Nagai[67,w], Y. Nagai[86], K. Nagano[67], Y. Nagasaka[60], K. Nagata[160], M. Nagel[101], E. Nagy[86], A.M. Nairz[31], Y. Nakahama[31], K. Nakamura[67], T. Nakamura[155], I. Nakano[112], H. Namasivayam[42], R.F. Naranjo Garcia[43], R. Narayan[32], D.I. Narrias Villar[59a], I. Naryshkin[123], T. Naumann[43], G. Navarro[20], R. Nayyar[7], H.A. Neal[90], P.Yu. Nechaeva[96], T.J. Neep[85], P.D. Nef[143], A. Negri[121a,121b], M. Negrini[21a], S. Nektarijevic[106], C. Nellist[117], A. Nelson[162], S. Nemecek[127], P. Nemethy[110], A.A. Nepomuceno[25a], M. Nessi[31,ad], M.S. Neubauer[165], M. Neumann[174], R.M. Neves[110], P. Nevski[26], P.R. Newman[18], D.H. Nguyen[6], R.B. Nickerson[120], R. Nicolaidou[136], B. Nicquevert[31], J. Nielsen[137], A. Nikiforov[16], V. Nikolaenko[130,ac], I. Nikolic-Audit[81], K. Nikolopoulos[18], J.K. Nilsen[119], P. Nilsson[26], Y. Ninomiya[155], A. Nisati[132a], R. Nisius[101], T. Nobe[155], L. Nodulman[6], M. Nomachi[118], I. Nomidis[30], T. Nooney[77], S. Norberg[113], M. Nordberg[31], N. Norjoharuddeen[120], O. Novgorodova[45], S. Nowak[101], M. Nozaki[67], L. Nozka[115], K. Ntekas[10], E. Nurse[79], F. Nuti[89], F. O'grady[7], D.C. O'Neil[142], A.A. O'Rourke[43], V. O'Shea[54], F.G. Oakham[30,d], H. Oberlack[101], T. Obermann[22], J. Ocariz[81], A. Ochi[68], I. Ochoa[36], J.P. Ochoa-Ricoux[33a], S. Oda[71], S. Odaka[67], H. Ogren[62], A. Oh[85], S.H. Oh[46], C.C. Ohm[15], H. Ohman[164], H. Oide[31], H. Okawa[160], Y. Okumura[32], T. Okuyama[67], A. Olariu[27b], L.F. Oleiro Seabra[126a], S.A. Olivares Pino[47], D. Oliveira Damazio[26], A. Olszewski[40], J. Olszowska[40], A. Onofre[126a,126e], K. Onogi[103], P.U.E. Onyisi[32,s], C.J. Oram[159a], M.J. Oreglia[32], Y. Oren[153], D. Orestano[134a,134b], N. Orlando[61b], R.S. Orr[158], B. Osculati[51a,51b], R. Ospanov[85], G. Otero y Garzon[28], H. Otono[71], M. Ouchrif[135d], F. Ould-Saada[119], A. Ouraou[136], K.P. Oussoren[107], Q. Ouyang[34a], A. Ovcharova[15], M. Owen[54], R.E. Owen[18], V.E. Ozcan[19a], N. Ozturk[8], K. Pachal[142], A. Pacheco Pages[12], C. Padilla Aranda[12], M. Pagáčová[49], S. Pagan Griso[15], F. Paige[26], P. Pais[87], K. Pajchel[119], G. Palacino[159b], S. Palestini[31], M. Palka[39b], D. Pallin[35], A. Palma[126a,126b], E.St. Panagiotopoulou[10], C.E. Pandini[81], J.G. Panduro Vazquez[78], P. Pani[146a,146b], S. Panitkin[26], D. Pantea[27b], L. Paolozzi[50], Th.D. Papadopoulou[10], K. Papageorgiou[154], A. Paramonov[6], D. Paredes Hernandez[175], M.A. Parker[29], K.A. Parker[139], F. Parodi[51a,51b], J.A. Parsons[36], U. Parzefall[49], V.R. Pascuzzi[158], E. Pasqualucci[132a], S. Passaggio[51a], F. Pastore[134a,134b,*], Fr. Pastore[78], G. Pásztor[30], S. Pataraia[174], N.D. Patel[150], J.R. Pater[85], T. Pauly[31], J. Pearce[168], B. Pearson[113], L.E. Pedersen[37], M. Pedersen[119], S. Pedraza Lopez[166], R. Pedro[126a,126b], S.V. Peleganchuk[109,c], D. Pelikan[164], O. Penc[127], C. Peng[34a], H. Peng[34b], J. Penwell[62], B.S. Peralva[25b], M.M. Perego[136], D.V. Perepelitsa[26], E. Perez Codina[159a], L. Perini[92a,92b], H. Pernegger[31], S. Perrella[104a,104b], R. Peschke[43], V.D. Peshekhonov[66], K. Peters[31], R.F.Y. Peters[85], B.A. Petersen[31], T.C. Petersen[37], E. Petit[56], A. Petridis[1], C. Petridou[154], P. Petroff[117], E. Petrolo[132a], M. Petrov[120], F. Petrucci[134a,134b], N.E. Pettersson[157], A. Peyaud[136], R. Pezoa[33b], P.W. Phillips[131], G. Piacquadio[143], E. Pianori[169], A. Picazio[87], E. Piccaro[77], M. Piccinini[21a,21b], M.A. Pickering[120], R. Piegaia[28], J.E. Pilcher[32], A.D. Pilkington[85], A.W.J. Pin[85], J. Pina[126a,126b,126d], M. Pinamonti[163a,163c,ae], J.L. Pinfold[3], A. Pingel[37], S. Pires[81], H. Pirumov[43], M. Pitt[171], L. Plazak[144a], M.-A. Pleier[26], V. Pleskot[84], E. Plotnikova[66], P. Plucinski[146a,146b], D. Pluth[65], R. Poettgen[146a,146b], L. Poggioli[117], D. Pohl[22], G. Polesello[121a], A. Poley[43], A. Policicchio[38a,38b], R. Polifka[158], A. Polini[21a], C.S. Pollard[54], V. Polychronakos[26], K. Pommès[31], L. Pontecorvo[132a], B.G. Pope[91], G.A. Popeneciu[27c], D.S. Popovic[13], A. Poppleton[31], S. Pospisil[128], K. Potamianos[15], I.N. Potrap[66], C.J. Potter[29], C.T. Potter[116], G. Poulard[31], J. Poveda[31], V. Pozdnyakov[66], M.E. Pozo Astigarraga[31], P. Pralavorio[86], A. Pranko[15], S. Prell[65], D. Price[85], L.E. Price[6], M. Primavera[74a], S. Prince[88], M. Proissl[47],

K. Prokofiev[61c], F. Prokoshin[33b], S. Protopopescu[26], J. Proudfoot[6], M. Przybycien[39a], D. Puddu[134a,134b], D. Puldon[148], M. Purohit[26,af], P. Puzo[117], J. Qian[90], G. Qin[54], Y. Qin[85], A. Quadt[55], W.B. Quayle[163a,163b], M. Queitsch-Maitland[85], D. Quilty[54], S. Raddum[119], V. Radeka[26], V. Radescu[59b], S.K. Radhakrishnan[148], P. Radloff[116], P. Rados[89], F. Ragusa[92a,92b], G. Rahal[177], S. Rajagopalan[26], M. Rammensee[31], C. Rangel-Smith[164], M.G. Ratti[92a,92b], F. Rauscher[100], S. Rave[84], T. Ravenscroft[54], M. Raymond[31], A.L. Read[119], N.P. Readioff[75], D.M. Rebuzzi[121a,121b], A. Redelbach[173], G. Redlinger[26], R. Reece[137], K. Reeves[42], L. Rehnisch[16], J. Reichert[122], H. Reisin[28], C. Rembser[31], H. Ren[34a], M. Rescigno[132a], S. Resconi[92a], O.L. Rezanova[109,c], P. Reznicek[129], R. Rezvani[95], R. Richter[101], S. Richter[79], E. Richter-Was[39b], O. Ricken[22], M. Ridel[81], P. Rieck[16], C.J. Riegel[174], J. Rieger[55], O. Rifki[113], M. Rijssenbeek[148], A. Rimoldi[121a,121b], L. Rinaldi[21a], B. Ristić[50], E. Ritsch[31], I. Riu[12], F. Rizatdinova[114], E. Rizvi[77], C. Rizzi[12], S.H. Robertson[88,l], A. Robichaud-Veronneau[88], D. Robinson[29], J.E.M. Robinson[43], A. Robson[54], C. Roda[124a,124b], Y. Rodina[86], A. Rodriguez Perez[12], D. Rodriguez Rodriguez[166], S. Roe[31], C.S. Rogan[58], O. Røhne[119], A. Romaniouk[98], M. Romano[21a,21b], S.M. Romano Saez[35], E. Romero Adam[166], N. Rompotis[138], M. Ronzani[49], L. Roos[81], E. Ros[166], S. Rosati[132a], K. Rosbach[49], P. Rose[137], O. Rosenthal[141], V. Rossetti[146a,146b], E. Rossi[104a,104b], L.P. Rossi[51a], J.H.N. Rosten[29], R. Rosten[138], M. Rotaru[27b], I. Roth[171], J. Rothberg[138], D. Rousseau[117], C.R. Royon[136], A. Rozanov[86], Y. Rozen[152], X. Ruan[145c], F. Rubbo[143], I. Rubinskiy[43], V.I. Rud[99], M.S. Rudolph[158], F. Rühr[49], A. Ruiz-Martinez[31], Z. Rurikova[49], N.A. Rusakovich[66], A. Ruschke[100], H.L. Russell[138], J.P. Rutherfoord[7], N. Ruthmann[31], Y.F. Ryabov[123], M. Rybar[165], G. Rybkin[117], S. Ryu[6], A. Ryzhov[130], A.F. Saavedra[150], G. Sabato[107], S. Sacerdoti[28], H.F-W. Sadrozinski[137], R. Sadykov[66], F. Safai Tehrani[132a], P. Saha[108], M. Sahinsoy[59a], M. Saimpert[136], T. Saito[155], H. Sakamoto[155], Y. Sakurai[170], G. Salamanna[134a,134b], A. Salamon[133a,133b], J.E. Salazar Loyola[33b], D. Salek[107], P.H. Sales De Bruin[138], D. Salihagic[101], A. Salnikov[143], J. Salt[166], D. Salvatore[38a,38b], F. Salvatore[149], A. Salvucci[61a], A. Salzburger[31], D. Sammel[49], D. Sampsonidis[154], A. Sanchez[104a,104b], J. Sánchez[166], V. Sanchez Martinez[166], H. Sandaker[119], R.L. Sandbach[77], H.G. Sander[84], M.P. Sanders[100], M. Sandhoff[174], C. Sandoval[20], R. Sandstroem[101], D.P.C. Sankey[131], M. Sannino[51a,51b], A. Sansoni[48], C. Santoni[35], R. Santonico[133a,133b], H. Santos[126a], I. Santoyo Castillo[149], K. Sapp[125], A. Sapronov[66], J.G. Saraiva[126a,126d], B. Sarrazin[22], O. Sasaki[67], Y. Sasaki[155], K. Sato[160], G. Sauvage[5,*], E. Sauvan[5], G. Savage[78], P. Savard[158,d], C. Sawyer[131], L. Sawyer[80,o], J. Saxon[32], C. Sbarra[21a], A. Sbrizzi[21a,21b], T. Scanlon[79], D.A. Scannicchio[162], M. Scarcella[150], V. Scarfone[38a,38b], J. Schaarschmidt[171], P. Schacht[101], D. Schaefer[31], R. Schaefer[43], J. Schaeffer[84], S. Schaepe[22], S. Schaetzel[59b], U. Schäfer[84], A.C. Schaffer[117], D. Schaile[100], R.D. Schamberger[148], V. Scharf[59a], V.A. Schegelsky[123], D. Scheirich[129], M. Schernau[162], C. Schiavi[51a,51b], C. Schillo[49], M. Schioppa[38a,38b], S. Schlenker[31], K. Schmieden[31], C. Schmitt[84], S. Schmitt[43], S. Schmitz[84], B. Schneider[159a], Y.J. Schnellbach[75], U. Schnoor[49], L. Schoeffel[136], A. Schoening[59b], B.D. Schoenrock[91], E. Schopf[22], A.L.S. Schorlemmer[44], M. Schott[84], D. Schouten[159a], J. Schovancova[8], S. Schramm[50], M. Schreyer[173], N. Schuh[84], M.J. Schultens[22], H.-C. Schultz-Coulon[59a], H. Schulz[16], M. Schumacher[49], B.A. Schumm[137], Ph. Schune[136], C. Schwanenberger[85], A. Schwartzman[143], T.A. Schwarz[90], Ph. Schwegler[101], H. Schweiger[85], Ph. Schwemling[136], R. Schwienhorst[91], J. Schwindling[136], T. Schwindt[22], G. Sciolla[24], F. Scuri[124a,124b], F. Scutti[89], J. Searcy[90], P. Seema[22], S.C. Seidel[105], A. Seiden[137], F. Seifert[128], J.M. Seixas[25a], G. Sekhniaidze[104a], K. Sekhon[90], S.J. Sekula[41], D.M. Seliverstov[123,*], N. Semprini-Cesari[21a,21b], C. Serfon[119], L. Serin[117], L. Serkin[163a,163b], M. Sessa[134a,134b], R. Seuster[159a], H. Severini[113], T. Sfiligoj[76], F. Sforza[31], A. Sfyrla[50], E. Shabalina[55], N.W. Shaikh[146a,146b], L.Y. Shan[34a], R. Shang[165], J.T. Shank[23], M. Shapiro[15], P.B. Shatalov[97], K. Shaw[163a,163b], S.M. Shaw[85], A. Shcherbakova[146a,146b], C.Y. Shehu[149], P. Sherwood[79], L. Shi[151,ag], S. Shimizu[68], C.O. Shimmin[162], M. Shimojima[102], M. Shiyakova[66,ah], A. Shmeleva[96], D. Shoaleh Saadi[95], M.J. Shochet[32], S. Shojaii[92a,92b], S. Shrestha[111], E. Shulga[98], M.A. Shupe[7], P. Sicho[127], P.E. Sidebo[147], O. Sidiropoulou[173], D. Sidorov[114],

A. Sidoti[21a,21b], F. Siegert[45], Dj. Sijacki[13], J. Silva[126a,126d], S.B. Silverstein[146a], V. Simak[128], O. Simard[5], Lj. Simic[13], S. Simion[117], E. Simioni[84], B. Simmons[79], D. Simon[35], M. Simon[84], P. Sinervo[158], N.B. Sinev[116], M. Sioli[21a,21b], G. Siragusa[173], S.Yu. Sivoklokov[99], J. Sjölin[146a,146b], T.B. Sjursen[14], M.B. Skinner[73], H.P. Skottowe[58], P. Skubic[113], M. Slater[18], T. Slavicek[128], M. Slawinska[107], K. Sliwa[161], R. Slovak[129], V. Smakhtin[171], B.H. Smart[5], L. Smestad[14], S.Yu. Smirnov[98], Y. Smirnov[98], L.N. Smirnova[99,ai], O. Smirnova[82], M.N.K. Smith[36], R.W. Smith[36], M. Smizanska[73], K. Smolek[128], A.A. Snesarev[96], G. Snidero[77], S. Snyder[26], R. Sobie[168,l], F. Socher[45], A. Soffer[153], D.A. Soh[151,ag], G. Sokhrannyi[76], C.A. Solans Sanchez[31], M. Solar[128], E.Yu. Soldatov[98], U. Soldevila[166], A.A. Solodkov[130], A. Soloshenko[66], O.V. Solovyanov[130], V. Solovyev[123], P. Sommer[49], H. Son[161], H.Y. Song[34b,z], A. Sood[15], A. Sopczak[128], V. Sopko[128], V. Sorin[12], D. Sosa[59b], C.L. Sotiropoulou[124a,124b], R. Soualah[163a,163c], A.M. Soukharev[109,c], D. South[43], B.C. Sowden[78], S. Spagnolo[74a,74b], M. Spalla[124a,124b], M. Spangenberg[169], F. Spanò[78], D. Sperlich[16], F. Spettel[101], R. Spighi[21a], G. Spigo[31], L.A. Spiller[89], M. Spousta[129], R.D. St. Denis[54,*], A. Stabile[92a], S. Staerz[31], J. Stahlman[122], R. Stamen[59a], S. Stamm[16], E. Stanecka[40], R.W. Stanek[6], C. Stanescu[134a], M. Stanescu-Bellu[43], M.M. Stanitzki[43], S. Stapnes[119], E.A. Starchenko[130], G.H. Stark[32], J. Stark[56], P. Staroba[127], P. Starovoitov[59a], R. Staszewski[40], P. Steinberg[26], B. Stelzer[142], H.J. Stelzer[31], O. Stelzer-Chilton[159a], H. Stenzel[53], G.A. Stewart[54], J.A. Stillings[22], M.C. Stockton[88], M. Stoebe[88], G. Stoicea[27b], P. Stolte[55], S. Stonjek[101], A.R. Stradling[8], A. Straessner[45], M.E. Stramaglia[17], J. Strandberg[147], S. Strandberg[146a,146b], A. Strandlie[119], M. Strauss[113], P. Strizenec[144b], R. Ströhmer[173], D.M. Strom[116], R. Stroynowski[41], A. Strubig[106], S.A. Stucci[17], B. Stugu[14], N.A. Styles[43], D. Su[143], J. Su[125], R. Subramaniam[80], S. Suchek[59a], Y. Sugaya[118], M. Suk[128], V.V. Sulin[96], S. Sultansoy[4c], T. Sumida[69], S. Sun[58], X. Sun[34a], J.E. Sundermann[49], K. Suruliz[149], G. Susinno[38a,38b], M.R. Sutton[149], S. Suzuki[67], M. Svatos[127], M. Swiatlowski[32], I. Sykora[144a], T. Sykora[129], D. Ta[49], C. Taccini[134a,134b], K. Tackmann[43], J. Taenzer[158], A. Taffard[162], R. Tafirout[159a], N. Taiblum[153], H. Takai[26], R. Takashima[70], H. Takeda[68], T. Takeshita[140], Y. Takubo[67], M. Talby[86], A.A. Talyshev[109,c], J.Y.C. Tam[173], K.G. Tan[89], J. Tanaka[155], R. Tanaka[117], S. Tanaka[67], B.B. Tannenwald[111], S. Tapia Araya[33b], S. Tapprogge[84], S. Tarem[152], G.F. Tartarelli[92a], P. Tas[129], M. Tasevsky[127], T. Tashiro[69], E. Tassi[38a,38b], A. Tavares Delgado[126a,126b], Y. Tayalati[135d], A.C. Taylor[105], G.N. Taylor[89], P.T.E. Taylor[89], W. Taylor[159b], F.A. Teischinger[31], P. Teixeira-Dias[78], K.K. Temming[49], D. Temple[142], H. Ten Kate[31], P.K. Teng[151], J.J. Teoh[118], F. Tepel[174], S. Terada[67], K. Terashi[155], J. Terron[83], S. Terzo[101], M. Testa[48], R.J. Teuscher[158,l], T. Theveneaux-Pelzer[86], J.P. Thomas[18], J. Thomas-Wilsker[78], E.N. Thompson[36], P.D. Thompson[18], R.J. Thompson[85], A.S. Thompson[54], L.A. Thomsen[175], E. Thomson[122], M. Thomson[29], M.J. Tibbetts[15], R.E. Ticse Torres[86], V.O. Tikhomirov[96,aj], Yu.A. Tikhonov[109,c], S. Timoshenko[98], P. Tipton[175], S. Tisserant[86], K. Todome[157], T. Todorov[5,*], S. Todorova-Nova[129], J. Tojo[71], S. Tokár[144a], K. Tokushuku[67], E. Tolley[58], L. Tomlinson[85], M. Tomoto[103], L. Tompkins[143,ak], K. Toms[105], B. Tong[58], E. Torrence[116], H. Torres[142], E. Torró Pastor[138], J. Toth[86,al], F. Touchard[86], D.R. Tovey[139], T. Trefzger[173], L. Tremblet[31], A. Tricoli[31], I.M. Trigger[159a], S. Trincaz-Duvoid[81], M.F. Tripiana[12], W. Trischuk[158], B. Trocmé[56], A. Trofymov[43], C. Troncon[92a], M. Trottier-McDonald[15], M. Trovatelli[168], L. Truong[163a,163b], M. Trzebinski[40], A. Trzupek[40], J.C-L. Tseng[120], P.V. Tsiareshka[93], G. Tsipolitis[10], N. Tsirintanis[9], S. Tsiskaridze[12], V. Tsiskaridze[49], E.G. Tskhadadze[52a], K.M. Tsui[61a], I.I. Tsukerman[97], V. Tsulaia[15], S. Tsuno[67], D. Tsybychev[148], A. Tudorache[27b], V. Tudorache[27b], A.N. Tuna[58], S.A. Tupputi[21a,21b], S. Turchikhin[99,ai], D. Turecek[128], D. Turgeman[171], R. Turra[92a,92b], A.J. Turvey[41], P.M. Tuts[36], M. Tylmad[146a,146b], M. Tyndel[131], G. Ucchielli[21a,21b], I. Ueda[155], R. Ueno[30], M. Ughetto[146a,146b], F. Ukegawa[160], G. Unal[31], A. Undrus[26], G. Unel[162], F.C. Ungaro[89], Y. Unno[67], C. Unverdorben[100], J. Urban[144b], P. Urquijo[89], P. Urrejola[84], G. Usai[8], A. Usanova[63], L. Vacavant[86], V. Vacek[128], B. Vachon[88], C. Valderanis[84], E. Valdes Santurio[146a,146b], N. Valencic[107], S. Valentinetti[21a,21b], A. Valero[166], L. Valery[12], S. Valkar[129], S. Vallecorsa[50], J.A. Valls Ferrer[166],

W. Van Den Wollenberg[107], P.C. Van Der Deijl[107], R. van der Geer[107], H. van der Graaf[107], N. van Eldik[152], P. van Gemmeren[6], J. Van Nieuwkoop[142], I. van Vulpen[107], M.C. van Woerden[31], M. Vanadia[132a,132b], W. Vandelli[31], R. Vanguri[122], A. Vaniachine[6], P. Vankov[107], G. Vardanyan[176], R. Vari[132a], E.W. Varnes[7], T. Varol[41], D. Varouchas[81], A. Vartapetian[8], K.E. Varvell[150], F. Vazeille[35], T. Vazquez Schroeder[88], J. Veatch[7], L.M. Veloce[158], F. Veloso[126a,126c], S. Veneziano[132a], A. Ventura[74a,74b], M. Venturi[168], N. Venturi[158], A. Venturini[24], V. Vercesi[121a], M. Verducci[132a,132b], W. Verkerke[107], J.C. Vermeulen[107], A. Vest[45,am], M.C. Vetterli[142,d], O. Viazlo[82], I. Vichou[165], T. Vickey[139], O.E. Vickey Boeriu[139], G.H.A. Viehhauser[120], S. Viel[15], R. Vigne[63], M. Villa[21a,21b], M. Villaplana Perez[92a,92b], E. Vilucchi[48], M.G. Vincter[30], V.B. Vinogradov[66], C. Vittori[21a,21b], I. Vivarelli[149], S. Vlachos[10], M. Vlasak[128], M. Vogel[174], P. Vokac[128], G. Volpi[124a,124b], M. Volpi[89], H. von der Schmitt[101], E. von Toerne[22], V. Vorobel[129], K. Vorobev[98], M. Vos[166], R. Voss[31], J.H. Vossebeld[75], N. Vranjes[13], M. Vranjes Milosavljevic[13], V. Vrba[127], M. Vreeswijk[107], R. Vuillermet[31], I. Vukotic[32], Z. Vykydal[128], P. Wagner[22], W. Wagner[174], H. Wahlberg[72], S. Wahrmund[45], J. Wakabayashi[103], J. Walder[73], R. Walker[100], W. Walkowiak[141], V. Wallangen[146a,146b], C. Wang[151], C. Wang[34d,86], F. Wang[172], H. Wang[15], H. Wang[41], J. Wang[43], J. Wang[150], K. Wang[88], R. Wang[6], S.M. Wang[151], T. Wang[22], T. Wang[36], X. Wang[175], C. Wanotayaroj[116], A. Warburton[88], C.P. Ward[29], D.R. Wardrope[79], A. Washbrook[47], P.M. Watkins[18], A.T. Watson[18], I.J. Watson[150], M.F. Watson[18], G. Watts[138], S. Watts[85], B.M. Waugh[79], S. Webb[84], M.S. Weber[17], S.W. Weber[173], J.S. Webster[6], A.R. Weidberg[120], B. Weinert[62], J. Weingarten[55], C. Weiser[49], H. Weits[107], P.S. Wells[31], T. Wenaus[26], T. Wengler[31], S. Wenig[31], N. Wermes[22], M. Werner[49], P. Werner[31], M. Wessels[59a], J. Wetter[161], K. Whalen[116], N.L. Whallon[138], A.M. Wharton[73], A. White[8], M.J. White[1], R. White[33b], S. White[124a,124b], D. Whiteson[162], F.J. Wickens[131], W. Wiedenmann[172], M. Wielers[131], P. Wienemann[22], C. Wiglesworth[37], L.A.M. Wiik-Fuchs[22], A. Wildauer[101], H.G. Wilkens[31], H.H. Williams[122], S. Williams[107], C. Willis[91], S. Willocq[87], J.A. Wilson[18], I. Wingerter-Seez[5], F. Winklmeier[116], O.J. Winston[149], B.T. Winter[22], M. Wittgen[143], J. Wittkowski[100], S.J. Wollstadt[84], M.W. Wolter[40], H. Wolters[126a,126c], B.K. Wosiek[40], J. Wotschack[31], M.J. Woudstra[85], K.W. Wozniak[40], M. Wu[56], M. Wu[32], S.L. Wu[172], X. Wu[50], Y. Wu[90], T.R. Wyatt[85], B.M. Wynne[47], S. Xella[37], D. Xu[34a], L. Xu[26], B. Yabsley[150], S. Yacoob[145a], R. Yakabe[68], D. Yamaguchi[157], Y. Yamaguchi[118], A. Yamamoto[67], S. Yamamoto[155], T. Yamanaka[155], K. Yamauchi[103], Y. Yamazaki[68], Z. Yan[23], H. Yang[34e], H. Yang[172], Y. Yang[151], Z. Yang[14], W-M. Yao[15], Y.C. Yap[81], Y. Yasu[67], E. Yatsenko[5], K.H. Yau Wong[22], J. Ye[41], S. Ye[26], I. Yeletskikh[66], A.L. Yen[58], E. Yildirim[43], K. Yorita[170], R. Yoshida[6], K. Yoshihara[122], C. Young[143], C.J.S. Young[31], S. Youssef[23], D.R. Yu[15], J. Yu[8], J.M. Yu[90], J. Yu[65], L. Yuan[68], S.P.Y. Yuen[22], I. Yusuff[29,an], B. Zabinski[40], R. Zaidan[34d], A.M. Zaitsev[130,ac], N. Zakharchuk[43], J. Zalieckas[14], A. Zaman[148], S. Zambito[58], L. Zanello[132a,132b], D. Zanzi[89], C. Zeitnitz[174], M. Zeman[128], A. Zemla[39a], J.C. Zeng[165], Q. Zeng[143], K. Zengel[24], O. Zenin[130], T. Ženiš[144a], D. Zerwas[117], D. Zhang[90], F. Zhang[172], G. Zhang[34b,z], H. Zhang[34c], J. Zhang[6], L. Zhang[49], R. Zhang[22], R. Zhang[34b,ao], X. Zhang[34d], Z. Zhang[117], X. Zhao[41], Y. Zhao[34d,117], Z. Zhao[34b], A. Zhemchugov[66], J. Zhong[120], B. Zhou[90], C. Zhou[46], L. Zhou[36], L. Zhou[41], M. Zhou[148], N. Zhou[34f], C.G. Zhu[34d], H. Zhu[34a], J. Zhu[90], Y. Zhu[34b], X. Zhuang[34a], K. Zhukov[96], A. Zibell[173], D. Zieminska[62], N.I. Zimine[66], C. Zimmermann[84], S. Zimmermann[49], Z. Zinonos[55], M. Zinser[84], M. Ziolkowski[141], L. Živković[13], G. Zobernig[172], A. Zoccoli[21a,21b], M. zur Nedden[16], G. Zurzolo[104a,104b], L. Zwalinski[31].

[1] Department of Physics, University of Adelaide, Adelaide, Australia
[2] Physics Department, SUNY Albany, Albany NY, United States of America
[3] Department of Physics, University of Alberta, Edmonton AB, Canada
[4] (a) Department of Physics, Ankara University, Ankara; (b) Istanbul Aydin University, Istanbul; (c) Division of Physics, TOBB University of Economics and Technology, Ankara, Turkey

[5] LAPP, CNRS/IN2P3 and Université Savoie Mont Blanc, Annecy-le-Vieux, France
[6] High Energy Physics Division, Argonne National Laboratory, Argonne IL, United States of America
[7] Department of Physics, University of Arizona, Tucson AZ, United States of America
[8] Department of Physics, The University of Texas at Arlington, Arlington TX, United States of America
[9] Physics Department, University of Athens, Athens, Greece
[10] Physics Department, National Technical University of Athens, Zografou, Greece
[11] Institute of Physics, Azerbaijan Academy of Sciences, Baku, Azerbaijan
[12] Institut de Física d'Altes Energies (IFAE), The Barcelona Institute of Science and Technology, Barcelona, Spain, Spain
[13] Institute of Physics, University of Belgrade, Belgrade, Serbia
[14] Department for Physics and Technology, University of Bergen, Bergen, Norway
[15] Physics Division, Lawrence Berkeley National Laboratory and University of California, Berkeley CA, United States of America
[16] Department of Physics, Humboldt University, Berlin, Germany
[17] Albert Einstein Center for Fundamental Physics and Laboratory for High Energy Physics, University of Bern, Bern, Switzerland
[18] School of Physics and Astronomy, University of Birmingham, Birmingham, United Kingdom
[19] [(a)] Department of Physics, Bogazici University, Istanbul; [(b)] Department of Physics Engineering, Gaziantep University, Gaziantep; [(d)] Istanbul Bilgi University, Faculty of Engineering and Natural Sciences, Istanbul,Turkey; [(e)] Bahcesehir University, Faculty of Engineering and Natural Sciences, Istanbul, Turkey, Turkey
[20] Centro de Investigaciones, Universidad Antonio Narino, Bogota, Colombia
[21] [(a)] INFN Sezione di Bologna; [(b)] Dipartimento di Fisica e Astronomia, Università di Bologna, Bologna, Italy
[22] Physikalisches Institut, University of Bonn, Bonn, Germany
[23] Department of Physics, Boston University, Boston MA, United States of America
[24] Department of Physics, Brandeis University, Waltham MA, United States of America
[25] [(a)] Universidade Federal do Rio De Janeiro COPPE/EE/IF, Rio de Janeiro; [(b)] Electrical Circuits Department, Federal University of Juiz de Fora (UFJF), Juiz de Fora; [(c)] Federal University of Sao Joao del Rei (UFSJ), Sao Joao del Rei; [(d)] Instituto de Fisica, Universidade de Sao Paulo, Sao Paulo, Brazil
[26] Physics Department, Brookhaven National Laboratory, Upton NY, United States of America
[27] [(a)] Transilvania University of Brasov, Brasov, Romania; [(b)] National Institute of Physics and Nuclear Engineering, Bucharest; [(c)] National Institute for Research and Development of Isotopic and Molecular Technologies, Physics Department, Cluj Napoca; [(d)] University Politehnica Bucharest, Bucharest; [(e)] West University in Timisoara, Timisoara, Romania
[28] Departamento de Física, Universidad de Buenos Aires, Buenos Aires, Argentina
[29] Cavendish Laboratory, University of Cambridge, Cambridge, United Kingdom
[30] Department of Physics, Carleton University, Ottawa ON, Canada
[31] CERN, Geneva, Switzerland
[32] Enrico Fermi Institute, University of Chicago, Chicago IL, United States of America
[33] [(a)] Departamento de Física, Pontificia Universidad Católica de Chile, Santiago; [(b)] Departamento de Física, Universidad Técnica Federico Santa María, Valparaíso, Chile
[34] [(a)] Institute of High Energy Physics, Chinese Academy of Sciences, Beijing; [(b)] Department of Modern Physics, University of Science and Technology of China, Anhui; [(c)] Department of Physics, Nanjing University, Jiangsu; [(d)] School of Physics, Shandong University, Shandong; [(e)] Department of Physics and Astronomy, Shanghai Key Laboratory for Particle Physics and Cosmology, Shanghai Jiao Tong University, Shanghai; (also affiliated with PKU-CHEP); [(f)] Physics Department, Tsinghua

University, Beijing 100084, China
[35] Laboratoire de Physique Corpusculaire, Clermont Université and Université Blaise Pascal and CNRS/IN2P3, Clermont-Ferrand, France
[36] Nevis Laboratory, Columbia University, Irvington NY, United States of America
[37] Niels Bohr Institute, University of Copenhagen, Kobenhavn, Denmark
[38] [(a)] INFN Gruppo Collegato di Cosenza, Laboratori Nazionali di Frascati; [(b)] Dipartimento di Fisica, Università della Calabria, Rende, Italy
[39] [(a)] AGH University of Science and Technology, Faculty of Physics and Applied Computer Science, Krakow; [(b)] Marian Smoluchowski Institute of Physics, Jagiellonian University, Krakow, Poland
[40] Institute of Nuclear Physics Polish Academy of Sciences, Krakow, Poland
[41] Physics Department, Southern Methodist University, Dallas TX, United States of America
[42] Physics Department, University of Texas at Dallas, Richardson TX, United States of America
[43] DESY, Hamburg and Zeuthen, Germany
[44] Institut für Experimentelle Physik IV, Technische Universität Dortmund, Dortmund, Germany
[45] Institut für Kern- und Teilchenphysik, Technische Universität Dresden, Dresden, Germany
[46] Department of Physics, Duke University, Durham NC, United States of America
[47] SUPA - School of Physics and Astronomy, University of Edinburgh, Edinburgh, United Kingdom
[48] INFN Laboratori Nazionali di Frascati, Frascati, Italy
[49] Fakultät für Mathematik und Physik, Albert-Ludwigs-Universität, Freiburg, Germany
[50] Section de Physique, Université de Genève, Geneva, Switzerland
[51] [(a)] INFN Sezione di Genova; [(b)] Dipartimento di Fisica, Università di Genova, Genova, Italy
[52] [(a)] E. Andronikashvili Institute of Physics, Iv. Javakhishvili Tbilisi State University, Tbilisi; [(b)] High Energy Physics Institute, Tbilisi State University, Tbilisi, Georgia
[53] II Physikalisches Institut, Justus-Liebig-Universität Giessen, Giessen, Germany
[54] SUPA - School of Physics and Astronomy, University of Glasgow, Glasgow, United Kingdom
[55] II Physikalisches Institut, Georg-August-Universität, Göttingen, Germany
[56] Laboratoire de Physique Subatomique et de Cosmologie, Université Grenoble-Alpes, CNRS/IN2P3, Grenoble, France
[57] Department of Physics, Hampton University, Hampton VA, United States of America
[58] Laboratory for Particle Physics and Cosmology, Harvard University, Cambridge MA, United States of America
[59] [(a)] Kirchhoff-Institut für Physik, Ruprecht-Karls-Universität Heidelberg, Heidelberg; [(b)] Physikalisches Institut, Ruprecht-Karls-Universität Heidelberg, Heidelberg; [(c)] ZITI Institut für technische Informatik, Ruprecht-Karls-Universität Heidelberg, Mannheim, Germany
[60] Faculty of Applied Information Science, Hiroshima Institute of Technology, Hiroshima, Japan
[61] [(a)] Department of Physics, The Chinese University of Hong Kong, Shatin, N.T., Hong Kong; [(b)] Department of Physics, The University of Hong Kong, Hong Kong; [(c)] Department of Physics, The Hong Kong University of Science and Technology, Clear Water Bay, Kowloon, Hong Kong, China
[62] Department of Physics, Indiana University, Bloomington IN, United States of America
[63] Institut für Astro- und Teilchenphysik, Leopold-Franzens-Universität, Innsbruck, Austria
[64] University of Iowa, Iowa City IA, United States of America
[65] Department of Physics and Astronomy, Iowa State University, Ames IA, United States of America
[66] Joint Institute for Nuclear Research, JINR Dubna, Dubna, Russia
[67] KEK, High Energy Accelerator Research Organization, Tsukuba, Japan
[68] Graduate School of Science, Kobe University, Kobe, Japan
[69] Faculty of Science, Kyoto University, Kyoto, Japan
[70] Kyoto University of Education, Kyoto, Japan

[71] Department of Physics, Kyushu University, Fukuoka, Japan
[72] Instituto de Física La Plata, Universidad Nacional de La Plata and CONICET, La Plata, Argentina
[73] Physics Department, Lancaster University, Lancaster, United Kingdom
[74] [(a)] INFN Sezione di Lecce; [(b)] Dipartimento di Matematica e Fisica, Università del Salento, Lecce, Italy
[75] Oliver Lodge Laboratory, University of Liverpool, Liverpool, United Kingdom
[76] Department of Physics, Jožef Stefan Institute and University of Ljubljana, Ljubljana, Slovenia
[77] School of Physics and Astronomy, Queen Mary University of London, London, United Kingdom
[78] Department of Physics, Royal Holloway University of London, Surrey, United Kingdom
[79] Department of Physics and Astronomy, University College London, London, United Kingdom
[80] Louisiana Tech University, Ruston LA, United States of America
[81] Laboratoire de Physique Nucléaire et de Hautes Energies, UPMC and Université Paris-Diderot and CNRS/IN2P3, Paris, France
[82] Fysiska institutionen, Lunds universitet, Lund, Sweden
[83] Departamento de Fisica Teorica C-15, Universidad Autonoma de Madrid, Madrid, Spain
[84] Institut für Physik, Universität Mainz, Mainz, Germany
[85] School of Physics and Astronomy, University of Manchester, Manchester, United Kingdom
[86] CPPM, Aix-Marseille Université and CNRS/IN2P3, Marseille, France
[87] Department of Physics, University of Massachusetts, Amherst MA, United States of America
[88] Department of Physics, McGill University, Montreal QC, Canada
[89] School of Physics, University of Melbourne, Victoria, Australia
[90] Department of Physics, The University of Michigan, Ann Arbor MI, United States of America
[91] Department of Physics and Astronomy, Michigan State University, East Lansing MI, United States of America
[92] [(a)] INFN Sezione di Milano; [(b)] Dipartimento di Fisica, Università di Milano, Milano, Italy
[93] B.I. Stepanov Institute of Physics, National Academy of Sciences of Belarus, Minsk, Republic of Belarus
[94] National Scientific and Educational Centre for Particle and High Energy Physics, Minsk, Republic of Belarus
[95] Group of Particle Physics, University of Montreal, Montreal QC, Canada
[96] P.N. Lebedev Physical Institute of the Russian Academy of Sciences, Moscow, Russia
[97] Institute for Theoretical and Experimental Physics (ITEP), Moscow, Russia
[98] National Research Nuclear University MEPhI, Moscow, Russia
[99] D.V. Skobeltsyn Institute of Nuclear Physics, M.V. Lomonosov Moscow State University, Moscow, Russia
[100] Fakultät für Physik, Ludwig-Maximilians-Universität München, München, Germany
[101] Max-Planck-Institut für Physik (Werner-Heisenberg-Institut), München, Germany
[102] Nagasaki Institute of Applied Science, Nagasaki, Japan
[103] Graduate School of Science and Kobayashi-Maskawa Institute, Nagoya University, Nagoya, Japan
[104] [(a)] INFN Sezione di Napoli; [(b)] Dipartimento di Fisica, Università di Napoli, Napoli, Italy
[105] Department of Physics and Astronomy, University of New Mexico, Albuquerque NM, United States of America
[106] Institute for Mathematics, Astrophysics and Particle Physics, Radboud University Nijmegen/Nikhef, Nijmegen, Netherlands
[107] Nikhef National Institute for Subatomic Physics and University of Amsterdam, Amsterdam, Netherlands
[108] Department of Physics, Northern Illinois University, DeKalb IL, United States of America

[109] Budker Institute of Nuclear Physics, SB RAS, Novosibirsk, Russia
[110] Department of Physics, New York University, New York NY, United States of America
[111] Ohio State University, Columbus OH, United States of America
[112] Faculty of Science, Okayama University, Okayama, Japan
[113] Homer L. Dodge Department of Physics and Astronomy, University of Oklahoma, Norman OK, United States of America
[114] Department of Physics, Oklahoma State University, Stillwater OK, United States of America
[115] Palacký University, RCPTM, Olomouc, Czech Republic
[116] Center for High Energy Physics, University of Oregon, Eugene OR, United States of America
[117] LAL, Univ. Paris-Sud, CNRS/IN2P3, Université Paris-Saclay, Orsay, France
[118] Graduate School of Science, Osaka University, Osaka, Japan
[119] Department of Physics, University of Oslo, Oslo, Norway
[120] Department of Physics, Oxford University, Oxford, United Kingdom
[121] [(a)] INFN Sezione di Pavia; [(b)] Dipartimento di Fisica, Università di Pavia, Pavia, Italy
[122] Department of Physics, University of Pennsylvania, Philadelphia PA, United States of America
[123] National Research Centre "Kurchatov Institute" B.P.Konstantinov Petersburg Nuclear Physics Institute, St. Petersburg, Russia
[124] [(a)] INFN Sezione di Pisa; [(b)] Dipartimento di Fisica E. Fermi, Università di Pisa, Pisa, Italy
[125] Department of Physics and Astronomy, University of Pittsburgh, Pittsburgh PA, United States of America
[126] [(a)] Laboratório de Instrumentação e Física Experimental de Partículas - LIP, Lisboa; [(b)] Faculdade de Ciências, Universidade de Lisboa, Lisboa; [(c)] Department of Physics, University of Coimbra, Coimbra; [(d)] Centro de Física Nuclear da Universidade de Lisboa, Lisboa; [(e)] Departamento de Fisica, Universidade do Minho, Braga; [(f)] Departamento de Fisica Teorica y del Cosmos and CAFPE, Universidad de Granada, Granada (Spain); [(g)] Dep Fisica and CEFITEC of Faculdade de Ciencias e Tecnologia, Universidade Nova de Lisboa, Caparica, Portugal
[127] Institute of Physics, Academy of Sciences of the Czech Republic, Praha, Czech Republic
[128] Czech Technical University in Prague, Praha, Czech Republic
[129] Faculty of Mathematics and Physics, Charles University in Prague, Praha, Czech Republic
[130] State Research Center Institute for High Energy Physics (Protvino), NRC KI, Russia
[131] Particle Physics Department, Rutherford Appleton Laboratory, Didcot, United Kingdom
[132] [(a)] INFN Sezione di Roma; [(b)] Dipartimento di Fisica, Sapienza Università di Roma, Roma, Italy
[133] [(a)] INFN Sezione di Roma Tor Vergata; [(b)] Dipartimento di Fisica, Università di Roma Tor Vergata, Roma, Italy
[134] [(a)] INFN Sezione di Roma Tre; [(b)] Dipartimento di Matematica e Fisica, Università Roma Tre, Roma, Italy
[135] [(a)] Faculté des Sciences Ain Chock, Réseau Universitaire de Physique des Hautes Energies - Université Hassan II, Casablanca; [(b)] Centre National de l'Energie des Sciences Techniques Nucleaires, Rabat; [(c)] Faculté des Sciences Semlalia, Université Cadi Ayyad, LPHEA-Marrakech; [(d)] Faculté des Sciences, Université Mohamed Premier and LPTPM, Oujda; [(e)] Faculté des sciences, Université Mohammed V, Rabat, Morocco
[136] DSM/IRFU (Institut de Recherches sur les Lois Fondamentales de l'Univers), CEA Saclay (Commissariat à l'Energie Atomique et aux Energies Alternatives), Gif-sur-Yvette, France
[137] Santa Cruz Institute for Particle Physics, University of California Santa Cruz, Santa Cruz CA, United States of America
[138] Department of Physics, University of Washington, Seattle WA, United States of America
[139] Department of Physics and Astronomy, University of Sheffield, Sheffield, United Kingdom

[140] Department of Physics, Shinshu University, Nagano, Japan
[141] Fachbereich Physik, Universität Siegen, Siegen, Germany
[142] Department of Physics, Simon Fraser University, Burnaby BC, Canada
[143] SLAC National Accelerator Laboratory, Stanford CA, United States of America
[144] [(a)] Faculty of Mathematics, Physics & Informatics, Comenius University, Bratislava; [(b)] Department of Subnuclear Physics, Institute of Experimental Physics of the Slovak Academy of Sciences, Kosice, Slovak Republic
[145] [(a)] Department of Physics, University of Cape Town, Cape Town; [(b)] Department of Physics, University of Johannesburg, Johannesburg; [(c)] School of Physics, University of the Witwatersrand, Johannesburg, South Africa
[146] [(a)] Department of Physics, Stockholm University; [(b)] The Oskar Klein Centre, Stockholm, Sweden
[147] Physics Department, Royal Institute of Technology, Stockholm, Sweden
[148] Departments of Physics & Astronomy and Chemistry, Stony Brook University, Stony Brook NY, United States of America
[149] Department of Physics and Astronomy, University of Sussex, Brighton, United Kingdom
[150] School of Physics, University of Sydney, Sydney, Australia
[151] Institute of Physics, Academia Sinica, Taipei, Taiwan
[152] Department of Physics, Technion: Israel Institute of Technology, Haifa, Israel
[153] Raymond and Beverly Sackler School of Physics and Astronomy, Tel Aviv University, Tel Aviv, Israel
[154] Department of Physics, Aristotle University of Thessaloniki, Thessaloniki, Greece
[155] International Center for Elementary Particle Physics and Department of Physics, The University of Tokyo, Tokyo, Japan
[156] Graduate School of Science and Technology, Tokyo Metropolitan University, Tokyo, Japan
[157] Department of Physics, Tokyo Institute of Technology, Tokyo, Japan
[158] Department of Physics, University of Toronto, Toronto ON, Canada
[159] [(a)] TRIUMF, Vancouver BC; [(b)] Department of Physics and Astronomy, York University, Toronto ON, Canada
[160] Faculty of Pure and Applied Sciences, and Center for Integrated Research in Fundamental Science and Engineering, University of Tsukuba, Tsukuba, Japan
[161] Department of Physics and Astronomy, Tufts University, Medford MA, United States of America
[162] Department of Physics and Astronomy, University of California Irvine, Irvine CA, United States of America
[163] [(a)] INFN Gruppo Collegato di Udine, Sezione di Trieste, Udine; [(b)] ICTP, Trieste; [(c)] Dipartimento di Chimica, Fisica e Ambiente, Università di Udine, Udine, Italy
[164] Department of Physics and Astronomy, University of Uppsala, Uppsala, Sweden
[165] Department of Physics, University of Illinois, Urbana IL, United States of America
[166] Instituto de Física Corpuscular (IFIC) and Departamento de Física Atómica, Molecular y Nuclear and Departamento de Ingeniería Electrónica and Instituto de Microelectrónica de Barcelona (IMB-CNM), University of Valencia and CSIC, Valencia, Spain
[167] Department of Physics, University of British Columbia, Vancouver BC, Canada
[168] Department of Physics and Astronomy, University of Victoria, Victoria BC, Canada
[169] Department of Physics, University of Warwick, Coventry, United Kingdom
[170] Waseda University, Tokyo, Japan
[171] Department of Particle Physics, The Weizmann Institute of Science, Rehovot, Israel
[172] Department of Physics, University of Wisconsin, Madison WI, United States of America
[173] Fakultät für Physik und Astronomie, Julius-Maximilians-Universität, Würzburg, Germany

[174] Fakultät für Mathematik und Naturwissenschaften, Fachgruppe Physik, Bergische Universität Wuppertal, Wuppertal, Germany
[175] Department of Physics, Yale University, New Haven CT, United States of America
[176] Yerevan Physics Institute, Yerevan, Armenia
[177] Centre de Calcul de l'Institut National de Physique Nucléaire et de Physique des Particules (IN2P3), Villeurbanne, France
[a] Also at Department of Physics, King's College London, London, United Kingdom
[b] Also at Institute of Physics, Azerbaijan Academy of Sciences, Baku, Azerbaijan
[c] Also at Novosibirsk State University, Novosibirsk, Russia
[d] Also at TRIUMF, Vancouver BC, Canada
[e] Also at Department of Physics & Astronomy, University of Louisville, Louisville, KY, United States of America
[f] Also at Department of Physics, California State University, Fresno CA, United States of America
[g] Also at Department of Physics, University of Fribourg, Fribourg, Switzerland
[h] Also at Departament de Fisica de la Universitat Autonoma de Barcelona, Barcelona, Spain
[i] Also at Departamento de Fisica e Astronomia, Faculdade de Ciencias, Universidade do Porto, Portugal
[j] Also at Tomsk State University, Tomsk, Russia
[k] Also at Universita di Napoli Parthenope, Napoli, Italy
[l] Also at Institute of Particle Physics (IPP), Canada
[m] Also at Department of Physics, St. Petersburg State Polytechnical University, St. Petersburg, Russia
[n] Also at Department of Physics, The University of Michigan, Ann Arbor MI, United States of America
[o] Also at Louisiana Tech University, Ruston LA, United States of America
[p] Also at Institucio Catalana de Recerca i Estudis Avancats, ICREA, Barcelona, Spain
[q] Also at Graduate School of Science, Osaka University, Osaka, Japan
[r] Also at Department of Physics, National Tsing Hua University, Taiwan
[s] Also at Department of Physics, The University of Texas at Austin, Austin TX, United States of America
[t] Also at Institute of Theoretical Physics, Ilia State University, Tbilisi, Georgia
[u] Also at CERN, Geneva, Switzerland
[v] Also at Georgian Technical University (GTU),Tbilisi, Georgia
[w] Also at Ochadai Academic Production, Ochanomizu University, Tokyo, Japan
[x] Also at Manhattan College, New York NY, United States of America
[y] Also at Hellenic Open University, Patras, Greece
[z] Also at Institute of Physics, Academia Sinica, Taipei, Taiwan
[aa] Also at Academia Sinica Grid Computing, Institute of Physics, Academia Sinica, Taipei, Taiwan
[ab] Also at School of Physics, Shandong University, Shandong, China
[ac] Also at Moscow Institute of Physics and Technology State University, Dolgoprudny, Russia
[ad] Also at Section de Physique, Université de Genève, Geneva, Switzerland
[ae] Also at International School for Advanced Studies (SISSA), Trieste, Italy
[af] Also at Department of Physics and Astronomy, University of South Carolina, Columbia SC, United States of America
[ag] Also at School of Physics and Engineering, Sun Yat-sen University, Guangzhou, China
[ah] Also at Institute for Nuclear Research and Nuclear Energy (INRNE) of the Bulgarian Academy of Sciences, Sofia, Bulgaria
[ai] Also at Faculty of Physics, M.V.Lomonosov Moscow State University, Moscow, Russia
[aj] Also at National Research Nuclear University MEPhI, Moscow, Russia
[ak] Also at Department of Physics, Stanford University, Stanford CA, United States of America

[al] Also at Institute for Particle and Nuclear Physics, Wigner Research Centre for Physics, Budapest, Hungary
[am] Also at Flensburg University of Applied Sciences, Flensburg, Germany
[an] Also at University of Malaya, Department of Physics, Kuala Lumpur, Malaysia
[ao] Also at CPPM, Aix-Marseille Université and CNRS/IN2P3, Marseille, France
[*] Deceased